Abstract

Title of Thesis: Dynamics of Low Immersion Milling

Sigmund Max Young, Master of Science, 2008

Directed by: Professor B. Balachandran
Department of Mechanical Engineering

In this thesis, dynamics of low immersion milling is explored through analytical and numerical means. Using linear and nonlinear cutting force models, maps are constructed for single degree-of-freedom and two degree-of-freedom systems where the time spent cutting is "small" compared to the spindle rotation period. These maps are used to study the possibilities for different nonlinear instabilities and construct stability charts in the space of cutting depth and spindle speed. The analytical predictions are compared with numerical results as well as prior experimental results. Good agreement amongst analytical, numerical, and experimental results is seen. Limitations of the analytical and numerical approaches are discussed and extensions for future work are suggested.

Dynamics of Low Immersion Milling

by

Sigmund Max Young

Thesis submitted to the Faculty of the Graduate School of the
University of Maryland, College Park, in partial fulfillment
of the requirements for the degree of
Master of Science
2008

Advisory Committee:
Professor B. Balachandran, Chair/Advisor
Professor A. Baz, Mechanical Engineering
Assistant Professor N. Chopra, Mechanical Engineering

Dedication

To my mother Sue,
my father Charles,
my sister Sigrid,
and my dear friends Silke and Edward.

Acknowledgements

I would like to express my deepest appreciation to Professor B. Balachandran for his utmost patience, encouragement, and guidance during my time here at University of Maryland, College Park (UMCP). His wisdom and selfless support made the completion of this thesis possible.

Much gratitude goes to Professor A. Baz and Professor N. Chopra for taking time out of their busy schedules to serve on my committee and help with the refinement of this thesis.

Special thanks goes out to Marcelo Valdez for helping me with the numerical integration of the delay differential equations and Professor Xinhua Long of Shanghai Jiao Tong University for helping me with the UMCP numerical stability prediction program.

I would also like to thank the Naval Surface Warfare Center, Carderock Division and the Code 7210 Signature Materials Physics Branch for providing financial support to my course work and thesis work.

Finally, I would like to thank my mother, my father, my sister, and my friends for their support and understanding during the completion of this thesis. Their insightful advice, comedic relief, and continuous encouragement, helped me immensely when facing the numerous challenges presented during the formation of this thesis.

Table of Contents

List of Tables

List of Figures

Chapter 1

Introduction and Background

1.1 Introduction

Machining is an industrial process where material is removed to form a desired shape on a workpiece. Traditional machining includes cutting operations such as turning, boring, drilling, and milling as well as abrading operations such as grinding, polishing, and buffing. There are non-traditional machining operations that include chemical machining, abrasive-jet machining, laser cutting, plasma cutting, and water-jet cutting. With advances of modern machining, the manufacturing of large, sculptured parts through material removal is faster and more economical than the production of a large number of simple parts (Halley, Helvey, Smith, and Winfough, 1999). The focus of this thesis will be on traditional machining methods, especially, that of milling.

1.2 Background

Milling is a process in which a rotating cutting tool uses the teeth or flutes on its edges to remove material on a workpiece.

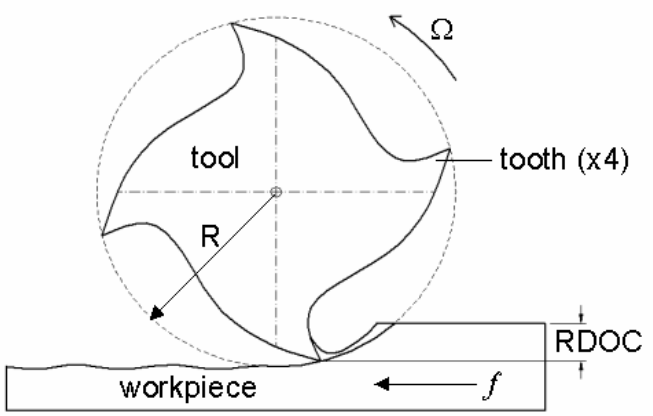

Figure 1.1: Milling diagram - section view.

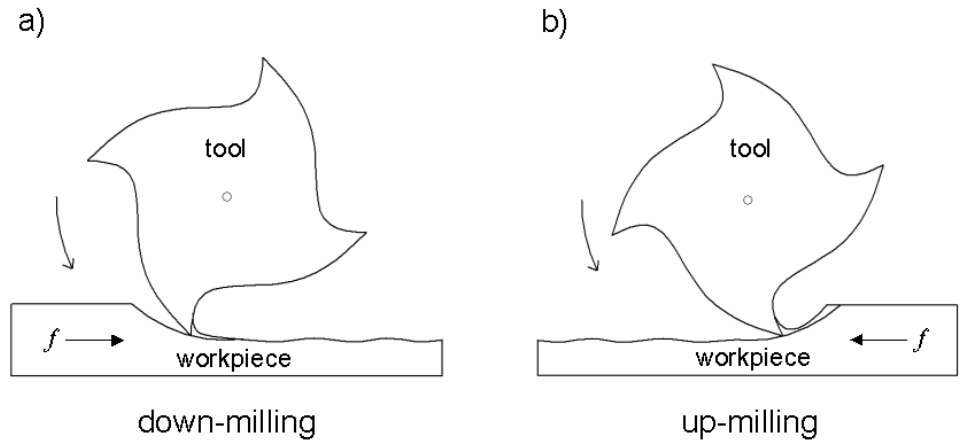

Figure 1.2: a) down-milling process and b) up-milling process.

As depicted in Figure 1.1, the workpiece is fed at a feed rate *f* into the tool of radius R, which spins at a high angular speed Ω. During the pass of each tooth, a little chip of material is removed from the workpiece. Material removal can be achieved through an up-milling process or a down-milling process.

During down-milling, the feed rate *f* is directed along the same direction as the rotation of the tool; in up-milling, the feed rate *f* is directed along the opposite direction to the rotation of the tool. The chip formation in down-milling is opposite to that seen in up-milling.

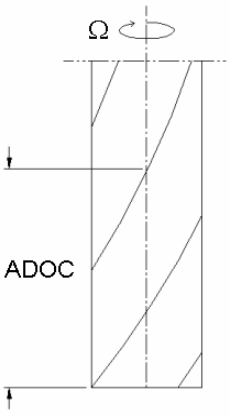

Figure 1.3: Milling tool diagram.

Under most conditions, the amount of material removed per tooth pass depends mostly on the feed rate and the axial depth of cut (ADOC), as shown in Figure 1.2. The rate of immersion is defined as

$$\text{rate of immersion} = \frac{\text{RDOC}}{2R} \tag{1.1}$$

where RDOC is the radial depth of cut.

In this thesis, the focus is on low immersion milling, which is assumed to occur when the RDOC is much less than the radius of the tool *R*. Another way to express the rate of immersion is through

$$\text{rate of immersion} \approx \left(\frac{\pi\rho}{N}\right)^2 \tag{1.2}$$

where N is the number of teeth on the tool and ρ is defined as the ratio of time spent cutting to the total spindle period τ ; it is noted that this assumption only holds valid for static cutting conditions, zero helix angle on the cutting tool, circular tool paths, and small angles of engagement (Davies, Pratt, and Dutterer, 2002). Therefore, by making ρ a small parameter, the rate of immersion also becomes small. Low immersion milling applies to modern cutting operations including the milling of hard-to-machine materials, contoured surfaces, and finishing operations on flexible components (Davies *et al*., 2002). In general, low immersion also occurs during high speed milling when the spindle speed Ω is greater than 10 krpm.

1.3 Chatter and Regenerative Effects

During the milling process, the cutting forces on the tool cause relative vibrations that are either stable or unstable. Stable vibrations from the cutting forces can be said to provide a net positive damping to the system that allow the vibrations to decay while unstable vibrations from the cutting forces can be said to provide a net negative damping to the system and therefore introduce energy to the system that cannot be dissipated (Tobias, 1965). The associated loss of dynamic stability is called chatter. Primary sources of chatter include the following: (1) regenerative instabilities that result from the undercutting of a previously cut surface and (2) driven oscillations that arise from the intermittent engagement between the workpiece and the tool (e.g., Davies and Balachandran, 2000).

The first case occurs most commonly during full immersion milling operations where at least one flute of the tool is engaged with the workpiece at all times. The stability analysis for this case can be treated like that of a turning problem, where the tool and workpiece system is modeled as a linear oscillator and the cutting force acting on the system is dependent on the previous and present positions of the tool.

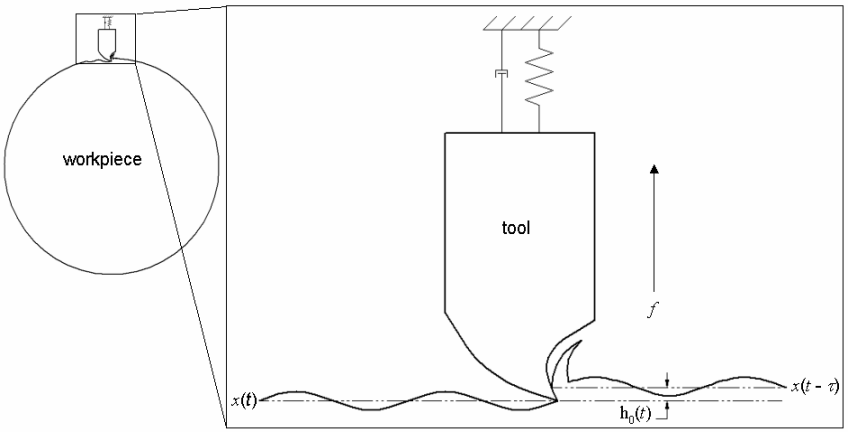

Figure 1.4: Regenerative effects of turning.

In Figure 1.4, the cutting force of the tool is determined from the difference of the time-delayed tool position $x(t-\tau)$ with the current tool position $x(t)$ plus the feed $h_0(t)$, which is equal to the feed rate f_0 multiplied by the total spindle period $\tau(t)$. This kind of regenerative system was first studied by Arnold (1946), who used a lathe with a stiff workpiece and flexible tool. The onset of chatter vibrations depends on parameters such as the feed rate, the RDOC, the axial depth of cut, and the spindle speed. Tlusty and Polacek (1963) and Tobias (1965) later showed that the chip thickness variation along with the dynamic cutting force and its regenerative effects are important mechanisms that lead to chatter.

1.4 Loss of Contact Effects

The second primary source for chatter is significant during low immersion operations where the cutting becomes highly interrupted. When this occurs, some of the cutting edges are not in contact with the workpiece for the majority of the time; this is also known as the loss of contact effect (e.g., Balachandran, 2001).

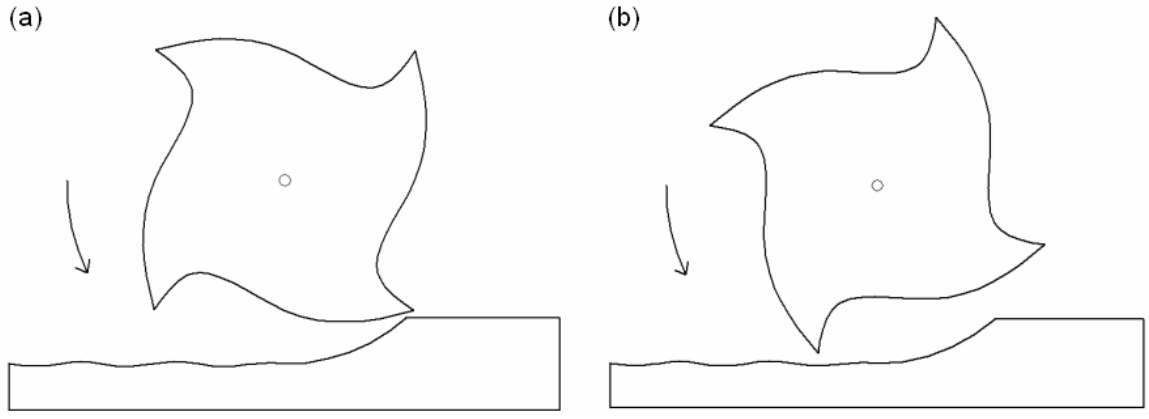

Figure 1.5: Loss of contact effects.

Therefore, the actual cutting or contact of a tooth with the workpiece occurs during short time intervals; that is $\rho << 1$. Through this small parameter assumption, the cutting force duration shrinks towards zero making the non-cutting period close to the total spindle period.

1.5 Cutting Forces

The cutting force is mostly dependent on the following properties: i) cutter geometry, ii) workpiece geometry, iii) cutting conditions, iv) workpiece material properties, and v) relative displacement between the workpiece and the tool. While Davies *et al*. (2002) examine a single degree-of-freedom (DOF) linear cutting force model, Szalai, Stepan, and Hogan (2004) modify this linear model by changing the cutting force into a nonlinear cutting force function that follows the 3/4 rule (Tlusty 2000). Zhao (2000) and Long (2006) model the cutting tool as an integrated set of thin disk elements while using linear dynamic uncut chip thickness variations.

1.6 Research Objectives

The motivation for this study includes increasing productivity and lowering the cost of material removal while achieving a high quality surface finish and keeping the tool wear low. Vibrations during the milling process play a major role in influencing the quality of the surface finish, the wear of the tool, and the material removal rate. While active damping can reduce and stabilize these vibrations, extensive modification of the system is required, which can be costly. In addition, there are limitations to the extent to which the damping levels can be increased. Therefore, a better approach is to look at the

operating parameters of the milling system. By observing cutting speeds and axial depth of cuts, ideal operating parameters can be identified for productive milling operations. Through a thorough examination of the dynamics on milling processes, the parameters for establishing stable chatter free operations can be determined and graphed to create a stability chart.

By using a stability chart like the one shown in Figure 1.6, a milling operator can find the ideal spindle speed and axial depth of cut to machine efficiently while producing parts with a high quality surface finish. Knowledge of the dynamics and stability behavior of milling processes is sought to improve the accuracy of stability prediction, and therefore, enhance milling performance.

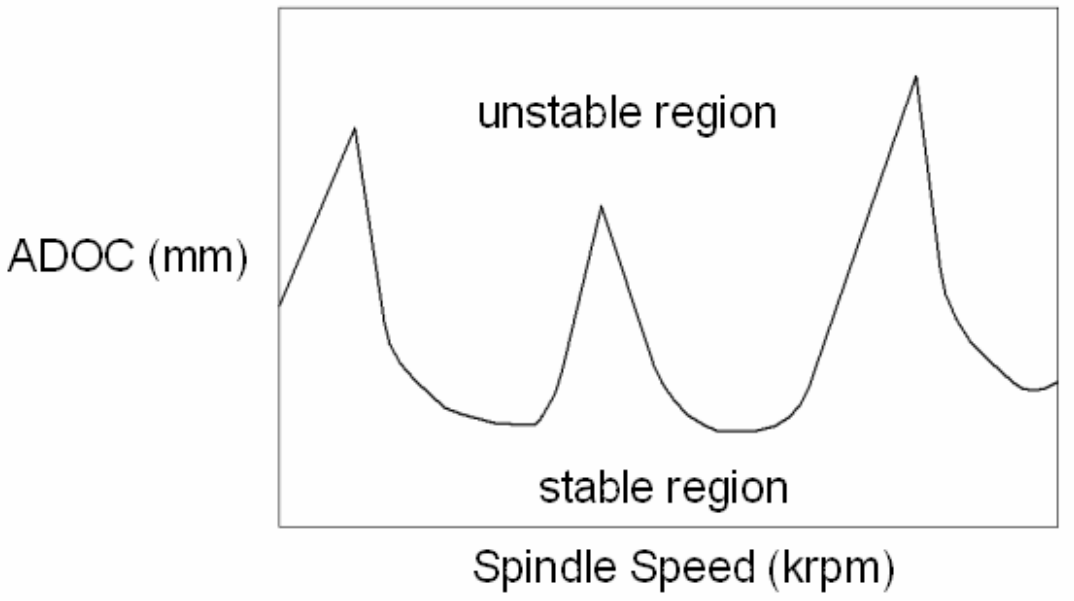

Figure 1.6: Sample stability chart for milling.

From the earlier discussion, the cutting forces during low immersion milling can be reasonably modeled with loss of contact assumptions. The non-cutting and cutting periods can be mapped through dynamic equations that incorporate regenerative effects. By conducting analytical and numerical stability analysis with these maps, bifurcation parameters can be identified. The results of this analysis are presented graphically through stability charts. The accuracy of these results is examined through comparison with existing experimental results.

This thesis effort has been carried out with the following objectives:

i) Develop single and two degree-of-freedom system equations of motion for low immersion milling with linear and 3/4 rule cutting force models
ii) Construct maps based on cutting and non-cutting periods, and conduct stability analysis predictions by using the developed maps
iii) Use delay differential equation numerical techniques to verify the analytical stability predictions
iv) Use the UMCP numerical stability prediction program developed by Zhao (2000) and Long (2006), and modify the linear dynamic uncut chip thickness variation in the program's cutting force model to incorporate the 3/4 rule
v) Compare the predictions obtained through analytical and numerical means with that of existing experimental data

1.7 Thesis Organization

This thesis is organized as follows. In the second chapter, the single degree-of-freedom system equations of motion with linear and 3/4 rule cutting forces are summarized from

Davies *et al*. (2002) and Szalai *et al*. (2004). These equations of motion and the cutting force models are then expanded to a two degree-of-freedom model. Development of maps from the single degree-of-freedom and the two degree-of-freedom models follow. In the third chapter, analytical stability prediction equations are obtained for the single degree-of-freedom maps and the derivations of the analytical stability prediction equations for the two degree-of-freedom system maps are detailed. In chapter four, the delay differential equation numerical verification of the analytical predictions is presented. Summaries detailing the UMCP numerical stability prediction program and its modification to include the 3/4 rule cutting force model are also included. In the fifth chapter, stability charts obtained by using the analytical models are compared with the predictions obtained from numerical simulations as well as data taken from existing experimental results found in the literature (Davies *et al*., 2002 and Stepan, Szalai, Mann, Bayly, Insperger, Gradisek, and Govekar, 2005). Concluding remarks and suggestions for future work are presented in the last chapter. Appendices are included to provide details of calculations as well as the codes used for the numerical simulations. References are listed at the end of the thesis.

Chapter 2

Milling Models

2.1 Single DOF System Equation of Motion

The following figure depicts a one degree-of-freedom milling configuration.

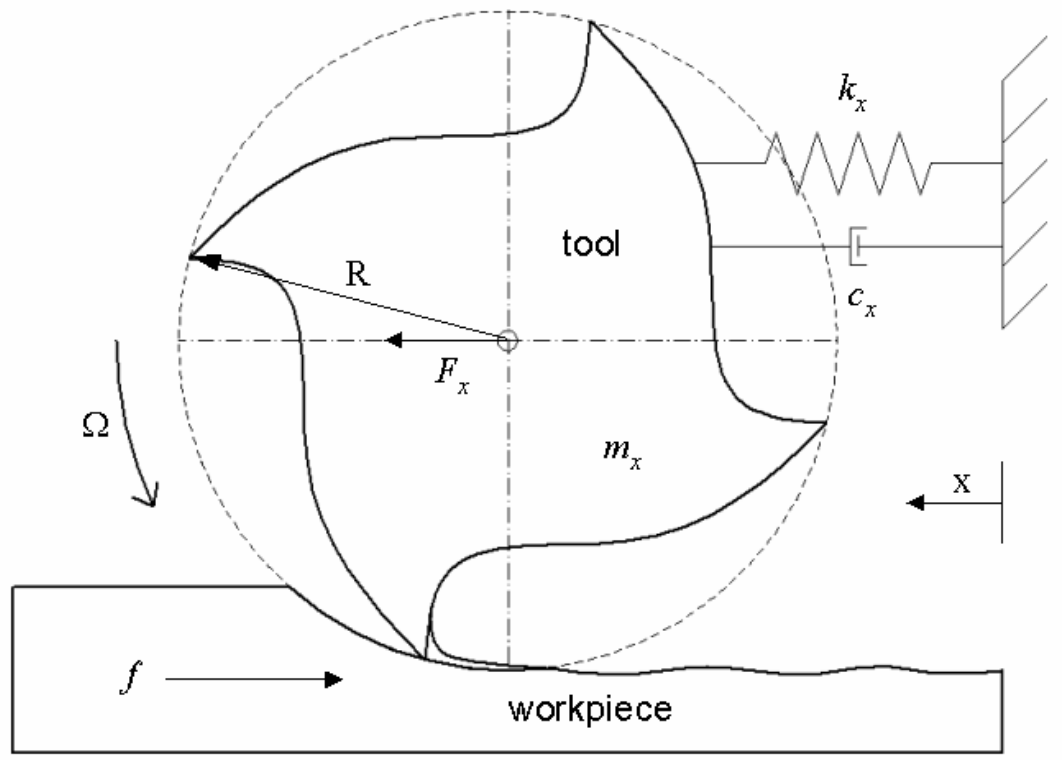

Figure 2.1: Schematic of a single DOF milling configuration.

The governing equations of this system are

$$m_x\ddot{q}_x(t)+c_x\dot{q}_x(t)+k_xq_x(t)=g(t)F_x\left(t,\tau(t)\right) \tag{2.1}$$

where

$$g(t)=0, \text{ is the free oscillation period } \tau_1,\ t_j \le t < t_{j+1}^-$$
$$g(t)=1, \text{ is the cutting period } \tau_2,\ t_{j+1}^- \le t < t_{j+1}$$

and τ, the total spindle time period, equals $\tau_1 + \tau_2$. Therefore, at the start of τ_1, from time t_j, to the end of τ_1, at the time just prior to t_{j+1}^-, the tool is not in contact with the workpiece; the equation of motion in (2.1) does not depend on the cutting force $F_x\left(t, \tau(t)\right)$ and becomes a linear, homogenous differential equation. Then at the start of τ_2, from the time t_{j+1}^-, to the end of τ_2, at the time just prior to t_{j+1}, the tool contacts the workpiece and thus, the equation of motion in (2.1) depends on the cutting force $F_x\left(t, \tau(t)\right)$. At the time t_{j+1}, a new spindle period begins. In both states of τ_1 and τ_2, the equation of motion of the tool includes displacement $q_x(t)$, constant stiffness k_x, and constant damping c_x. The tool rotates with a constant angular speed Ω and has N number of teeth. The constant feed rate f of the workpiece runs opposite to the major mode of motion $q_x(t)$. According to previous research as mentioned in Long (2006), a circular tooth path is assumed, which therefore creates the constant time delay $\tau = 2\pi / N\Omega$. Through the definition of ρ, $\tau_2 = \rho\tau$. The linear cutting force is given by

$$F_x\left(t, \tau(t)\right) = K_t w\left[q_x(t-\tau) - q_x(t) + \mathrm{h}_0\right] \tag{2.2}$$

while the 3/4 rule cutting force is given by

$$F_x\left(t, \tau(t)\right) = Kw\left[q_x(t-\tau) - q_x(t) + \mathrm{h}_0\right]^{3/4} \tag{2.3}$$

where K_t is the workpiece material constant, K is the modified workpiece material constant and is related to K_t by

$$K = K_t \mathrm{h}_0^{1/4}, \tag{2.4}$$

w is the axial depth of cut or constant chip width, and h_0 is the feed, which is defined as $\mathrm{h}_0 = f\tau$. Note that both h_0 and τ are dependent on t.

2.2 Two DOF System Equations of Motion

The following figure depicts a two degree-of-freedom milling configuration.

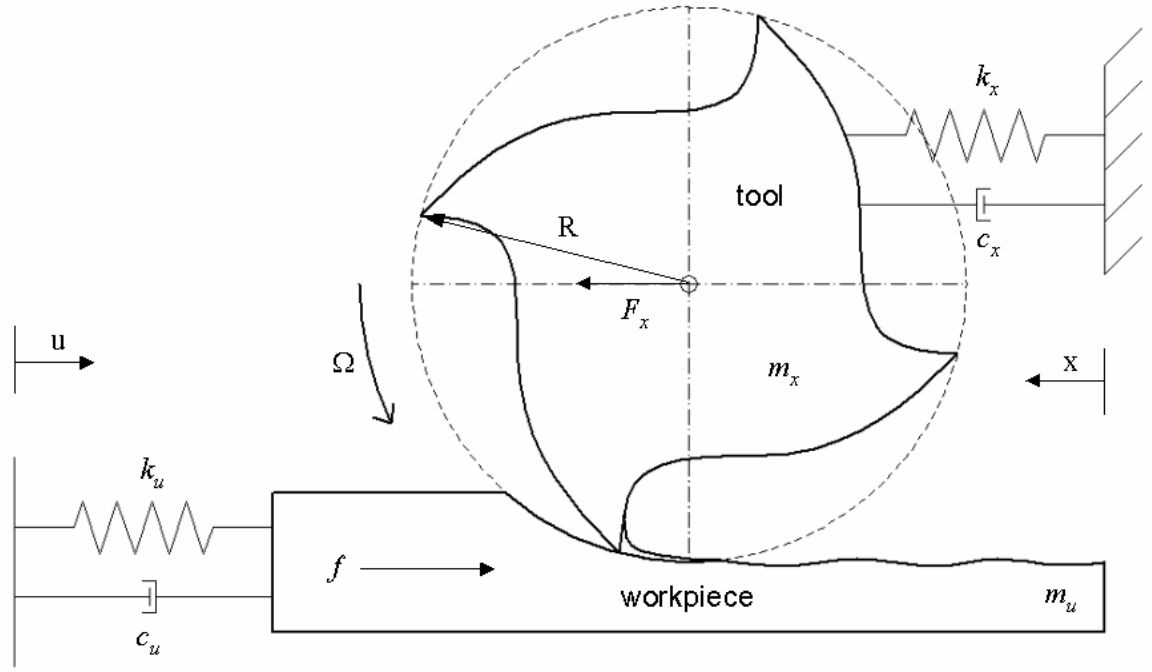

Figure 2.2: Schematic of a two DOF milling configuration.

The governing equations of this system are

$$\begin{aligned} m_x\ddot{q}_x(t)+c_x\dot{q}_x(t)+k_xq_x(t) &= g(t)F_x\left(t,\tau(t)\right) \\ m_u\ddot{q}_u(t)+c_u\dot{q}_u(t)+k_uq_u(t) &= g(t)F_u\left(t,\tau(t)\right) \end{aligned} \tag{2.5}$$

where

$$\begin{aligned} g(t)=0, \text{ the free oscillation period } \tau_1,\ t_j \le t < t_{j+1}^- \\ g(t)=1, \text{ the cutting period } \tau_2,\ t_{j+1}^- \le t < t_{j+1} \end{aligned}$$

and τ, the total time period, equals $\tau_1+\tau_2$. As in the one degree-of-freedom case, at the start of τ_1, from time t_j, to the end of τ_1, at the time just prior to t_{j+1}^-, the tool is not in contact with the workpiece, so the equations of motion in (2.5) do not depend on the

cutting forces $F_x\left(t,\tau(t)\right)$ and $F_u\left(t,\tau(t)\right)$; the system becomes a set of linear, homogenous differential equations. Then at the start of τ_2, from the time t_{j+1}^-, to the end of τ_2, at the time just prior to t_{j+1}, the tool contacts the workpiece and the equations of motion in (2.5) depend on the cutting forces $F_x\left(t,\tau(t)\right)$ and $F_u\left(t,\tau(t)\right)$. At the time t_{j+1}, a new spindle period begins. As in the single degree-of-freedom case, the equation of motion for the tool includes displacement $q_x(t)$, constant stiffness k_x, and constant damping c_x. The equation of motion for the workpiece includes displacement $q_u(t)$, constant stiffness k_u, and constant damping c_u. The constant feed rate f of the workpiece runs along the major mode of motion on the workpiece $q_u(t)$. The linear cutting force is given by

$$F_x\left(t,\tau(t)\right) = K_t w\left[q_x(t-\tau) - q_x(t) + q_u(t-\tau) - q_u(t) + \mathrm{h}_0\right] \tag{2.6}$$

while the 3/4 rule cutting force is given by

$$F_x\left(t,\tau(t)\right) = Kw\left[q_x(t-\tau) - q_x(t) + q_u(t-\tau) - q_u(t) + \mathrm{h}_0\right]^{3/4} \tag{2.7}$$

Applying Newton's Third Law, the cutting force $F_x\left(t,\tau(t)\right)$ acting on the tool is equal and opposite to the cutting force $F_u\left(t,\tau(t)\right)$ acting on the workpiece. Thus, the equations of motion become

$$\begin{aligned} m_x\ddot{q}_x(t) + c_x\dot{q}_x(t) + k_x q_x(t) &= g(t)F_x\left(t,\tau(t)\right) \\ m_u\ddot{q}_u(t) + c_u\dot{q}_u(t) + k_u q_u(t) &= g(t)F_x\left(t,\tau(t)\right) \end{aligned} \tag{2.8}$$

2.3 Single DOF System Map

The key to determining stability is to find the appropriate maps and their solutions for the interrupted cutting process. For ease of notation, one manipulates the equation of motion from (2.1) into

$$\ddot{q}_x(t) + 2\zeta_x \omega_x \dot{q}_x(t) + \omega_x{}^2 q_x(t) = \frac{g(t)}{m_x} F_x\left(t, \tau(t)\right) \tag{2.9}$$

where $\omega_x = \sqrt{k_x / m_x}$ is the natural frequency for the tool and $\zeta_x = c_x / 2\sqrt{k_x m_x}$ is the constant damping ratio for the tool. The free vibration non-cutting phase ($g(t) = 0$) that maps the state $\left(q_x(t_j), \dot{q}_x(t_j)\right)$ to the state $\left(q_x(t_{j+1}^-), \dot{q}_x(t_{j+1}^-)\right)$ is derived to be

$$\begin{bmatrix} q_x(t_{j+1}^-) \\ \dot{q}_x(t_{j+1}^-) \end{bmatrix} = \mathrm{A} \begin{bmatrix} q_x(t_j) \\ \dot{q}_x(t_j) \end{bmatrix} \tag{2.10}$$

where the state-transition matrix A is

$$\mathrm{A} = \exp(-\zeta_x \omega_x \tau) \begin{bmatrix} \cos(\omega_{xd}\tau) + \dfrac{\zeta_x \omega_x}{\omega_{xd}} \sin(\omega_{xd}\tau) & \dfrac{1}{\omega_{xd}} \sin(\omega_{xd}\tau) \\ -\dfrac{\omega_x{}^2}{\omega_{xd}} \sin(\omega_{xd}\tau) & \cos(\omega_{xd}\tau) - \dfrac{\zeta_x \omega_x}{\omega_{xd}} \sin(\omega_{xd}\tau) \end{bmatrix} \tag{2.11}$$

and $\omega_{xd} = \omega_x \sqrt{1 - \zeta_x{}^2}$ is defined to be the damped natural frequency for free oscillations of the tool. Note that it has been assumed that $\tau_1 \approx \tau$, as explained next.

In instances where the time period of cutting is very short; that is, $\tau_2 \to 0$, τ_1 can be approximated by τ (e.g. Szalai *et al*., 2004). For the cutting period $\tau_2 \to 0$, the spring and damping forces can be neglected (e.g. Davies *et al*., 2002) and the position of the tool can be assumed to experience a negligible change during cutting, which leaves

$$\ddot{q}_x(t) \approx \frac{K_t w}{m_x}\left[q_x(t_j) - q_x(t_{j+1}^-) + \mathrm{h}_0 \right] , \quad t_{j+1}^- \le t < t_{j+1} \tag{2.12}$$

for the linear cutting force model and

$$\ddot{q}_x(t) \approx \frac{K w}{m_x}\left[q_x(t_j) - q_x(t_{j+1}^-) + \mathrm{h}_0 \right]^{3/4} , \quad t_{j+1}^- \le t < t_{j+1} \tag{2.13}$$

for the 3/4 rule cutting force model.

Integrating the above equation over the period $[t_{j+1}^-, t_{j+1}]$, one finds

$$\dot{q}_x(t_{j+1}) = \dot{q}_x(t_{j+1}^-) + \tau_2 \frac{K_t w}{m_x}\left[q_x(t_j) - q_x(t_{j+1}^-) + \mathrm{h}_0 \right] \tag{2.14}$$

for the linear cutting force model and

$$\dot{q}_x(t_{j+1}) = \dot{q}_x(t_{j+1}^-) + \tau_2 \frac{K w}{m_x}\left[q_x(t_j) - q_x(t_{j+1}^-) + \mathrm{h}_0 \right]^{3/4} \tag{2.15}$$

for the 3/4 rule cutting force model.

Combining equations (2.10) and (2.14) together for the linear cutting force model, and equations (2.10) and (2.15) together for the 3/4 rule cutting force model, and assuming that the position of the oscillating tool remains constant during the interaction with the workpiece so that $q_x(t_{j+1}) \approx q_x(t_{j+1}^-)$, one arrives at

$$\begin{bmatrix} q_x(t_{j+1}) \\ \dot{q}_x(t_{j+1}) \end{bmatrix} = \mathrm{A} \begin{bmatrix} q_x(t_j) \\ \dot{q}_x(t_j) \end{bmatrix} + \begin{bmatrix} 0 \\ \tau_2 \frac{K_t w}{m_x}[(1-\mathrm{A}_{11}) q_x(t_j) - \mathrm{A}_{12} \dot{q}_x(t_j) + \mathrm{h}_0] \end{bmatrix} \tag{2.16}$$

and

$$\begin{bmatrix} q_x(t_{j+1}) \\ \dot{q}_x(t_{j+1}) \end{bmatrix} = \mathrm{A}\begin{bmatrix} q_x(t_j) \\ \dot{q}_x(t_j) \end{bmatrix} + \begin{bmatrix} 0 \\ \tau_2 \dfrac{Kw}{m_x}[(1-\mathrm{A}_{11})q_x(t_j) - \mathrm{A}_{12}\dot{q}_x(t_j) + \mathrm{h}_0]^{3/4} \end{bmatrix} \tag{2.17}$$

for the linear and 3/4 rule cutting forces, respectively, where A_{ij} corresponds to the elements of A in (2.11).

By using fixed point and stability techniques such as those found in Nayfeh and Balachandran (1995), the maps in (2.16) and (2.17) are found to have the fixed points

$$\begin{bmatrix} x_e \\ v_e \end{bmatrix} = \frac{K_t w \tau_2 \mathrm{h}_0}{m_x\left[1+\det(\mathrm{A})-\mathrm{tr}(\mathrm{A})\right]}\begin{bmatrix} \mathrm{A}_{12} \\ 1-\mathrm{A}_{11} \end{bmatrix} \tag{2.18}$$

and

$$\begin{bmatrix} x_e \\ v_e \end{bmatrix} = \frac{Kw\tau_2 \mathrm{h}_0{}^{3/4}}{m_x\left[1+\det(\mathrm{A})-\mathrm{tr}(\mathrm{A})\right]}\begin{bmatrix} \mathrm{A}_{12} \\ 1-\mathrm{A}_{11} \end{bmatrix} \tag{2.19}$$

The linearized Jacobian matrix for (2.16) and (2.17) is

$$\mathrm{B} = \begin{bmatrix} \mathrm{A}_{11} & \mathrm{A}_{12} \\ \mathrm{A}_{21} + \hat{w}_x(1-\mathrm{A}_{11}) & \mathrm{A}_{22} - \hat{w}_x\mathrm{A}_{12} \end{bmatrix} \tag{2.20}$$

where the dimensionless chip width for the linear cutting force model is

$$\hat{w}_x = \frac{K_t w \tau_2}{m_x} \tag{2.21}$$

and the dimensionless chip width for the 3/4 cutting force model is

$$\hat{w}_x = \frac{3}{4}\frac{Kw\tau_2}{m_x \mathrm{h}_0{}^{1/4}} \tag{2.22}$$

Linearizing around the fixed points, the generalized local dynamics is described by

$$\begin{bmatrix} q_x(t_{j+1}) \\ \dot{q}_x(t_{j+1}) \end{bmatrix} = \begin{bmatrix} x_e \\ v_e \end{bmatrix} + \mathrm{B} \begin{bmatrix} q_x(t_j) \\ \dot{q}_x(t_j) \end{bmatrix} \tag{2.23}$$

where x_e, v_e, and $\hat{w}_x$ are based on their respective cutting force models.

2.4 Two DOF System Map

As in the case of the single degree-of-freedom map, one simplifies the notation in the equations of motion (2.8) to yield

$$\begin{aligned} \ddot{q}_x(t) + 2\zeta_x \omega_x \dot{q}_x(t) + \omega_x{}^2 q_x(t) &= \frac{g(t)}{m_x} F_x\left(t, \tau(t)\right) \\ \ddot{q}_u(t) + 2\zeta_u \omega_u \dot{q}_u(t) + \omega_u{}^2 q_u(t) &= \frac{g(t)}{m_u} F_x\left(t, \tau(t)\right) \end{aligned} \tag{2.24}$$

where, as in the single degree-of-freedom case, $\omega_x = \sqrt{k_x / m_x}$ is the natural frequency for the tool and $\zeta_x = c_x / 2\sqrt{k_x m_x}$ is the constant damping ratio for the tool. $\omega_u = \sqrt{k_u / m_u}$ is the natural frequency for the workpiece and $\zeta_u = c_u / 2\sqrt{k_u m_u}$ is the constant damping ratio for the workpiece. With equation (2.24), the non-cutting phase ($g(t) = 0$) that maps the state $\left(q_x(t_j), \dot{q}_x(t_j), q_u(t_j), \dot{q}_u(t_j)\right)$ to the state $\left(q_x(t_{j+1}^-), \dot{q}_x(t_{j+1}^-), q_u(t_{j+1}^-), \dot{q}_u(t_{j+1}^-)\right)$ is derived as

$$\begin{bmatrix} q_x(t_{j+1}^-) \\ q_u(t_{j+1}^-) \\ \dot{q}_x(t_{j+1}^-) \\ \dot{q}_u(t_{j+1}^-) \end{bmatrix} = \mathrm{C} \begin{bmatrix} q_x(t_j) \\ q_u(t_j) \\ \dot{q}_x(t_j) \\ \dot{q}_u(t_j) \end{bmatrix} \tag{2.25}$$

where the state-transition matrix C is

$$\begin{bmatrix} e^{-\zeta_x\omega_x\tau}[\hat{c}_x+\frac{\zeta_x\omega_x}{\omega_{xd}}\hat{s}_x] & 0 & \frac{e^{-\zeta_x\omega_x\tau}}{\omega_{xd}}\hat{s}_x & 0 \\ 0 & e^{-\zeta_u\omega_u\tau}[\hat{c}_u+\frac{\zeta_u\omega_u}{\omega_{ud}}\hat{s}_u] & 0 & \frac{e^{-\zeta_u\omega_u\tau}}{\omega_{ud}}\hat{s}_u \\ -\frac{\omega_x^{\,2}}{\omega_{xd}}e^{-\zeta_x\omega_x\tau}\hat{s}_x & 0 & e^{-\zeta_x\omega_x\tau}[\hat{c}_x-\frac{\zeta_x\omega_x}{\omega_{xd}}\hat{s}_x] & 0 \\ 0 & -\frac{\omega_u^{\,2}}{\omega_{ud}}e^{-\zeta_u\omega_u\tau}\hat{s}_u & 0 & e^{-\zeta_u\omega_u\tau}[\hat{c}_u-\frac{\zeta_u\omega_u}{\omega_{ud}}\hat{s}_u] \end{bmatrix} \quad (2.26)$$

and $\hat{c}_x=\cos(\omega_{xd}\tau)$, $\hat{s}_x=\sin(\omega_{xd}\tau)$, $\hat{c}_u=\cos(\omega_{ud}\tau)$, and $\hat{s}_u=\sin(\omega_{ud}\tau)$.

$\hat{\mathrm{C}}$ is obtained from the state-transition matrix A of the tool in equation (2.11)

$$\hat{\mathrm{C}}=\mathrm{A}=\begin{bmatrix}\mathrm{A}_{11} & \mathrm{A}_{12}\\ \mathrm{A}_{21} & \mathrm{A}_{22}\end{bmatrix}=\begin{bmatrix}\mathrm{C}_{11} & \mathrm{C}_{13}\\ \mathrm{C}_{31} & \mathrm{C}_{33}\end{bmatrix}$$

and $\overset{*}{\mathrm{C}}$ is the state-transition matrix of the workpiece

$$\overset{*}{\mathrm{C}}=\begin{bmatrix}\mathrm{C}_{22} & \mathrm{C}_{24}\\ \mathrm{C}_{42} & \mathrm{C}_{44}\end{bmatrix} \quad (2.27)$$

where again, $\omega_{xd}=\omega_x\sqrt{1-\zeta_x^{\,2}}$ is the damped natural frequency for the freely oscillating tool and $\omega_{ud}=\omega_u\sqrt{1-\zeta_u^{\,2}}$ is introduced as the damped natural frequency for the freely oscillating workpiece.

As in the single degree-of-freedom case, with $\tau_2\to 0$, the spring and damping forces can be neglected and the position of the tool can be assumed to experience negligible change during the cutting, which leads to

$$\begin{aligned}\ddot{q}_x(t) &\approx \frac{K_t w}{m_x}\left[q_x(t_j) - q_x(t_{j+1}^-) + q_u(t_j) - q_u(t_{j+1}^-) + \mathrm{h}_0\right] \\ \ddot{q}_u(t) &\approx \frac{K_t w}{m_u}\left[q_x(t_j) - q_x(t_{j+1}^-) + q_u(t_j) - q_u(t_{j+1}^-) + \mathrm{h}_0\right]\end{aligned}, \quad t_{j+1}^- \le t < t_{j+1} \tag{2.28}$$

for the linear cutting force model and

$$\begin{aligned}\ddot{q}_x(t) &\approx \frac{Kw}{m_x}\left[q_x(t_j) - q_x(t_{j+1}^-) + q_u(t_j) - q_u(t_{j+1}^-) + \mathrm{h}_0\right]^{3/4} \\ \ddot{q}_u(t) &\approx \frac{Kw}{m_u}\left[q_x(t_j) - q_x(t_{j+1}^-) + q_u(t_j) - q_u(t_{j+1}^-) + \mathrm{h}_0\right]^{3/4}\end{aligned}, \quad t_{j+1}^- \le t < t_{j+1} \tag{2.29}$$

for the 3/4 rule cutting force model.

Integrating the above equation over the interval $[t_{j+1}^-, t_{j+1}]$ one finds

$$\begin{aligned}\dot{q}_x(t_{j+1}) &= \dot{q}_x(t_{j+1}^-) + \tau_2 \frac{K_t w}{m_x}\left[q_x(t_j) - q_x(t_{j+1}^-) + q_u(t_j) - q_u(t_{j+1}^-) + \mathrm{h}_0\right] \\ \dot{q}_u(t_{j+1}) &= \dot{q}_u(t_{j+1}^-) + \tau_2 \frac{K_t w}{m_u}\left[q_x(t_j) - q_x(t_{j+1}^-) + q_u(t_j) - q_u(t_{j+1}^-) + \mathrm{h}_0\right]\end{aligned} \tag{2.30}$$

for the linear cutting force model and

$$\begin{aligned}\dot{q}_x(t_{j+1}) &= \dot{q}_x(t_{j+1}^-) + \tau_2 \frac{Kw}{m_x}\left[q_x(t_j) - q_x(t_{j+1}^-) + q_u(t_j) - q_u(t_{j+1}^-) + \mathrm{h}_0\right]^{3/4} \\ \dot{q}_u(t_{j+1}) &= \dot{q}_u(t_{j+1}^-) + \tau_2 \frac{Kw}{m_u}\left[q_x(t_j) - q_x(t_{j+1}^-) + q_u(t_j) - q_u(t_{j+1}^-) + \mathrm{h}_0\right]^{3/4}\end{aligned} \tag{2.31}$$

for the 3/4 rule cutting force model.

For the linear cutting force model, combining equations (2.25) and (2.30) together yields

$$\begin{bmatrix} q_x(t_{j+1}) \\ q_u(t_{j+1}) \\ \dot{q}_x(t_{j+1}) \\ \dot{q}_u(t_{j+1}) \end{bmatrix} = \mathrm{C} \begin{bmatrix} q_x(t_j) \\ q_u(t_j) \\ \dot{q}_x(t_j) \\ \dot{q}_u(t_j) \end{bmatrix} + \begin{bmatrix} 0 \\ 0 \\ \tau_2 \dfrac{K_t w}{m_x}[(1-\mathrm{C}_{11})q_x(t_j) - \mathrm{C}_{13}\dot{q}_x(t_j) + (1-\mathrm{C}_{22})q_u(t_j) - \mathrm{C}_{24}\dot{q}_u(t_j) + \mathrm{h}_0] \\ \tau_2 \dfrac{K_t w}{m_u}[(1-\mathrm{C}_{11})q_x(t_j) - \mathrm{C}_{13}\dot{q}_x(t_j) + (1-\mathrm{C}_{22})q_u(t_j) - \mathrm{C}_{24}\dot{q}_u(t_j) + \mathrm{h}_0] \end{bmatrix} \tag{2.32}$$

while combining equations (2.25) and (2.31) together for the 3/4 rule cutting force model yields

$$\begin{bmatrix} q_x(t_{j+1}) \\ q_u(t_{j+1}) \\ \dot{q}_x(t_{j+1}) \\ \dot{q}_u(t_{j+1}) \end{bmatrix} = \mathrm{C} \begin{bmatrix} q_x(t_j) \\ q_u(t_j) \\ \dot{q}_x(t_j) \\ \dot{q}_u(t_j) \end{bmatrix} + \begin{bmatrix} 0 \\ 0 \\ \tau_2 \dfrac{Kw}{m_x}[(1-\mathrm{C}_{11})q_x(t_j) - \mathrm{C}_{13}\dot{q}_x(t_j) + (1-\mathrm{C}_{22})q_u(t_j) - \mathrm{C}_{24}\dot{q}_u(t_j) + \mathrm{h}_0]^{3/4} \\ \tau_2 \dfrac{Kw}{m_u}[(1-\mathrm{C}_{11})q_x(t_j) - \mathrm{C}_{13}\dot{q}_x(t_j) + (1-\mathrm{C}_{22})q_u(t_j) - \mathrm{C}_{24}\dot{q}_u(t_j) + \mathrm{h}_0]^{3/4} \end{bmatrix} \tag{2.33}$$

where C_{ij} corresponds to the elements of C in equation (2.26). The fixed points of equation (2.32) are

$$\begin{bmatrix} x_e \\ v_e \end{bmatrix} = \frac{K_t w \tau_2 \mathrm{h}_0}{m_x\left[1+\det(\hat{\mathrm{C}})-\mathrm{tr}(\hat{\mathrm{C}})\right]} \begin{bmatrix} \mathrm{C}_{13} \\ 1-\mathrm{C}_{11} \end{bmatrix}$$
$$\begin{bmatrix} u_e \\ w_e \end{bmatrix} = \frac{K_t w \tau_2 \mathrm{h}_0}{m_u\left[1+\det(\overset{*}{\mathrm{C}})-\mathrm{tr}(\overset{*}{\mathrm{C}})\right]} \begin{bmatrix} \mathrm{C}_{24} \\ 1-\mathrm{C}_{22} \end{bmatrix} \tag{2.34}$$

while the fixed points of equation of the system (2.33) are

$$\begin{bmatrix} x_e \\ v_e \end{bmatrix} = \frac{Kw\tau_2 h_0^{3/4}}{m_x\left[1+\det(\hat{C})-\mathrm{tr}(\hat{C})\right]}\begin{bmatrix} C_{13} \\ 1-C_{11} \end{bmatrix}$$
$$\begin{bmatrix} u_e \\ w_e \end{bmatrix} = \frac{Kw\tau_2 h_0^{3/4}}{m_u\left[1+\det(\overset{*}{C})-\mathrm{tr}(\overset{*}{C})\right]}\begin{bmatrix} C_{24} \\ 1-C_{22} \end{bmatrix} \tag{2.35}$$

The linearized Jacobian matrix of equations (2.32) and (2.33) can be formed as

$$D=\begin{bmatrix} C_{11} & 0 & C_{13} & 0 \\ 0 & C_{22} & 0 & C_{24} \\ C_{31}+\hat{w}_x(1-C_{11}) & \hat{w}_x(1-C_{22}) & C_{33}-\hat{w}_x C_{13} & -\hat{w}_x C_{24} \\ \hat{w}_u(1-C_{11}) & C_{42}+\hat{w}_u(1-C_{22}) & -\hat{w}_u C_{13} & C_{44}-\hat{w}_u C_{24} \end{bmatrix} \tag{2.36}$$

where the dimensionless chip widths for the linear cutting force are

$$\hat{w}_x = \frac{K_t w\tau_2}{m_x}$$

$$\hat{w}_u = \frac{K_t w\tau_2}{m_u} \tag{2.37}$$

and the dimensionless chip widths for the 3/4 rule cutting force are

$$\hat{w}_x = \frac{3}{4}\frac{Kw\tau_2}{m_x h_0^{1/4}}$$

$$\hat{w}_u = \frac{3}{4}\frac{Kw\tau_2}{m_u h_0^{1/4}} \tag{2.38}$$

An important parameter that will appear during the stability analysis is

$$\hat{m} = m_x / m_u \tag{2.39}$$

which equates

$$\hat{w}_u = \hat{m}\hat{w}_x \tag{2.40}$$

for both cases.

From (2.20),

$$\hat{\mathrm{D}} = \mathrm{B} = \begin{bmatrix} \mathrm{A}_{11} & \mathrm{A}_{12} \\ \mathrm{A}_{21} + \hat{w}_x(1-\mathrm{A}_{11}) & \mathrm{A}_{22} - \hat{w}_x\mathrm{A}_{12} \end{bmatrix} = \begin{bmatrix} \mathrm{C}_{11} & \mathrm{C}_{13} \\ \mathrm{C}_{31} + \hat{w}_x(1-\mathrm{C}_{11}) & \mathrm{C}_{33} - \hat{w}_x\mathrm{C}_{13} \end{bmatrix}$$

and

$$\overset{*}{\mathrm{D}} = \begin{bmatrix} \mathrm{C}_{22} & \mathrm{C}_{24} \\ \mathrm{C}_{42} + \hat{w}_u(1-\mathrm{C}_{22}) & \mathrm{C}_{44} - \hat{w}_u\mathrm{C}_{24} \end{bmatrix} \tag{2.41}$$

With the linearization around the fixed points, the generalized local dynamics for the two degree-of-freedom system is described by

$$\begin{bmatrix} q_x(t_{j+1}) \\ q_u(t_{j+1}) \\ \dot{q}_x(t_{j+1}) \\ \dot{q}_u(t_{j+1}) \end{bmatrix} = \begin{bmatrix} x_e \\ u_e \\ v_e \\ w_e \end{bmatrix} + \mathrm{D} \begin{bmatrix} q_x(t_j) \\ q_u(t_j) \\ q_x(t_j) \\ \dot{q}_u(t_j) \end{bmatrix} \tag{2.42}$$

where x_e, u_e, v_e, w_e, $\hat{w}_x$, and $\hat{w}_u$ are based on the respective cutting force models.

Chapter 3

Analytical Stability Predictions

3.1 Introduction

The stability of the one or two degree-of-freedom system is determined by the respective system's Jacobian matrix given by B (2.20) or D (2.36). If the eigenvalues lie outside the unit circle of the complex plane meaning that the magnitude of each eigenvalue is greater than one, the amplitude of a perturbation about the system's fixed point will grow without bound on further iterations of the system map; in this scenario, the system is unstable. Conversely, if the eigenvalues lie within the unit circle of the complex plane, all subsequent perturbations about the fixed point of the system map will decay to zero; in this scenario, the system is stable, (e.g., Nayfeh and Balachandran, 1995). To determine the stability of the system, one must look at the conditions when one or more eigenvalues leave the unit circle.

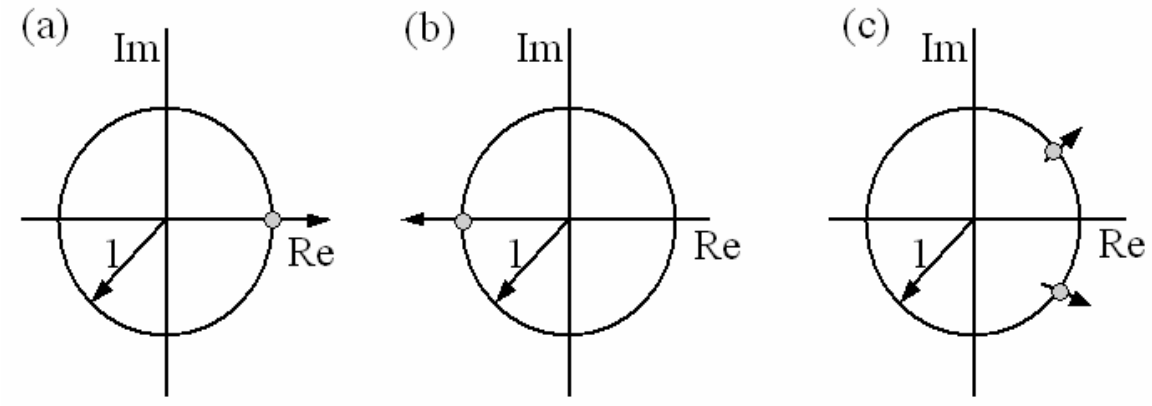

Figure 3.1: Bifurcation types - (a) cyclic fold bifurcation, (b) flip bifurcation, and (c) Neimark-Sacker bifurcation.

According to stability analysis (e.g. Nayfeh and Balachandran, 1995), there are three conditions under which the system can become unstable:

i) a real-valued eigenvalue traveling left to right through +1, which is a necessary condition for a cyclic fold bifurcation (see Figure 3.1 (a))

ii) a real-valued eigenvalue traveling right to left through -1, which is a necessary condition for a flip or period doubling bifurcation (see Figure 3.1 (b))

iii) a pair of complex-conjugate eigenvalues leaving the unit circle through the complex boundary of this circle, which is a necessary condition for a Neimark-Sacker or secondary Hopf bifurcation (see Figure 3.1 (c))

For both the one and two degree-of-freedom systems, all three possibilities are examined.

3.2 Characteristic Equation for the Single DOF System

The eigenvalues λ of the single degree-of-freedom map (2.23) are calculated from the characteristic equation of the Jacobian matrix B given by (2.20), leading to

$$\lambda^2 - \mathrm{tr}(B)\lambda + \det(B) = 0 \tag{3.1}$$

where tr(B) is the trace of B and det(B) is the determinant of B. Following some algebraic manipulations, one can obtain

$$\begin{aligned} \mathrm{tr}(B) &= \mathrm{tr}(A) - \hat{w}_x A_{12} \\ \det(B) &= \det(A) - \hat{w}_x A_{12} \end{aligned} \tag{3.2}$$

Without further analysis, immediate conclusions can be drawn by using (3.2); for values of parameters in which $A_{12} = 0$, the characteristic equation reduces to that of a simple, damped harmonic oscillating tool described by matrix A (2.11); thus, the system is stable

(Davies *et al*., 2002). Since this is a limited special case, the other cases are now examined.

3.3 Case 1: λ = +1 for the Single DOF System

Setting $\lambda = 1$ in the characteristic equation (3.1) produces

$$1 - \mathrm{tr(A)} + \det(\mathrm{A}) = 0 \tag{3.3}$$

This equation is independent of the axial depth of cut or chip width and therefore cannot be a route to instability, when the chip width is used as a bifurcation control parameter.

3.4 Case 2: λ = -1 for the Single DOF System

Setting $\lambda = -1$ in the characteristic equation (3.1), the critical dimensionless chip width, which is the chosen control parameter, is determined as

$$\hat{w}_{xcr}^{f} = \frac{\det(\mathrm{A}) + \mathrm{tr(A)} + 1}{2\mathrm{A}_{12}} = \omega_{xd}\left(\frac{\cosh(\zeta_x \omega_x \tau) + \cos(\omega_{xd}\tau)}{\sin(\omega_{xd}\tau)}\right) \tag{3.4}$$

A map experiencing a flip bifurcation at its critical point results in the creation or destruction of two branches of period-two points (e.g. Nayfeh and Balachandran, 1995). An iteration of a map initiated at either of the period-two points flips back and forth between those points if x_{20} and x_{30} are period-two critical bifurcation points of map $M(x)$; that is,

$$M(x_{20}) = x_{30} \text{ and } \mathrm{M}(x_{30}) = x_{20} \tag{3.5}$$

Thus, the stability lobes formed from $\hat{w}_{xcr}^{f}$ in (3.4) correspond to flip bifurcation points.

3.5 Case 3: $\lambda\bar{\lambda}$ = 1 for the Single DOF System

Setting $\lambda\bar{\lambda} = 1$, where $\bar{\lambda}$ is the complex conjugate of λ, one arrives at the general form $\lambda = e^{i\phi}$ and $\bar{\lambda} = e^{-i\phi}$ for Case 3, where ϕ is an angle that needs to be solved. For Case 3, the general form of the characteristic equation is derived to be

$$\lambda^2 - (2\cos\phi)\lambda + 1 = 0 \tag{3.6}$$

Equating like radicals, the radicals of λ^1 from (3.1) and (3.6) are used to solve for

$$\phi = \cos^{-1}\frac{\mathrm{tr(B)}}{2} \tag{3.7}$$

By using the radicals of λ^0 from equations (3.1) and (3.6), the following condition for Neimark-Sacker bifurcations is obtained:

$$\det(\mathrm{B}) = 1 \tag{3.8}$$

Applying this condition, the critical dimensionless chip width for this case is determined as

$$\hat{w}_{xcr}^{ns} = \frac{\det(\mathrm{A}) - 1}{\mathrm{A}_{12}} = -2\omega_{xd}\frac{\sinh(\omega_x\zeta_x\tau)}{\sin(\omega_{xd}\tau)} \tag{3.9}$$

Branches of stable periodic solutions at a critical point that exist prior to the Neimark-Sacker bifurcation split as a pair of unstable branches after the bifurcation (e.g. Nayfeh and Balachandran, 1995). The stability lobes formed through $\hat{w}_{xcr}^{ns}$ in (3.9) predict the occurrence of Neimark-Sacker bifurcations along its boundary. As Davies *et al*. (2002) point out, the Neimark-Sacker bifurcation produces unstable, self-excited vibrations with frequencies that are not proportional to corresponding spindle rotation frequencies. This type of bifurcation also appears in continuous turning and gives rise to chatter frequency.

3.6 Characteristic Equation for the Two DOF System

The eigenvalues λ of the two degree-of-freedom map (2.42) are calculated from the characteristic equation of the Jacobian matrix D in equation (2.36), leading to

$$\begin{aligned}&\lambda^4 - \mathrm{tr(D)}\lambda^3 + [\det(\hat{\mathrm{D}}) + \det(\overset{*}{\mathrm{D}}) + \mathrm{tr}(\hat{\mathrm{D}})\mathrm{tr}(\overset{*}{\mathrm{D}}) - \hat{m}\hat{w}_x{}^2\mathrm{C}_{13}\mathrm{C}_{24}]\lambda^2 \\ &- [\mathrm{tr}(\hat{\mathrm{D}})\det(\overset{*}{\mathrm{D}}) + \mathrm{tr}(\overset{*}{\mathrm{D}})\det(\hat{\mathrm{D}}) - 2\hat{m}\hat{w}_x{}^2\mathrm{C}_{13}\mathrm{C}_{24}]\lambda + \det(\mathrm{D}) = 0\end{aligned} \tag{3.10}$$

In this regard, useful algebraic relationships include the following:

$$\begin{aligned}&\mathrm{tr(D)} = \mathrm{tr(C)} - \mathrm{C}_{13}\hat{w}_x - \mathrm{C}_{24}\hat{m}\hat{w}_x \\ &\det(\hat{\mathrm{D}}) = \det(\hat{\mathrm{C}}) - \mathrm{C}_{13}\hat{w}_x \\ &\det(\overset{*}{\mathrm{D}}) = \det(\overset{*}{\mathrm{C}}) - \mathrm{C}_{24}\hat{m}\hat{w}_x \\ &\mathrm{tr}(\hat{\mathrm{D}})\mathrm{tr}(\overset{*}{\mathrm{D}}) = \mathrm{tr}(\hat{\mathrm{C}})\mathrm{tr}(\overset{*}{\mathrm{C}}) - \mathrm{tr}(\overset{*}{\mathrm{C}})\mathrm{C}_{13}\hat{w}_x - \mathrm{tr}(\hat{\mathrm{C}})\mathrm{C}_{24}\hat{m}\hat{w}_x + \hat{m}\hat{w}_x{}^2\mathrm{C}_{13}\mathrm{C}_{24} \\ &\mathrm{tr}(\hat{\mathrm{D}})\det(\overset{*}{\mathrm{D}}) = \mathrm{tr}(\hat{\mathrm{C}})\det(\overset{*}{\mathrm{C}}) - \det(\overset{*}{\mathrm{C}})\mathrm{C}_{13}\hat{w}_x - \mathrm{tr}(\hat{\mathrm{C}})\mathrm{C}_{24}\hat{m}\hat{w}_x + \hat{m}\hat{w}_x{}^2\mathrm{C}_{13}\mathrm{C}_{24} \\ &\mathrm{tr}(\overset{*}{\mathrm{D}})\det(\hat{\mathrm{D}}) = \mathrm{tr}(\overset{*}{\mathrm{C}})\det(\hat{\mathrm{C}}) - \mathrm{tr}(\overset{*}{\mathrm{C}})\mathrm{C}_{13}\hat{w}_x - \det(\hat{\mathrm{C}})\mathrm{C}_{24}\hat{m}\hat{w}_x + \hat{m}\hat{w}_x{}^2\mathrm{C}_{13}\mathrm{C}_{24} \\ &\det(\mathrm{D}) = \det(\mathrm{C}) - \det(\overset{*}{\mathrm{C}})\mathrm{C}_{13}\hat{w}_x - \det(\hat{\mathrm{C}})\mathrm{C}_{24}\hat{m}\hat{w}_x\end{aligned} \tag{3.11}$$

As in the one degree-of-freedom case, one can immediately conclude by using (3.11) that for values of parameters in which $\mathrm{C}_{13} = \mathrm{C}_{24} = 0$, the characteristic equation reduces to that of a simple, damped harmonic oscillating tool and workpiece described by matrix C (2.26); thus, the system is stable. Again, since this is a limited special case, the other cases are examined for the two degree-of-freedom system.

3.7 Case 1: λ = +1 for the Two DOF System

Setting $\lambda = 1$ for the characteristic equation in (3.10) and by using the relationships defined in (3.11) leads to

$$1 - \mathrm{tr}(\mathrm{C}) + \det(\hat{\mathrm{C}}) + \det(\overset{*}{\mathrm{C}}) + \mathrm{tr}(\hat{\mathrm{C}})\mathrm{tr}(\overset{*}{\mathrm{C}}) - \mathrm{tr}(\hat{\mathrm{C}})\det(\overset{*}{\mathrm{C}}) - \mathrm{tr}(\overset{*}{\mathrm{C}})\det(\hat{\mathrm{C}}) + \det(\mathrm{C}) = 0 \quad (3.12)$$

Like in the one degree-of-freedom case, this equation is independent to the axial depth of cut or chip width, and therefore this scenario cannot be a route to instability.

3.8 Case 2: λ = -1 for the Two DOF System

Setting $\lambda = -1$ for the characteristic equation (3.10) and using the relationships defined in (3.11), the critical dimensionless flip bifurcation chip width becomes

$$\hat{w}_{xcr}^{f} = \frac{1}{2}\frac{1 + \mathrm{tr}(\mathrm{C}) + \det(\mathrm{C}) + \mathrm{tr}(\hat{\mathrm{C}})\mathrm{tr}(\overset{*}{\mathrm{C}}) + \mathrm{tr}(\hat{\mathrm{C}})\det(\overset{*}{\mathrm{C}}) + \mathrm{tr}(\overset{*}{\mathrm{C}})\det(\hat{\mathrm{C}}) + \det(\hat{\mathrm{C}}) + \det(\overset{*}{\mathrm{C}})}{[1 + \mathrm{tr}(\overset{*}{\mathrm{C}}) + \det(\overset{*}{\mathrm{C}})]\mathrm{C}_{13} + [1 + \mathrm{tr}(\hat{\mathrm{C}}) + \det(\hat{\mathrm{C}})]\hat{m}\mathrm{C}_{24}} \quad (3.13)$$

$$= \frac{1}{2}\frac{1 + e^{-2\zeta_x\omega_x\tau}(\hat{c}_x^{\,2} + \omega_x^{\,2}\hat{s}_x^{\,2}) + e^{-2\zeta_u\omega_u\tau}(\hat{c}_u^{\,2} + \omega_u^{\,2}\hat{s}_u^{\,2}) + 2e^{-\zeta_x\omega_x\tau}\hat{c}_x + 2e^{-\zeta_u\omega_u\tau}\hat{c}_u}{[1 + 2e^{-\zeta_u\omega_u\tau}\hat{c}_u + e^{-2\zeta_u\omega_u\tau}(\hat{c}_u^{\,2} + \omega_u^{\,2}\hat{s}_u^{\,2})]\frac{e^{-\zeta_x\omega_x\tau}}{\omega_{xd}}\hat{s}_x + [1 + 2e^{-\zeta_x\omega_x\tau}\hat{c}_x + e^{-2\zeta_x\omega_x\tau}(\hat{c}_x^{\,2} + \omega_x^{\,2}\hat{s}_x^{\,2})]\frac{\hat{m}e^{-\zeta_u\omega_u\tau}}{\omega_{ud}}\hat{s}_u}$$

$$+ \frac{1}{2}\frac{e^{-2(\zeta_x\omega_x + \zeta_u\omega_u)\tau}(\hat{c}_x^{\,2} + \omega_x^{\,2}\hat{s}_x^{\,2})(\hat{c}_u^{\,2} + \omega_u^{\,2}\hat{s}_u^{\,2}) + 4e^{-(\zeta_x\omega_x + \zeta_u\omega_u)\tau}\hat{c}_x\hat{c}_u}{[1 + 2e^{-\zeta_u\omega_u\tau}\hat{c}_u + e^{-2\zeta_u\omega_u\tau}(\hat{c}_u^{\,2} + \omega_u^{\,2}\hat{s}_u^{\,2})]\frac{e^{-\zeta_x\omega_x\tau}}{\omega_{xd}}\hat{s}_x + [1 + 2e^{-\zeta_x\omega_x\tau}\hat{c}_x + e^{-2\zeta_x\omega_x\tau}(\hat{c}_x^{\,2} + \omega_x^{\,2}\hat{s}_x^{\,2})]\frac{\hat{m}e^{-\zeta_u\omega_u\tau}}{\omega_{ud}}\hat{s}_u}$$

$$+ \frac{1}{2}\frac{2e^{-(\zeta_x\omega_x + 2\zeta_u\omega_u)\tau}\hat{c}_x(\hat{c}_u^{\,2} + \omega_u^{\,2}\hat{s}_u^{\,2}) + 2e^{-(2\zeta_x\omega_x + \zeta_u\omega_u)\tau}\hat{c}_u(\hat{c}_x^{\,2} + \omega_x^{\,2}\hat{s}_x^{\,2})}{[1 + 2e^{-\zeta_u\omega_u\tau}\hat{c}_u + e^{-2\zeta_u\omega_u\tau}(\hat{c}_u^{\,2} + \omega_u^{\,2}\hat{s}_u^{\,2})]\frac{e^{-\zeta_x\omega_x\tau}}{\omega_{xd}}\hat{s}_x + [1 + 2e^{-\zeta_x\omega_x\tau}\hat{c}_x + e^{-2\zeta_x\omega_x\tau}(\hat{c}_x^{\,2} + \omega_x^{\,2}\hat{s}_x^{\,2})]\frac{\hat{m}e^{-\zeta_u\omega_u\tau}}{\omega_{ud}}\hat{s}_u}$$

where $\hat{c}_x = \cos(\omega_{xd}\tau)$, $\hat{s}_x = \sin(\omega_{xd}\tau)$, $\hat{c}_u = \cos(\omega_{ud}\tau)$, and $\hat{s}_u = \sin(\omega_{ud}\tau)$. As in the one degree-of-freedom case, the stability lobes formed from $\hat{w}_{xcr}^{f}$ in (3.13) correspond to the flip bifurcation points.

3.9 Case 3: $\lambda\overline{\lambda}$ = 1 for the Two DOF System

Just like in the one degree-of-freedom system analysis, one can use $\lambda_1 = e^{i\phi}$ and $\overline{\lambda_1} = e^{-i\phi}$ as the general form for the Neimark-Sacker bifurcation case. In order for the map in (2.42) to experience a Neimark-Sacker bifurcation, not only do two complex conjugate eigenvalues have to leave the unit circle away from the real axis such that $\lambda_1\overline{\lambda_1}$ = 1, but the other two eigenvalues must be complex conjugates within the unit circle. The general solution of the second pair of eigenvalues is assumed to be $\lambda_2 = a + bi$ and $\overline{\lambda_2} = a - bi$ where *a* and *b* are real values. By using all four general forms of the eigenvalues, the characteristic equation in (3.10) becomes

$$\begin{aligned}&\lambda^4 - 2(a+\cos\phi)\lambda^3 + (a^2+b^2+4a\cos\phi+1)\lambda^2 \\ &-2[(a^2+b^2)\cos\phi + a]\lambda + a^2 + b^2 = 0\end{aligned} \tag{3.14}$$

Equating the radicals of λ^0 from (3.10) and (3.14), the following condition for Neimark-Sacker bifurcations is obtained

$$\det(\mathrm{D}) = a^2 + b^2 \tag{3.15}$$

Even when equating the rest of the radicals from (3.10) and (3.14), unlike the one degree-of-freedom case, there is no explicit form for the critical dimensionless Neimark-Sacker bifurcation chip width. Therefore, numerical means need to be used to predict the occurrence of Neimark-Sacker bifurcations along the stability lobe boundaries. A computational code for these solutions can be found in Section B.2 of Appendix B.

3.10 Analytical Stability Lobe Predictions

In order to compare the stability lobe boundaries with that of the numerical and experimental data, the dimensionless chip widths for both the linear cutting force model

and 3/4 rule cutting force model must be converted into chip widths that have dimensions. By using equations (2.21) and (2.22) from the one degree-of-freedom map, recalling from equation (2.4) that $K = K_t h_0^{1/4}$ for the 3/4 rule cutting force model, and remembering that $\tau_2 = \rho\tau$, where $\tau = 2\pi / N\Omega$, the following generalized stability prediction equations are derived in terms of their corresponding dimensionless chip widths for the linear cutting force model

$$w_{cr} = \frac{N\Omega m_x}{2\pi K_t \rho} \hat{w}_{xcr} \tag{3.16}$$

and for the 3/4 rule cutting force model

$$w_{cr} = \frac{4}{3} \frac{N\Omega m_x}{2\pi K_t \rho} \hat{w}_{xcr} \tag{3.17}$$

By using equations (2.37), (2.38), (2.39), and (2.40) for the two degree-of-freedom maps, one arrives at the exact same generalized stability prediction equations of (3.16) and (3.17). It is noted that through linearization, the linear cutting force model and the 3/4 rule cutting force model differ only by a factor of 4/3.

Chapter 4

Numerical Stability Predictions

The conditions detailed in Chapter 3 are necessary for bifurcations to occur, and additional analysis is needed to verify the occurrence of a bifurcation. In Szalai *et al*. (2004), asymptotic analysis is used to determine the criticality of each bifurcation for the single degree-of-freedom system. In this section, the analytical stability predictions are numerically verified by time integration of the delay differential equations.

4.1 Numerical Verification of the Analytical Predictions

To numerically solve the equations of motion given by (2.1) for the single degree-of-freedom case and (2.5) for the two degree-of-freedom case, the respective equations of motion are placed in state space form with their corresponding cutting force models. First, one defines

$$\begin{bmatrix} q_1(t) \\ q_2(t) \\ q_3(t) \\ q_4(t) \end{bmatrix} = \begin{bmatrix} q_x(t) \\ q_u(t) \\ \dot{q}_x(t) \\ \dot{q}_u(t) \end{bmatrix} \tag{4.1}$$

The single degree-of-freedom linear cutting force model is then derived to be

$$\begin{aligned} \dot{q}_1(t) &= q_2(t) \\ \dot{q}_2(t) &= -\frac{k_x}{m_x} q_1(t) - \frac{c_x}{m_x} q_2(t) + g(t) \frac{K_t w}{m_x} [q_1(t-\tau) - q_1(t) + f\tau] \end{aligned} \tag{4.2}$$

and the single degree-of-freedom 3/4 rule cutting force model is derived to be

$$\begin{aligned}\dot{q}_1(t) &= q_2(t)\\ \dot{q}_2(t) &= -\frac{k_x}{m_x}q_1(t) - \frac{c_x}{m_x}q_2(t) + g(t)\frac{K_t w(f\tau)^{1/4}}{m_x}[q_1(t-\tau) - q_1(t) + f\tau]^{3/4}\end{aligned} \tag{4.3}$$

while the two degree-of-freedom linear cutting force model is derived to be

$$\begin{aligned}\dot{q}_1(t) &= q_3(t)\\ \dot{q}_2(t) &= q_4(t)\\ \dot{q}_3(t) &= -\frac{k_x}{m_x}q_1(t) - \frac{c_x}{m_x}q_3(t) + g(t)\frac{K_t w}{m_x}[q_1(t-\tau) + q_2(t-\tau) - q_1(t) - q_2(t) + f\tau]\\ \dot{q}_4(t) &= -\frac{k_u}{m_u}q_2(t) - \frac{c_u}{m_u}q_4(t) + g(t)\frac{K_t w}{m_u}[q_1(t-\tau) + q_2(t-\tau) - q_1(t) - q_2(t) + f\tau]\end{aligned} \tag{4.4}$$

and the two degree-of-freedom 3/4 rule cutting force model is derived to be

$$\begin{aligned}\dot{q}_1(t) &= q_3(t)\\ \dot{q}_2(t) &= q_4(t)\\ \dot{q}_3(t) &= -\frac{k_x}{m_x}q_1(t) - \frac{c_x}{m_x}q_3(t) + g(t)\frac{K_t w(f\tau)^{1/4}}{m_x}[q_1(t-\tau) + q_2(t-\tau) - q_1(t) - q_2(t) + f\tau]^{3/4}\\ \dot{q}_4(t) &= -\frac{k_u}{m_u}q_2(t) - \frac{c_u}{m_u}q_4(t) + g(t)\frac{K_t w(f\tau)^{1/4}}{m_u}[q_1(t-\tau) + q_2(t-\tau) - q_1(t) - q_2(t) + f\tau]^{3/4}\end{aligned} \tag{4.5}$$

Recalling that the cutting force is only active (*g(t)* = 1) during the cutting period τ_2 and that $\tau_2 = \rho\tau$, the non-cutting period τ_1 can be found as $(1-\rho)\tau$. With the cutting and non-cutting periods defined, each state of each equation of motion is solved, respectively, by using a user defined axial depth of cut and spindle speed, and is then summed up to equal the total spindle period τ. Matlab's *dde23* solver is used to resolve each linear, homogeneous equation during τ_1 as well as each non-linear, non-homogeneous delay differential equation during τ_2. The solutions are then summed up to form the complete solution for τ. Initial conditions are carried from the solution at the end of the current

spindle period and entered into the next period for calculation. This process is iterated for a user designated number of spindle cycles. The solution generated across the chosen number of cycles is displayed in graphical form in terms of a response history and a phase portrait diagram. In Figure 4.1, an example of the response of a single degree-of-freedom system is shown for stable cutting conditions.

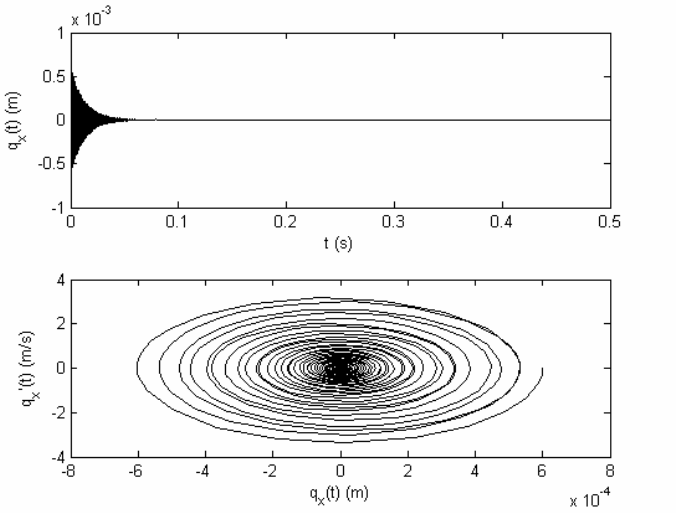

Figure 4.1: Response and phase portrait diagrams for stable cutting conditions.

In Figure 4.2, an example of the response of the same system is shown at the stability boundary.

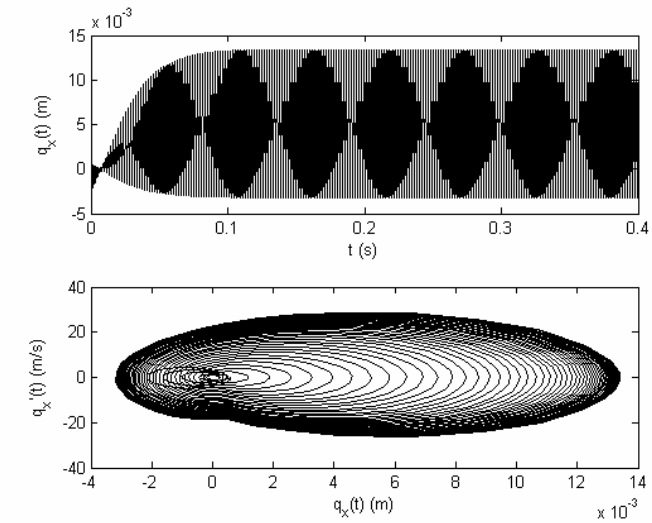

Figure 4.2: Response and phase portrait diagrams at stability boundary.

In Figure 4.3, an example of the system response is shown for unstable cutting conditions.

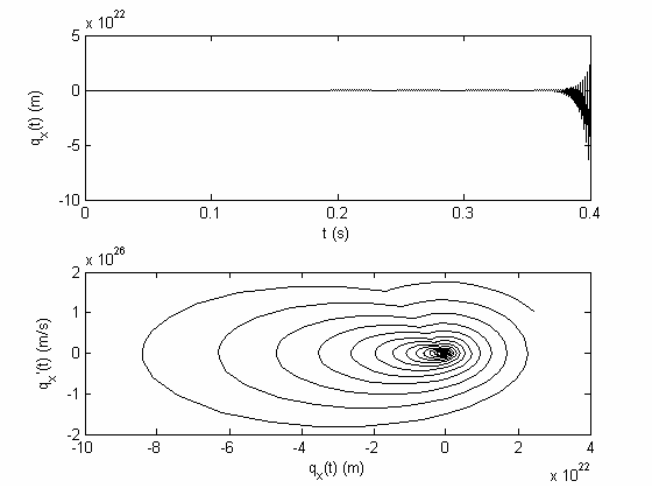

Figure 4.3: Response and phase portrait diagrams for unstable cutting conditions.

The Matlab code used to find the numerical solutions of equations (4.2) to (4.5) can be found in Appendix C.

4.2 UMCP Numerical Stability Prediction Program

The following figure depicts a four degree-of-freedom milling configuration.

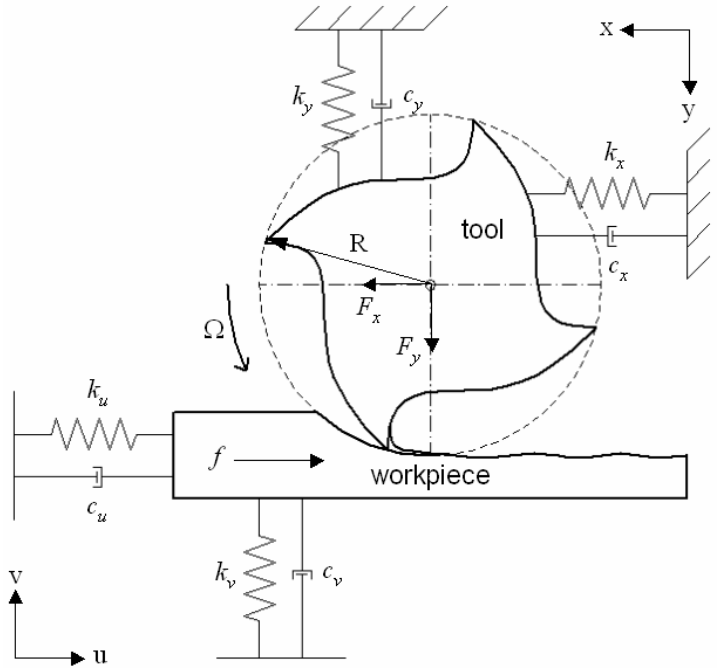

Figure 4.4: Schematic of a four DOF milling configuration.

The governing equations of this system are given by

$$\begin{aligned} m_x\ddot{q}_x(t)+c_x\dot{q}_x(t)+k_xq_x(t)&=F_x\left(t;\tau(t,i,z)\right)\\ m_y\ddot{q}_y(t)+c_y\dot{q}_y(t)+k_yq_y(t)&=F_y\left(t;\tau(t,i,z)\right)\\ m_u\ddot{q}_u(t)+c_u\dot{q}_u(t)+k_uq_u(t)&=F_u\left(t;\tau(t,i,z)\right)\\ m_v\ddot{q}_v(t)+c_v\dot{q}_v(t)+k_vq_v(t)&=F_v\left(t;\tau(t,i,z)\right) \end{aligned} \tag{4.6}$$

The equations of motion for the tool include, respectively, the horizontal and vertical displacements $q_x(t)$ and $q_y(t)$, the constant stiffnesses k_x and k_y, and the constant damping terms c_x and c_y. The equations of motion for the workpiece include, respectively, the horizontal and vertical displacements $q_u(t)$ and $q_v(t)$, the constant stiffnesses k_u and k_v, and the constant damping terms c_u and c_v. The constant feed rate f of the workpiece is directed along the major horizontal mode of motion on the workpiece $q_u(t)$.

Based on previous work carried out by Zhao (2000) and Long (2006), the cutter is modeled as a stack of infinitesimal disk elements. A summary of the derivation of the cutting forces is provided here. The detailed derivation of the cutting forces can be found in Chapter 2 of Long (2006).

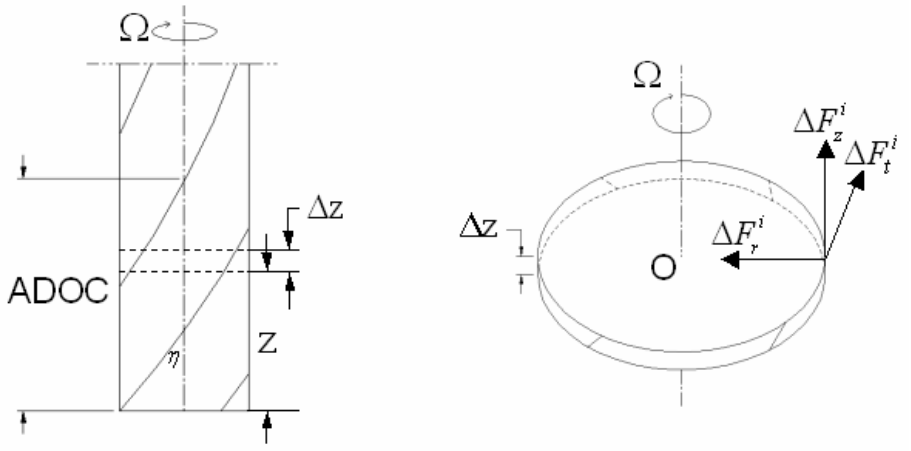

Figure 4.5: Cylindrical end mill with infinitesimal disk elements.

In Figure 4.5, each disk element is located at an axial distance z along the tool from the bottom of the end mill up to the axial depth of cut. The helix angle is η. For the *i*th tooth, the infinitesimal cutting-force components on the disk element are represented by ΔF_r^i for the radial direction, ΔF_t^i for the tangential direction, and ΔF_z^i for the axial direction. The cutting forces along each component of the infinitesimal disk element are found from the dynamic uncut chip thickness for the *i*th flute of the cutter at time *t* and height *z* as

$$h(t,i,z) = A(t,i,z)\sin\theta(t,i,z) + B(t,i,z)\cos\theta(t,i,z) + h_{sv} \tag{4.7}$$

where the static uncut chip thickness is

$$h_{sv} = \tau f \sin\theta + \frac{1}{2R}(\tau f \cos\theta)^2 \tag{4.8}$$

The relative displacements are found to be

$$\begin{aligned} A(t,i,z) &= q_x(t) - q_x(t-\tau(t,i,z)) + q_u(t) - q_u(t-\tau(t,i,z)) \\ B(t,i,z) &= q_y(t) - q_y(t-\tau(t,i,z)) + q_v(t) - q_v(t-\tau(t,i,z)) \end{aligned} \tag{4.9}$$

The cutting forces are then found to be

$$\begin{bmatrix} \Delta F_r^i \\ \Delta F_t^i \\ \Delta F_z^i \end{bmatrix} = \begin{bmatrix} 1 & 0 & 0 \\ 0 & \cos\eta & \sin\eta \\ 0 & -\sin\eta & \cos\eta \end{bmatrix} \begin{bmatrix} k_t \\ k_n k_t \\ \mu k_t(\cos\phi_n - k_n\cos\phi_n) \end{bmatrix} h(t,i,z)\frac{\Delta z}{\cos\eta} \tag{4.10}$$

Transforming the cutting forces into cartesian coordinates, integrating the infinitesimal cutting force components from $z_1(t,i)$ to $z_2(t,i)$ at the cutting zone, which is defined to be $\theta_s' < \theta(i,t,z) < \theta_e'$, and ignoring forces along the *z* direction, the cutting forces are found as

$$\begin{bmatrix} F_x^i(t) \\ F_y^i(t) \end{bmatrix} = \int_{z_1(t,i)}^{z_2(t,i)} \begin{bmatrix} \hat{k}_{11}^i(t,z) & \hat{k}_{12}^i(t,z) \\ \hat{k}_{21}^i(t,z) & \hat{k}_{22}^i(t,z) \end{bmatrix} \begin{bmatrix} A(t,i,z) \\ B(t,i,z) \end{bmatrix} dz + \int_{z_1(t,i)}^{z_2(t,i)} \begin{bmatrix} \hat{c}_1^i(t,z) \\ \hat{c}_2^i(t,z) \end{bmatrix} \left[\tau f \sin\theta(t,i,z) + \frac{1}{2R} \left(\tau f \cos\theta(t,i,z) \right)^2 \right] dz \tag{4.11}$$

where

$$\begin{bmatrix} \hat{k}_{11}^i(t,z) & \hat{k}_{12}^i(t,z) \\ \hat{k}_{21}^i(t,z) & \hat{k}_{22}^i(t,z) \end{bmatrix} = \begin{bmatrix} -\sin\theta(t,i,z) & -\cos\theta(t,i,z) \\ -\cos\theta(t,i,z) & \sin\theta(t,i,z) \end{bmatrix} \begin{bmatrix} k_1 k_t \\ k_2 k_t \end{bmatrix} [-\sin\theta(t,i,z) \quad \cos\theta(t,i,z)] \tag{4.12}$$

$$\begin{bmatrix} \hat{c}_1^i(t,z) \\ \hat{c}_2^i(t,z) \end{bmatrix} = \begin{bmatrix} -\sin\theta(t,i,z) & -\cos\theta(t,i,z) \\ -\cos\theta(t,i,z) & \sin\theta(t,i,z) \end{bmatrix} \begin{bmatrix} k_1 k_t \\ k_2 k_t \end{bmatrix} \tag{4.13}$$

$$\begin{aligned} k_1 &= \frac{k_n}{\cos\eta} \\ k_2 &= 1 + \tan\eta[\mu(\cos\phi_n - k_n \sin\phi_n)] \end{aligned} \tag{4.14}$$

and k_t is the specific cutting energy, ϕ_n is the normal rake angle, k_n is a proportionality constant, and μ is the friction coefficient. From Newton's Third Law of Motion, the forces acting on the workpiece are determined as

$$\begin{bmatrix} F_u\left(t;\tau(t,i,z)\right) \\ F_v\left(t;\tau(t,i,z)\right) \end{bmatrix} = \begin{bmatrix} F_x\left(t;\tau(t,i,z)\right) \\ F_y\left(t;\tau(t,i,z)\right) \end{bmatrix} \tag{4.15}$$

When the tool is outside of the cutting zone, there is loss of contact, which makes the cutting force components equal to zero. The determination of the cutting and non-cutting zones can be found in Chapter 3 of Zhao (2000). The derived state space equations from (4.6), by using the cutting forces described in (4.11), can be found in Chapter 2 of Long (2006). Stability analysis carried out by using the semi-discretization method is detailed in Chapter 3 of Long (2006). A copy of the UMCP numerical stability prediction program is given in Section D.1 of Appendix D.

4.3 Modified UMCP Numerical Stability Prediction Program for the 3/4 Rule

The dynamic uncut chip thickness given by equation (4.7) is based on a linear cutting force model. Applying the 3/4 rule to this expression yields

$$h^{3/4}(t,i,z) = [A(t,i,z)\sin\theta(t,i,z) + B(t,i,z)\cos\theta(t,i,z) + h_{sv}]^{3/4} \tag{4.16}$$

To incorporate this change into the UMCP numerical stability prediction program, the Taylor expansion is taken; that is,

$$\begin{aligned} h^{3/4}(t,i,z) &= [h_{sv} + \Delta h(t,i,z)]^{3/4} \\ &\approx h_{sv}^{3/4} + \frac{3}{4}\frac{\Delta h(t,i,z)}{h_{sv}^{1/4}} - \frac{3}{32}\frac{[\Delta h(t,i,z)]^2}{h_{sv}^{5/4}} + \frac{5}{128}\frac{[\Delta h(t,i,z)]^3}{h_{sv}^{9/4}} - \ldots \end{aligned} \tag{4.17}$$

where

$$\Delta h(t,i,z) = A(t,i,z)\sin\theta(t,i,z) + B(t,i,z)\cos\theta(t,i,z) \tag{4.18}$$

h_{sv} is previously defined in (4.8) and $A(t,i,z)$ along with $B(t,i,z)$ are previously defined in (4.9).

The linearized form of equation (4.17) becomes

$$h^{3/4}(t,i,z) \approx \frac{3}{4}\frac{A(t,i,z)\sin\theta(t,i,z) + B(t,i,z)\cos\theta(t,i,z)}{h_{sv}^{1/4}} + h_{sv}^{3/4} \tag{4.19}$$

Making use of equations (4.19) and (4.11), the cutting forces are found to be

$$\begin{aligned} \begin{bmatrix} F_x^i(t) \\ F_y^i(t) \end{bmatrix} = & \\ & \int_{z_1(t,i)}^{z_2(t,i)} \begin{bmatrix} \hat{k}_{11}^i(t,z) & \hat{k}_{12}^i(t,z) \\ \hat{k}_{21}^i(t,z) & \hat{k}_{22}^i(t,z) \end{bmatrix} \begin{bmatrix} A(t,i,z) \\ B(t,i,z) \end{bmatrix} \left\{ \frac{3}{4}[\tau f \sin\theta(t,i,z) + \frac{1}{2R}\left(\tau f \cos\theta(t,i,z)\right)^2]^{-1/4} \right\} dz \\ & + \int_{z_1(t,i)}^{z_2(t,i)} \begin{bmatrix} \hat{c}_1^i(t,z) \\ \hat{c}_2^i(t,z) \end{bmatrix} \left\{ [\tau f \sin\theta(t,i,z) + \frac{1}{2R}\left(\tau f \cos\theta(t,i,z)\right)^2]^{3/4} \right\} dz \end{aligned} \tag{4.20}$$

A copy of the modified UMCP numerical stability prediction program is given in Section D.2 of Appendix D.

Chapter 5

Results and Discussion

5.1 Single DOF System Results and Discussion

For the analytical results obtained for the single degree-of-freedom system with the linear cutting force, one uses equations (3.4) and (3.16) to arrive at the flip bifurcation predictions, while equations (3.9) and (3.16) are used to obtain the Neimark-Sacker bifurcation predictions. The analytical results obtained for the 3/4 rule cutting force model make use of equations (3.4) and (3.17) to arrive at the flip bifurcation predictions, while equations (3.9) and (3.17) are used to arrive at the Neimark-Sacker bifurcation predictions. As previously stated, negative and infinite axial depth of cut terms do not make physical sense and they are therefore not included in the results. The analytical results are compared with the results of the delay differential equation (DDE) numerical simulations detailed in Section 4.1.

From Davies *et al*. (2002), the following input parameters are used for making the single degree-of-freedom model predictions.

Properties	Parameters	Units
m_x	0.0431	kg
ζ_x	0.0167	-
k_x	1.40E+06	N/m
K_t	5.00E+08	N/m^2
N	2	-
f	0.000102	m/tooth
R	0.00635	m

Table 5.1: Input parameters from Davies *et al*. (2002) for analytical predictions.

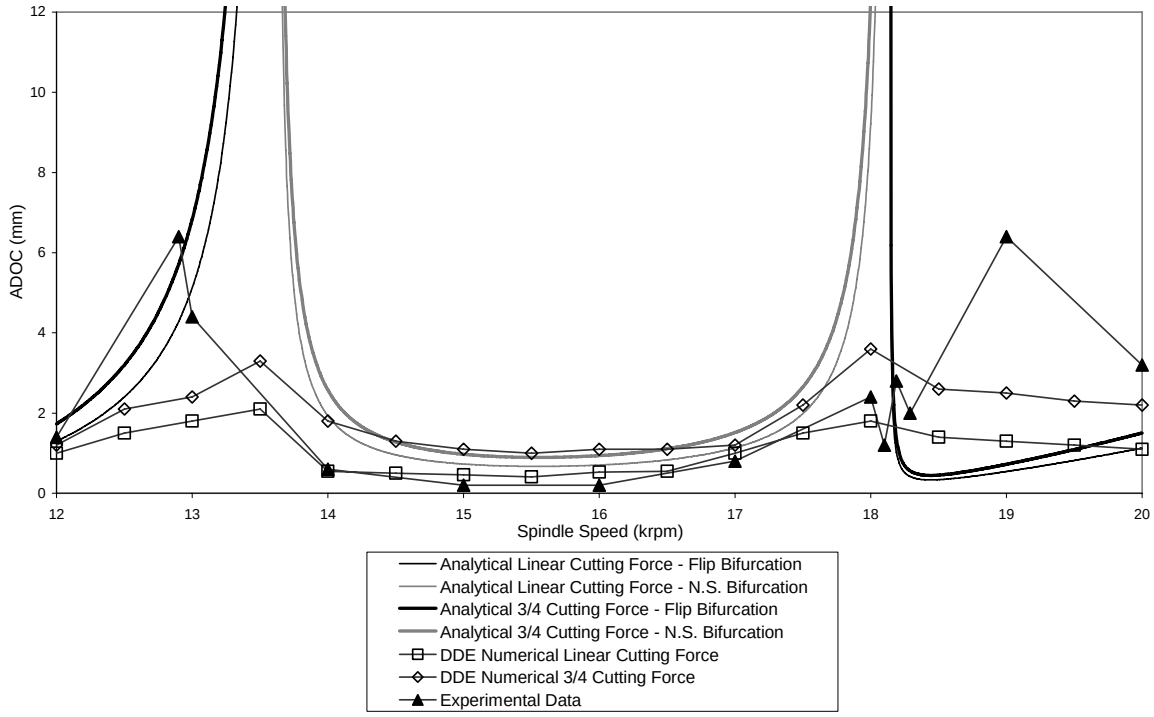

Figure 5.1: Analytical prediction and delay differential equation numerical prediction comparisons with experimental data for 5% immersion.

By using equation (1.2), the immersion rate is determined from $\rho = 0.14$ to be approximately 5%. Experimental data from Figure 7 (b) of Davies *et al*. (2002) is also included for comparison. For the next four graphs, the spindle speeds range from 12 to 20 krpm.

As expected, the delay differential equation numerical predictions shown in Figure 5.1 follow the trend of the analytical predictions. The 3/4 rule cutting force model predicts slightly higher regions of stability when compared with the results obtained with the linear cutting force model. The peak in the stability lobe predicted around 13.5 krpm, by using analytical means, compares reasonably well to the peak at 13 krpm seen in the experimental data; the predictions at 18 krpm, however, do not correspond well to the

experimental results that show a peak at 19 krpm. Outside of these regions of higher stability, the analytical results and the numerical results obtained by integrating the delay differential equations compare well with the experimental predictions.

The following parameters were used to run the UMCP numerical stability prediction program as well as the modified program for 3/4 rule cutting.

Properties	Parameters	Units
m_x	0.0431	kg
ζ_x	0.0167	-
k_x	1.40E+06	N/m
m_y	1.00E+05	kg
ζ_y	1	-
k_y	1.00E+15	N/m

Properties	Parameters	Units
m_u	1.00E+05	kg
ζ_u	1	-
k_u	1.00E+15	N/m
m_v	1.00E+05	kg
ζ_v	1	-
k_v	1.00E+15	N/m

Properties	Parameters	Units
K_t	5.00E+08	N/m^2
K_n	0.3	-
R	0.00635	m
N	2	-
f	0.000102	m/tooth
helix angle	0	degrees
rake angle	15	degrees
friction	0.2	-

Table 5.2: Input parameters from Davies *et al*. (2002) for numerical calculations.

In Figure 5.2, the 5% immersion analytical predictions are shown along with the predictions made from the UMCP numerical stability programs for both linear and 3/4 rule cutting force models; these predictions are compared with the 5% immersion experimental data. As shown in Figure 5.1, the analytical results are reasonably accurate in predicting the peak seen in the experimental results at 13 krpm. The UMCP programs, however, are too generous in their stability predictions from 12 to 18.5 krpm. It is only

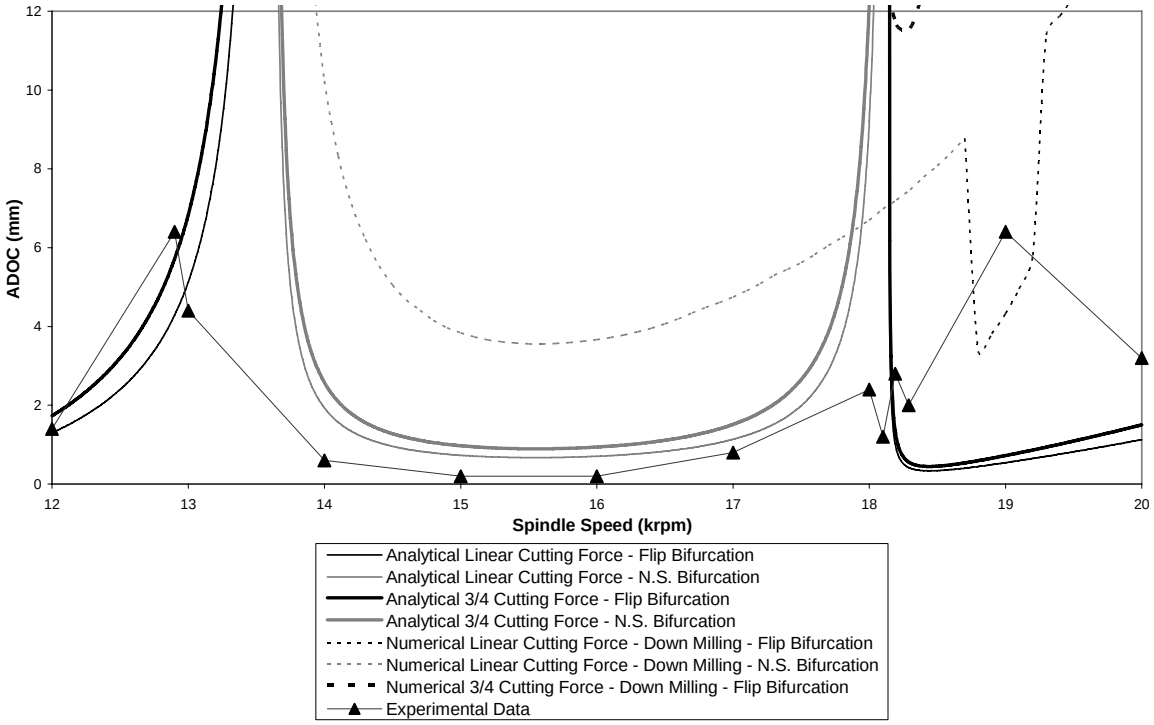

Figure 5.2: Analytical prediction and UMCP numerical stability program prediction comparisons with experimental data for 5% immersion.

around 19 krpm, where the UMCP program with the linear cutting force model compares reasonably well to the experimental data. The predictions made from the modified 3/4 rule UMCP numerical stability prediction program, results in generous operating regions for stability that mostly go beyond the scale of the figure. This is most likely due to the linearization of the cutting force model from the Taylor series expansion. Factors such as rake angle and friction that are included in the UMCP numerical program are not accounted for in the analytical predictions and therefore, may be the cause of certain discrepancies.

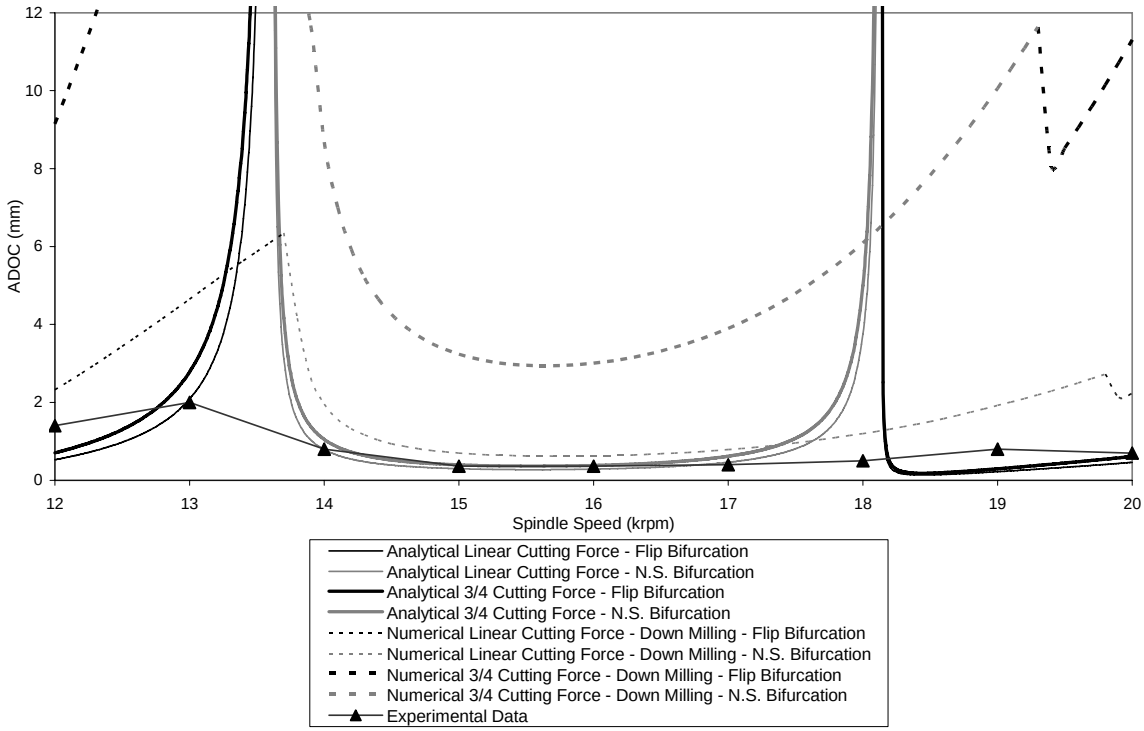

Figure 5.3: Analytical prediction and UMCP numerical stability program prediction comparisons with experimental data for 29% immersion.

In Figure 5.3, a higher immersion rate of 29% is now used for $\rho = 0.35$ to see if the stability predictions break down due to the loss of contact and low immersion assumptions made in the analytical model.

From the experimental results, the high immersion rate in Figure 5.3 causes the local peaks seen at 13 krpm and 19 krpm to reduce in size, compared with Figure 5.2, thereby reducing the region of stability. The UMCP numerical stability prediction program shrinks the region of stability as well so that the predictions for the linear cutting force compare well with the experimental data from 14 krpm to 18 krpm. However, like the analytical predictions, the UMCP numerical predictions do not compare well with experimental data, especially around the regions of 13 krpm and 19 krpm. As in the

previous case, the modified UMCP program with the 3/4 rule cutting force does not fare well in predicting results with the assumed parameters.

The UMCP numerical stability prediction program distinguishes between down-milling and up-milling processes. During the up-milling process, the flip and Neimark-Sacker bifurcation boundaries are different from those obtained during the down-milling process. The analytical predictions do not distinguish between these processes and they favor the numerical predictions made for the down-milling process as shown in Figures 5.2 and 5.3. This agreement may be due to an assumption in the analytical equations that places the cutting period at the start or the end of the spindle period.

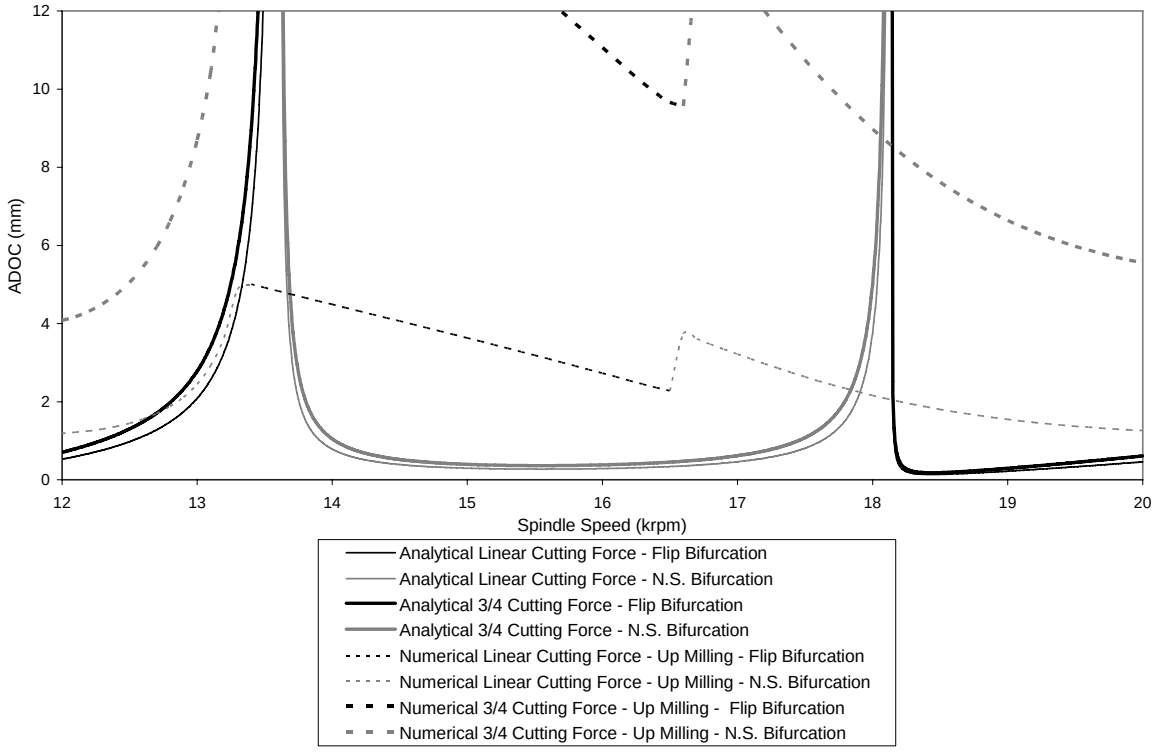

Figure 5.4 - Up-Milling Case: Comparison of the UMCP numerical stability prediction program with the analytical prediction results for 29% immersion.

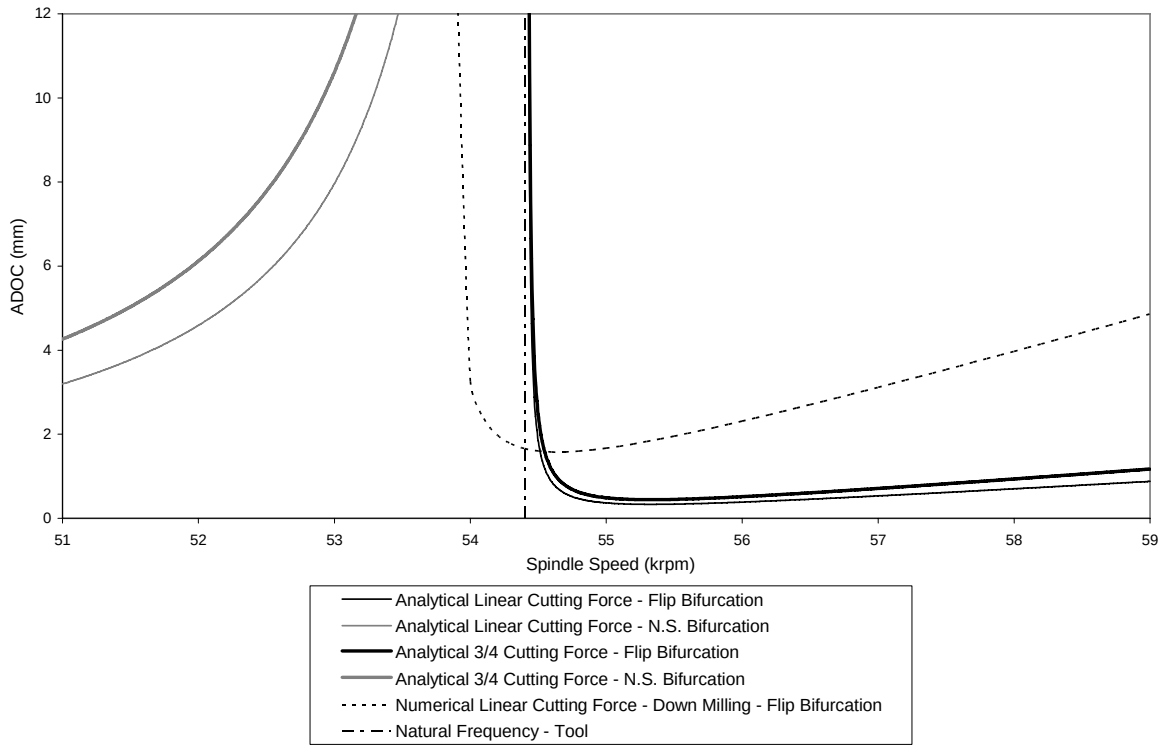

Figure 5.5: Analytical prediction and UMCP numerical stability program prediction comparisons for 5% immersion around the tool natural frequency of 54.4 krpm.

The natural frequency of the tool at 54.4 krpm (or 907 Hz) is included in Figure 5.5, along with stability lobes in its vicinity. As shown in this figure, the natural frequency of the tool lies directly in a high region of stability predicted by the analytical results while the UMCP program with the linear cutting force model predicts a high region to the left of the natural frequency. The stability lobes predicted by using both methods must be discounted in this region as the natural frequency of the tool dictates a region of instability around 54.4 krpm. Fortunately, milling operations are rarely carried out at such high spindle speeds, thereby reducing the possibility of operating around the natural frequency of the tool.

By using the work reported by Stepan *et al*. (2005), a new set of input parameters are used to compare the single degree-of-freedom analytical results in a lower range of spindle speeds.

Properties	Parameters	Units
m_x	2.586	kg
ζ_x	0.0038	-
k_x	2.20E+06	N/m
K_t	1.89E+09	N/m^2
N	1	-
h_0	0.0001016	m
R	0.009525	m

Table 5.3: Input parameters from Stepan *et al*. (2005) for analytical predictions.

Properties	Parameters	Units
m_x	2.586	kg
ζ_x	0.0038	-
k_x	2.20E+06	N/m
m_y	1.00E+05	kg
ζ_y	1	-
k_y	1.00E+15	N/m

Properties	Parameters	Units
m_u	1.00E+05	kg
ζ_u	1	-
k_u	1.00E+15	N/m
m_v	1.00E+05	kg
ζ_v	1	-
k_v	1.00E+15	N/m

Properties	Parameters	Units
K_t	1.89E+09	N/m^2
K_n	0.3	-
R	0.009525	m
N	1	-
h_0	0.0001016	m
helix angle	0	degrees
rake angle	15	degrees
friction	0.2	-

Table 5.4: Input parameters from Stepan *et al*. (2005) for numerical calculations.

The spindle speeds in the next two figures range from 2.9 to 3.7 krpm. ρ is set at 0.1082, which is approximated to be 3% immersion. The analytical and numerical stability predictions fare quite well when compared with the experimental data. In the 2.9 to 3.2 krpm range, the results favor the analytical 3/4 rule cutting force model predictions as

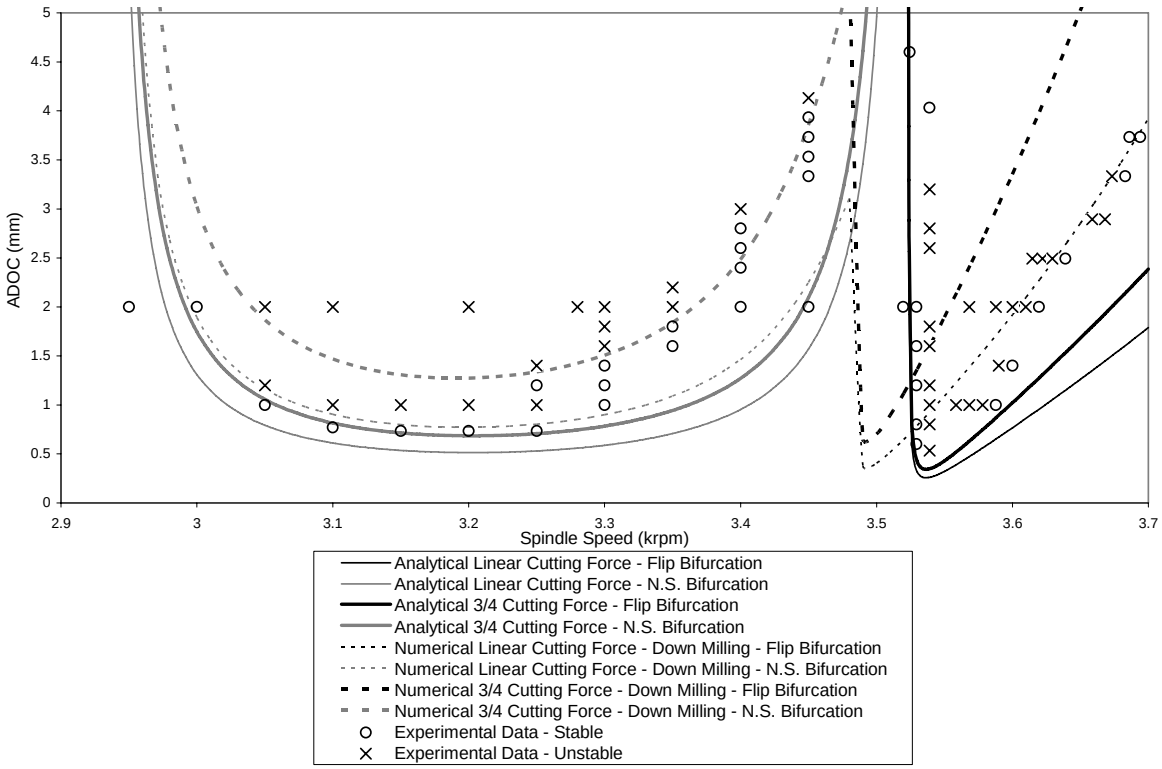

Figure 5.6: Analytical prediction and UMCP numerical stability program prediction comparisons with experimental data for 3% immersion.

well as the UMCP stability program predictions with the linear cutting force model. However, in the 3.3 to 3.48 krpm range, the results favor the predictions made by the modified UMCP program with the 3/4 rule cutting force model. The accuracy of the predictions from the numerical programs breaks down in the 3.5 to 3.55 krpm range where the results favor the predictions from analytical methods. In the 3.62 to 3.7 krpm range, though, the results again favor the predictions from the modified 3/4 rule UMCP program.

Figure 5.7 reaffirms the fact that the analytical model does not differentiate between up-milling and down-milling cases. Figure 5.8 shows that regions of high stability around

the natural frequency of the tool at 8.81 krpm (or 147 Hz) are predicted by both the analytical and numerical methods.

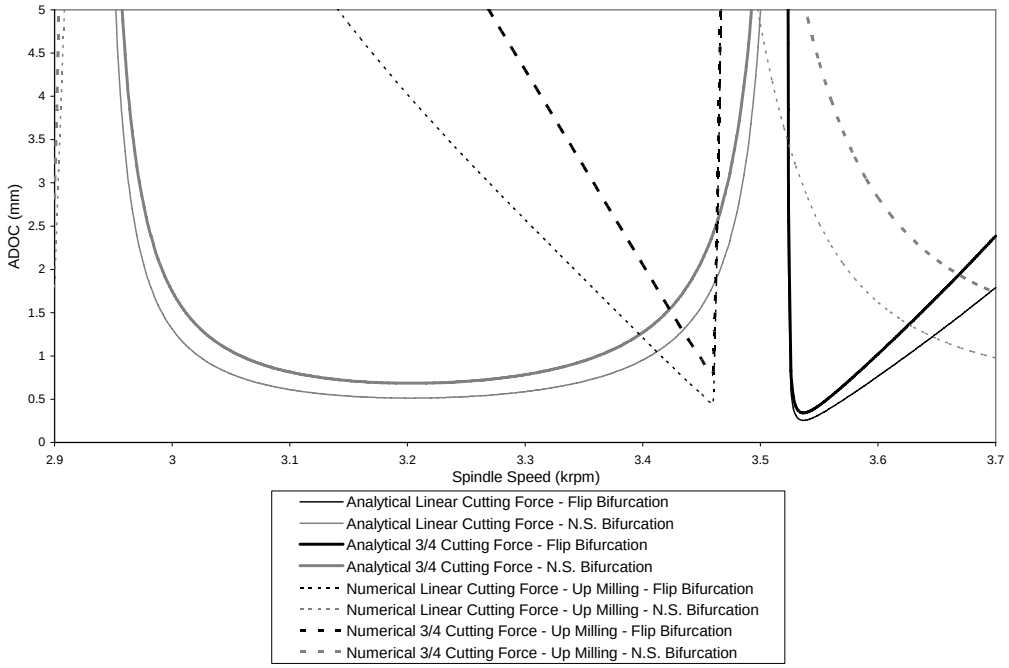

Figure 5.7 - Up-Milling Case: Comparison of the UMCP numerical stability prediction program with the analytical prediction results for 3% immersion.

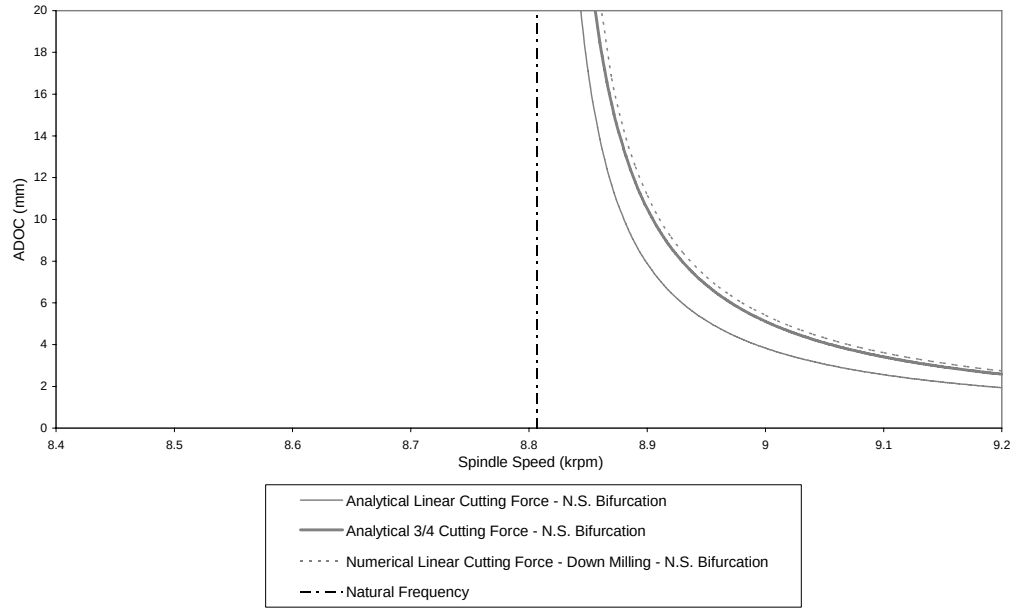

Figure 5.8: Analytical prediction and UMCP numerical stability prediction comparisons for 5% immersion around the tool natural frequency of 8.81 krpm.

5.2 Two DOF System Results and Discussion

The analytical results obtained for the two degree-of-freedom system with the linear cutting force make use of equations (3.13) and (3.16) to arrive at the flip bifurcation predictions. To obtain the Neimark-Sacker bifurcation predictions for the linear cutting force model, solutions based on the analysis of Section 3.4 are used in conjunction with equation (3.16). The analytical 3/4 rule cutting force results make use of equations (3.13) and (3.17) to arrive at the flip bifurcation predictions, while for the Neimark-Sacker bifurcation case, the solutions obtained from equation (3.17) is used to arrive at the stability predictions. As before, negative and infinite axial depth of cut terms do not make physical sense and they are not shown in the results. The analytical results are also compared with the results obtained by numerically integrating the delay differential equations.

Properties	Parameters	Units
m_x	0.02	kg
ζ_x	0.01	-
k_x	8.00E+05	N/m
m_u	0.1	kg
ζ_u	0.01	-
k_u	1.00E+06	N/m
K_t	6.00E+08	N/m^2
N	2	-
f	0.00051	m/tooth
R	0.00635	m
helix angle	30	degrees

Table 5.5: Input parameters for two DOF system analytical predictions.

After an extensive search, no existing experimental results were found for a two degree-of-freedom milling model that uses a single degree of freedom for the tool and a single degree of freedom for the workpiece. Therefore, the input parameters in Table 5.5 have been chosen to compare the two degree-of-freedom results. ρ is chosen to equal 0.1.

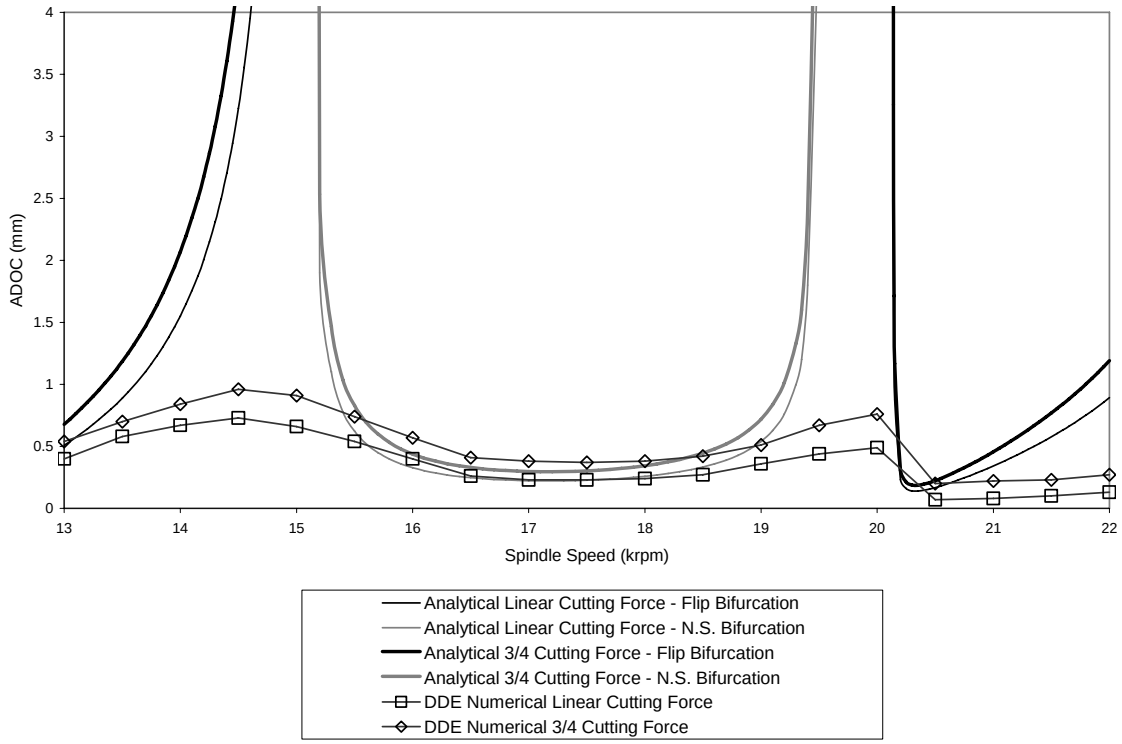

Figure 5.9 - Two DOF System: Analytical prediction and delay differential equation numerical prediction comparisons for $\rho = 0.1$.

In Figures 5.9 to 5.12, the spindle speeds range from 13 to 22 krpm. The predictions are first compared with the delay differential equation numerical results. As in the case of the single degree-of-freedom system results, the delay differential equation numerical predictions follow the trend of the analytical predictions. The 3/4 rule cutting force model predicts slightly higher regions of stability compared to the predictions from the linear cutting force model. Local peaks around 14.5 krpm and 20 krpm are seen in both the analytical and delay differential equation numerical results.

The analytical results are next compared with the numerical results obtained from the UMCP stability prediction program. In this case, the assumption given by equation (1.2) is invalid due to the 30° helix angle. Estimates of 5% and 10% immersions are used for comparison with the analytical predictions.

Properties	Parameters	Units
m_x	0.02	kg
ζ_x	0.01	-
k_x	8.00E+05	N/m
m_y	1.00E+05	kg
ζ_y	1	-
k_y	1.00E+15	N/m

Properties	Parameters	Units
m_u	0.1	kg
ζ_u	0.01	-
k_u	1.00E+06	N/m
m_v	1.00E+05	kg
ζ_v	1	-
k_v	1.00E+15	N/m

Properties	Parameters	Units
K_t	6.00E+08	N/m^2
K_n	0.3	-
R	0.00635	m
N	2	-
f	0.00051	m/tooth
helix angle	30	degrees
rake angle	15	degrees
friction	0.2	-

Table 5.6: Input parameters for two DOF system numerical calculations.

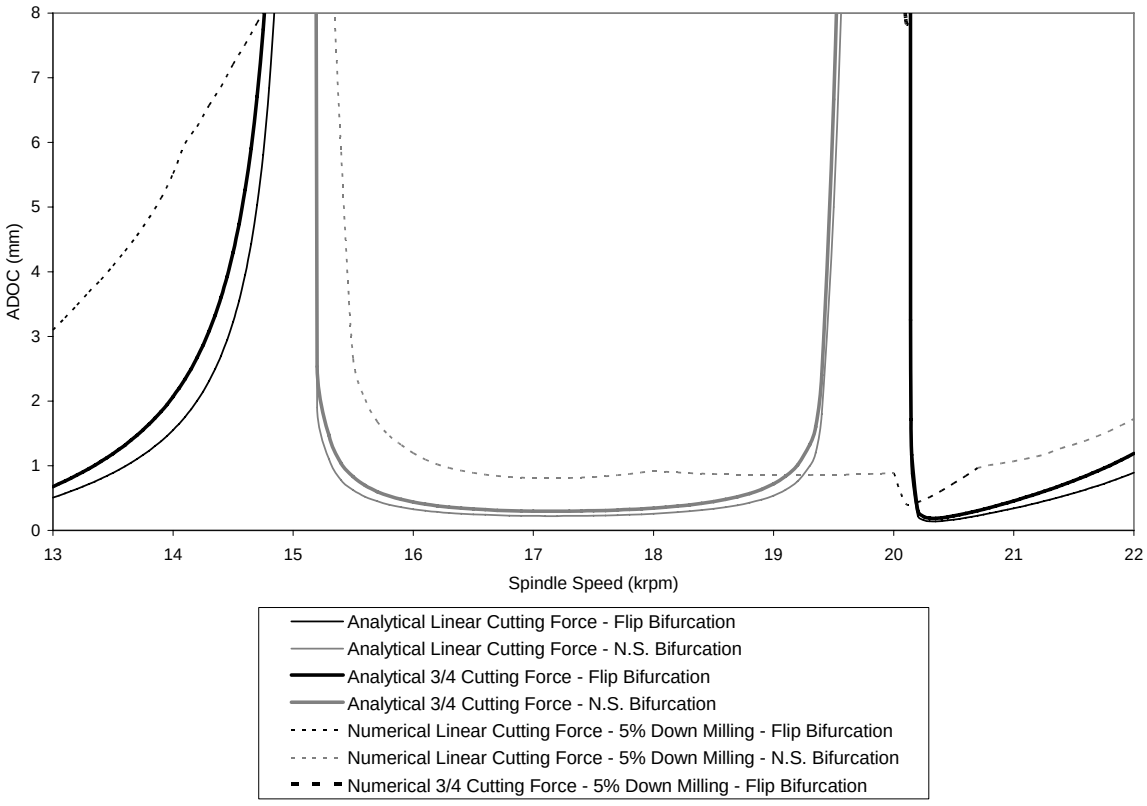

Figure 5.10 - Two DOF System: Analytical prediction for ρ = 0.1 and UMCP numerical stability program prediction for 5% immersion comparisons.

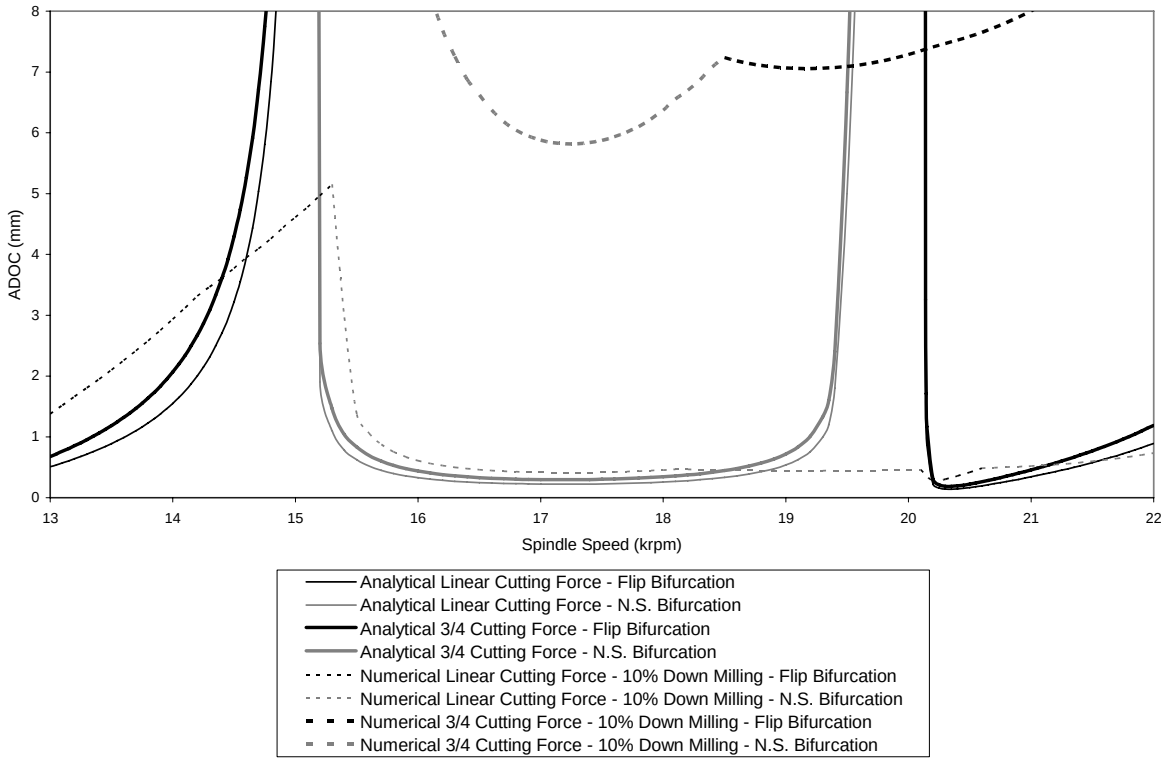

Figure 5.11 - Two DOF System: Analytical prediction for $\rho = 0.1$ and UMCP numerical stability program prediction for 10% immersion comparisons.

Comparing Figure 5.10 to 5.11, the 10% immersion results from the UMCP numerical stability prediction program agree more favorably with the analytical data. The local peak around 15 krpm appears in both the analytical and numerical predictions. However, the region of stability around this peak is wider for the numerical predictions. The local peak predicted at around 20 krpm for the analytical predictions does not appear in the numerical predictions. Nevertheless, there is agreement in the predictions for a change from a Neimark-Sacker bifurcation to a flip bifurcation at around 20 krpm. However, the change from a flip bifurcation back to a Neimark-Sacker bifurcation at around 20.5 krpm is only observed in the UMCP model predictions. These inconsistencies may be due to factors such as helix angle, rake angle, and friction properties that are included in the

UMCP model; these are not accounted for in the analytical models. As in the single degree-of-freedom cases, the predictions from the modified UMCP numerical stability prediction program for the 3/4 rule cutting force model show regions of stability that are much higher than the analytical and UMCP numerical linear cutting force model results. As discussed previously, the linearization assumption of the 3/4 rule cutting force model may play a role in these generous predictions.

As in the case of the single degree-of-freedom system, Figure 5.12 confirms that the analytical model does not differentiate between up-milling and down-milling in the two degree-of-freedom system case. As in the single degree-of-freedom case, there is an assumption in the map development that places the cutting period at either the start or the end of the spindle period.

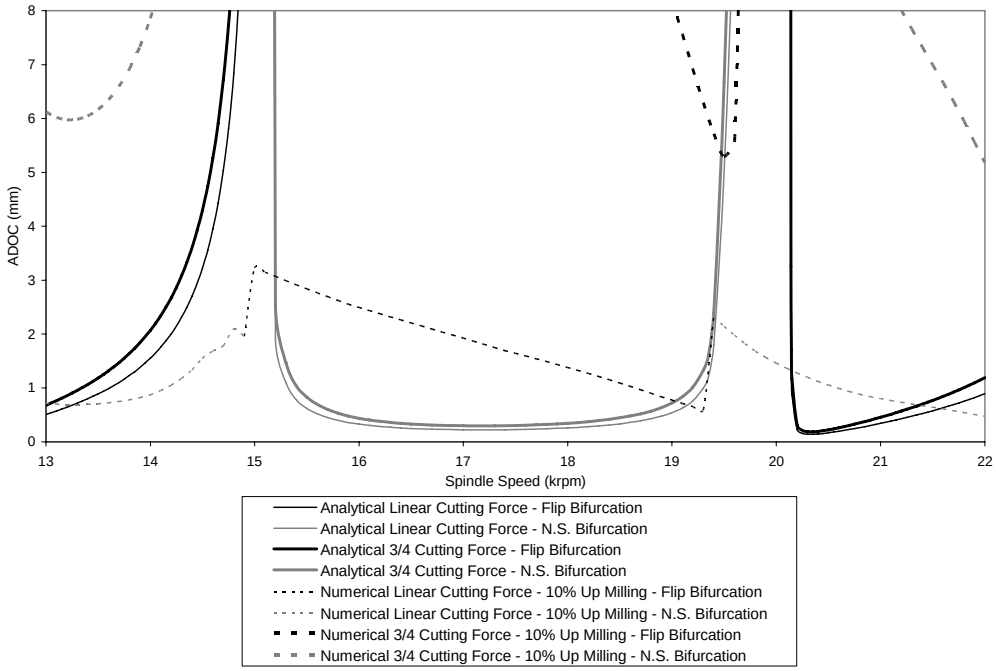

Figure 5.12 - Two DOF Up-Milling Case: Comparison of the UMCP numerical stability prediction program for ρ = 0.1 with the analytical prediction results for 10% immersion.

As in the case of the single degree-of-freedom system results, Figures 5.13 and 5.14 confirm that the analytical and numerical predictions generate high regions of stability around the natural frequencies of the tool and the workpiece at 60.4 krpm (or 1007 Hz) and at 30.2 krpm (or 503 Hz), respectively. The stability lobes predicted around these natural frequencies must be ignored.

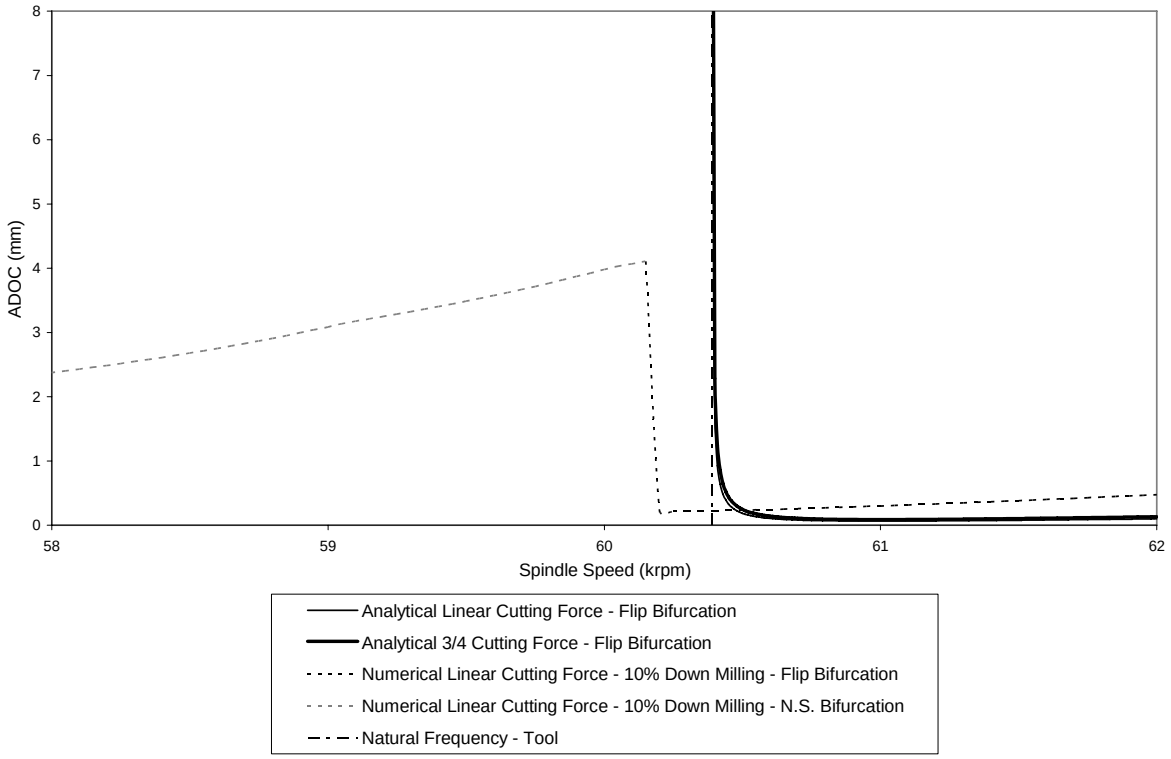

Figure 5.13 - Two DOF System: Analytical prediction for ρ = 0.1 and UMCP numerical stability program prediction for 10% immersion comparisons around the tool natural frequency of 60.4 krpm.

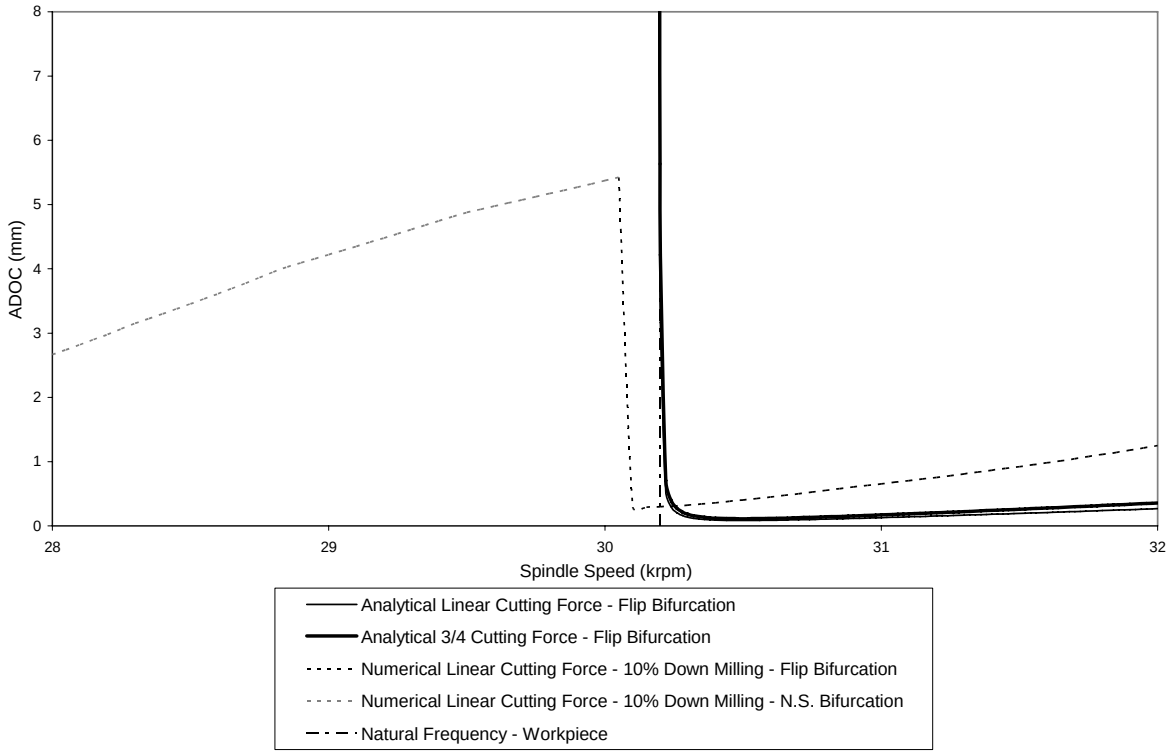

Figure 5.14 - Two DOF System: Analytical prediction for ρ = 0.1 and UMCP numerical stability prediction for 10% immersion comparisons around the workpiece natural frequency of 30.2 krpm.

Chapter 6

Conclusion

6.1 Concluding Remarks

In this thesis, maps derived from single degree-of-freedom models by using both linear and 3/4 rule cutting force models have been expanded to a model with two degrees of freedom. Due to loss of contact effects, the cutting period is minimized while the free vibration, non-cutting period is maximized during an entire spindle cycle period. Two numerical schemes are introduced to compare the predictions from the analytical models. The first is based on a direct numerical integration of the governing delay differential equations. The second is based on a UMCP numerical stability prediction program that uses a semi-discretization method to determine the stability boundaries. Linear and 3/4 rule cutting force models are incorporated in both numerical schemes. Analytical predictions and numerical results are then compared with existing experimental results. The following conclusions are made based on these comparisons:

i) The stability charts obtained analytically by using the linearized cutting force model and the 3/4 rule cutting force model differ by a factor of 4/3. This is due to the linearization of the 3/4 rule cutting force model during the formation of the single and two degree-of-freedom system maps.

ii) The analytical predictions compare well, in most instances, with the numerical and experimental results at the stability boundaries. In areas, where the comparisons break down, additional milling properties such as helix angle, rake

angle, and friction may play an effect pointing to the limitations of the analytical predictions.

iii) With certain parameters, the modified UMCP numerical stability prediction program for the 3/4 rule cutting force model produces generous stability boundaries when compared with the linear cutting force model used in the existing UMCP numerical stability prediction program. This is due to the linearization of the variable chip thickness terms in the Taylor series expansion.

iv) The analytical predictions do not differentiate between up-milling and down-milling processes and tend to favor the results obtained for the down-milling numerical predictions. The analytical models are based on an assumption where the cutting period is placed at either the start or the end of the entire spindle period.

v) Both the analytical and numerical predictions generate regions of high stability around the natural frequencies of the system, which does not appear to be correct given that loss of contact effects occur during a low immersion process.

6.2 Suggestions for Future Work

The following suggestions are made for future work:

i) Incorporate properties such as helix angle, rake angle, and friction into the analytical map models

ii) Modify the UMCP numerical stability prediction program to include nonlinear variable chip thickness terms for the 3/4 rule cutting force model

iii) Explore the dynamics with feed rate variability

iv) Explore the dynamics with damping that vary with spindle speeds

v) Conduct careful low immersion experiments to study effects of different parameters as well as the suitability of using different reduced-order models

Appendix A

Map Derivations

In this appendix, detailed steps used to derive the single degree-of-freedom and two degree-of-freedom system maps are provided. The final forms of the single and two degree-of-freedom maps can be found, respectively, in Sections 2.3 and 2.4 of Chapter 2.

A.1 Derivation of the Single DOF System Map

Recalling the single degree-of-freedom equation of motion found in equation (2.9),

$$\ddot{q}_x(t) + 2\zeta_x\omega_x\dot{q}_x(t) + \omega_x{}^2 q_x(t) = \frac{g(t)}{m_x} F_x\left(t, \tau(t)\right)$$

the equation of motion during the non-cutting period $t_j \le t < t_{j+1}^-$ is found to be

$$\ddot{q}_x(t) + 2\zeta_x\omega_x\dot{q}_x(t) + \omega_x{}^2 q_x(t) = 0$$

This linear, homogenous differential equation can be solved to obtain

$$q_x(t) = c_1 e^{-\zeta_x\omega_x t}\cos(\omega_x\sqrt{1-\zeta_x{}^2}\,t) + c_2 e^{-\zeta_x\omega_x t}\sin(\omega_x\sqrt{1-\zeta_x{}^2}\,t)$$

where c_1 and c_2 are constants of integration. The first derivative of this solution yields

$$\begin{aligned}\dot{q}_x(t) = &-c_1\zeta_x\omega_x e^{-\zeta_x\omega_x t}\cos(\omega_x\sqrt{1-\zeta_x{}^2}\,t) - c_1\omega_x\sqrt{1-\zeta_x{}^2}\,e^{-\zeta_x\omega_x t}\sin(\omega_x\sqrt{1-\zeta_x{}^2}\,t)\\ &-c_2\zeta_x\omega_x e^{-\zeta_x\omega_x t}\sin(\omega_x\sqrt{1-\zeta_x{}^2}\,t) + c_2\omega_x\sqrt{1-\zeta_x{}^2}\,e^{-\zeta_x\omega_x t}\cos(\omega_x\sqrt{1-\zeta_x{}^2}\,t)\end{aligned}$$

The starting time of the non-cutting period t_j can be chosen for any initial conditions.

$$\begin{aligned}q_x(t_j) &= q_x(0) = c_1\\ \dot{q}_x(t_j) &= \dot{q}_x(0) = -\zeta_x\omega_x c_1 + \omega_x\sqrt{1-\zeta_x{}^2}\,c_2\end{aligned}$$

c_2 then equals

$$c_2 = \frac{\dot{q}_x(0) + \zeta_x \omega_x q_x(0)}{\omega_x \sqrt{1-\zeta_x{}^2}} = \frac{\dot{q}_x(t_j) + \zeta_x \omega_x q_x(t_j)}{\omega_x \sqrt{1-\zeta_x{}^2}}$$

To describe the state at the end of the non-cutting period for $q_x(t_{j+1}^-)$ and $\dot{q}_x(t_{j+1}^-)$, the time *t* is allowed to travel for one period τ_1. Due to loss of contact effects $\tau_2 \to 0$, and hence, $\tau_1 \to \tau$. By substituting the constants of integration and by using the initial conditions established for $q_x(t_j)$ and $\dot{q}_x(t_j)$, the equations mapping the end of the non-cutting period to its beginning are derived to be

$$q_x(t_{j+1}^-) = [e^{-\zeta_x \omega_x \tau} \cos(\omega_x \sqrt{1-\zeta_x{}^2}\tau) + \frac{\zeta_x \omega_x e^{-\zeta_x \omega_x \tau}}{\omega_x \sqrt{1-\zeta_x{}^2}} \sin(\omega_x \sqrt{1-\zeta_x{}^2}\tau)] q_x(t_j)$$
$$+ [\frac{e^{-\zeta_x \omega_x \tau}}{\omega_x \sqrt{1-\zeta_x{}^2}} \sin(\omega_x \sqrt{1-\zeta_x{}^2}\tau)] \dot{q}_x(t_j)$$

$$\dot{q}_x(t_{j+1}^-) = [-\omega_x \sqrt{1-\zeta_x{}^2} e^{-\zeta_x \omega_x \tau} \sin(\omega_x \sqrt{1-\zeta_x{}^2}\tau) - \frac{\zeta_x{}^2 \omega_x{}^2 e^{-\zeta_x \omega_x \tau}}{\omega_x \sqrt{1-\zeta_x{}^2}} \sin(\omega_x \sqrt{1-\zeta_x{}^2}\tau)] q_x(t_j)$$
$$+ [e^{-\zeta_x \omega_x \tau} \cos(\omega_x \sqrt{1-\zeta_x{}^2}\tau) - \frac{\zeta_x \omega_x e^{-\zeta_x \omega_x \tau}}{\omega_x \sqrt{1-\zeta_x{}^2}} \sin(\omega_x \sqrt{1-\zeta_x{}^2}\tau)] \dot{q}_x(t_j)$$

Simplifying these equations produces the single degree-of-freedom non-cutting phase map (2.10)

$$\begin{bmatrix} q_x(t_{j+1}^-) \\ \dot{q}_x(t_{j+1}^-) \end{bmatrix} = \mathrm{A} \begin{bmatrix} q_x(t_j) \\ \dot{q}_x(t_j) \end{bmatrix}$$

where the state-transition matrix A (2.11) is

$$\mathrm{A} = \exp(-\zeta_x \omega_x \tau) \begin{bmatrix} \cos(\omega_{xd}\tau) + \frac{\zeta_x \omega_x}{\omega_{xd}} \sin(\omega_{xd}\tau) & \frac{1}{\omega_{xd}} \sin(\omega_{xd}\tau) \\ -\frac{\omega_x{}^2}{\omega_{xd}} \sin(\omega_{xd}\tau) & \cos(\omega_{xd}\tau) - \frac{\zeta_x \omega_x}{\omega_{xd}} \sin(\omega_{xd}\tau) \end{bmatrix}$$

and $\omega_{xd} = \omega_x \sqrt{1-\zeta_x^{\,2}}$ is defined to be the damped natural frequency of the tool free oscillations.

Inserting the lower expression from equation (2.10)

$$\dot{q}_x(t_{j+1}^-) = \mathrm{A}_{21} q_x(t_j) + \mathrm{A}_{22} \dot{q}_x(t_j)$$

into equation (2.14),

$$\dot{q}_x(t_{j+1}) = \dot{q}_x(t_{j+1}^-) + \tau_2 \frac{K_t w}{m_x} \left[q_x(t_j) - q_x(t_{j+1}^-) + \mathrm{h}_0 \right]$$

the following equation for the linear cutting force can be obtained:

$$\begin{aligned} \dot{q}_x(t_{j+1}) = {} & \mathrm{A}_{11} q_x(t_j) + \mathrm{A}_{12} \dot{q}_x(t_j) \\ & + \tau_2 \frac{K_t w}{m_x} [q_x(t_j) - \mathrm{A}_{11} q_x(t_j) - \mathrm{A}_{12} \dot{q}_x(t_j) + \mathrm{h}_0] \end{aligned}$$

Assuming that the position of the oscillating tool remains constant during the interaction with the workpiece so that $q_x(t_{j+1}) \approx q_x(t_{j+1}^-)$,

$$q_x(t_{j+1}) = \mathrm{A}_{11} q_x(t_j) + \mathrm{A}_{12} \dot{q}_x(t_j)$$

from the upper expression in equation (2.10). Combining the previous two equations together, one arrives at equation (2.16) for the linear cutting force model.

$$\begin{bmatrix} q_x(t_{j+1}) \\ \dot{q}_x(t_{j+1}) \end{bmatrix} = \mathrm{A} \begin{bmatrix} q_x(t_j) \\ \dot{q}_x(t_j) \end{bmatrix} + \begin{bmatrix} 0 \\ \tau_2 \frac{K_t w}{m_x} [(1-\mathrm{A}_{11}) q_x(t_j) - \mathrm{A}_{12} \dot{q}_x(t_j) + \mathrm{h}_0] \end{bmatrix}$$

By using equations (2.10) and (2.15), the same process can be carried out for the 3/4 rule cutting force model to obtain equation (2.17).

$$\begin{bmatrix} q_x(t_{j+1}) \\ \dot{q}_x(t_{j+1}) \end{bmatrix} = \mathrm{A} \begin{bmatrix} q_x(t_j) \\ \dot{q}_x(t_j) \end{bmatrix} + \begin{bmatrix} 0 \\ \tau_2 \frac{K w}{m_x} [(1-\mathrm{A}_{11}) q_x(t_j) - \mathrm{A}_{12} \dot{q}_x(t_j) + \mathrm{h}_0]^{3/4} \end{bmatrix}$$

To derive the fixed points for the single degree-of-freedom system by using the linear cutting force model, one sets

$$x_e = q_x(t_{j+1}) = q_x(t_j)$$
$$v_e = \dot{q}_x(t_{j+1}) = \dot{q}_x(t_j)$$

By substituting x_e and v_e into equation (2.16),

$$\begin{bmatrix} x_e \\ v_e \end{bmatrix} = \begin{bmatrix} \mathrm{A}_{11} & \mathrm{A}_{12} \\ \mathrm{A}_{21} & \mathrm{A}_{22} \end{bmatrix} \begin{bmatrix} x_e \\ v_e \end{bmatrix} + \begin{bmatrix} 0 \\ \tau_2 \dfrac{K_t w}{m_x} [(1-\mathrm{A}_{11})x_e - \mathrm{A}_{12} v_e + \mathrm{h}_0] \end{bmatrix}$$

and solving explicitly for x_e and v_e, the fixed points using the linear cutting force are found to be

$$x_e = \frac{K_t w \tau_2 \mathrm{h}_0 \mathrm{A}_{12}}{m_x[1 + \det(\mathrm{A}) - \mathrm{tr}(\mathrm{A})]}$$
$$v_e = \frac{K_t w \tau_2 \mathrm{h}_0 (1\text{-}\mathrm{A}_{11})}{m_x[1 + \det(\mathrm{A}) - \mathrm{tr}(\mathrm{A})]}$$

To solve for the fixed points for the 3/4 rule cutting force model, the Taylor series is expanded for

$$h_x^{3/4}(t_j) = [\mathrm{h}_0 + \Delta \mathrm{h}_x(t_j)]^{3/4}$$

where

$$\Delta \mathrm{h}_x(t_j) = (1-\mathrm{A}_{11}) q_x(t_j) - \mathrm{A}_{12} \dot{q}_x(t_j)$$

Taking only linear terms from the Taylor series expansion

$$\begin{aligned} \mathrm{h}_x^{3/4}(t_j) &\approx \mathrm{h}_0^{3/4} + \frac{3}{4} \frac{\Delta \mathrm{h}_x(t_j)}{\mathrm{h}_0^{1/4}} \\ &\approx \mathrm{h}_0^{3/4} + \frac{3}{4} \frac{(1-\mathrm{A}_{11}) q_x(t_j) - \mathrm{A}_{12} \dot{q}_x(t_j)}{\mathrm{h}_0^{1/4}} \end{aligned}$$

the linearized form of equation (2.17) now becomes

$$\begin{bmatrix} q_x(t_{j+1}) \\ \dot{q}_x(t_{j+1}) \end{bmatrix} = \mathrm{A}\begin{bmatrix} q_x(t_j) \\ \dot{q}_x(t_j) \end{bmatrix} + \begin{bmatrix} 0 \\ \tau_2 \dfrac{Kw}{m_x}[\mathrm{h_0}^{3/4} + \dfrac{3}{4}\dfrac{(1-\mathrm{A}_{11})q_x(t_j) - \mathrm{A}_{12}\dot{q}_x(t_j)}{\mathrm{h_0}^{1/4}}] \end{bmatrix}$$

By substituting x_e and v_e into this linearized form

$$\begin{bmatrix} x_e \\ v_e \end{bmatrix} = \mathrm{A}\begin{bmatrix} x_e \\ v_e \end{bmatrix} + \begin{bmatrix} 0 \\ \tau_2 \dfrac{Kw}{m_x}[\mathrm{h_0}^{3/4} + \dfrac{3}{4}\dfrac{(1-\mathrm{A}_{11})x_e - \mathrm{A}_{12}v_e}{\mathrm{h_0}^{1/4}}] \end{bmatrix}$$

and solving explicitly for x_e and v_e, the fixed points for the model with the 3/4 rule cutting force are found to be

$$x_e = \frac{Kw\tau_2 \mathrm{h_0}^{3/4}\mathrm{A}_{12}}{m_x[1+\det(\mathrm{A})-\mathrm{tr}(\mathrm{A})]}$$
$$v_e = \frac{Kw\tau_2 \mathrm{h_0}^{3/4}(1-\mathrm{A}_{11})}{m_x[1+\det(\mathrm{A})-\mathrm{tr}(\mathrm{A})]}$$

To solve for the Jacobian matrix of the linear cutting force model, equation (2.16) is rearranged to form

$$\begin{bmatrix} q_x(t_{j+1}) \\ \dot{q}_x(t_{j+1}) \end{bmatrix} = \mathrm{E}_{\mathrm{LCF}}^{1\mathrm{DOF}} + \begin{bmatrix} 0 \\ \tau_2 \dfrac{K_t w \mathrm{h_0}}{m_x} \end{bmatrix}$$

where matrix $\mathrm{E}_{\mathrm{LCF}}^{1\mathrm{DOF}}$ is determined to be

$$\mathrm{E}_{\mathrm{LCF}}^{1\mathrm{DOF}} = \begin{bmatrix} \mathrm{A}_{11}q_x(t_j) & \mathrm{A}_{12}\dot{q}_x(t_j) \\ [\mathrm{A}_{21} + \dfrac{K_t w\tau_2}{m_x}(1-\mathrm{A}_{11})]q_x(t_j) & [\mathrm{A}_{22} - \dfrac{K_t w\tau_2}{m_x}\mathrm{A}_{12}]\dot{q}_x(t_j) \end{bmatrix}$$

Constructing the Jacobian from $\mathrm{E}_{\mathrm{LCF}}^{1\mathrm{DOF}}$ leads to

$$\mathrm{B} = \begin{bmatrix} \mathrm{A}_{11} & \mathrm{A}_{12} \\ \mathrm{A}_{21} + \hat{w}_x(1-\mathrm{A}_{11}) & \mathrm{A}_{22} - \hat{w}_x\mathrm{A}_{12} \end{bmatrix}$$

where the dimensionless chip width for the linear cutting force model is

$$\hat{w}_x = \frac{K_t w \tau_2}{m_x}$$

To determine the Jacobian matrix for the 3/4 rule cutting force model, the linearized form of equation (2.17) is rearranged to become

$$\begin{bmatrix} q_x(t_{j+1}) \\ \dot{q}_x(t_{j+1}) \end{bmatrix} = \mathrm{E}_{3/4\mathrm{CF}}^{1\mathrm{DOF}} + \begin{bmatrix} 0 \\ \tau_2 \dfrac{K w \mathrm{h}_0^{\,3/4}}{m_x} \end{bmatrix}$$

where matrix $\mathrm{E}_{3/4\mathrm{CF}}^{1\mathrm{DOF}}$ is determined to be

$$\mathrm{E}_{3/4\mathrm{CF}}^{1\mathrm{DOF}} = \begin{bmatrix} \mathrm{A}_{11} q_x(t_j) & \mathrm{A}_{12} \dot{q}_x(t_j) \\ [\mathrm{A}_{21} + \dfrac{3}{4} \dfrac{K w \tau_2}{m_x \mathrm{h}_0^{\,1/4}} (1 - \mathrm{A}_{11})] q_x(t_j) & [\mathrm{A}_{22} - \dfrac{3}{4} \dfrac{K w \tau_2}{m_x \mathrm{h}_0^{\,1/4}} \mathrm{A}_{12}] \dot{q}_x(t_j) \end{bmatrix}$$

Finding the Jacobian from $\mathrm{E}_{3/4\mathrm{CF}}^{1\mathrm{DOF}}$ leads to

$$\mathrm{B} = \begin{bmatrix} \mathrm{A}_{11} & \mathrm{A}_{12} \\ \mathrm{A}_{21} + \hat{w}_x (1 - \mathrm{A}_{11}) & \mathrm{A}_{22} - \hat{w}_x \mathrm{A}_{12} \end{bmatrix}$$

where the dimensionless chip width for the 3/4 cutting force model is $\hat{w}_x = \dfrac{3}{4} \dfrac{K w \tau_2}{m_x \mathrm{h}_0^{\,1/4}}$

Linearizing around the fixed points, the generalized local dynamics is described by

$$\begin{bmatrix} q_x(t_{j+1}) \\ \dot{q}_x(t_{j+1}) \end{bmatrix} = \begin{bmatrix} x_e \\ v_e \end{bmatrix} + \mathrm{B} \begin{bmatrix} q_x(t_j) \\ \dot{q}_x(t_j) \end{bmatrix}$$

where x_e, v_e, and $\hat{w}_x$ are based on their respective cutting force models.

A.2 Derivation of the Two DOF System Map

Recalling the two degree-of-freedom equation of motion found in equation (2.24), is given by

$$\ddot{q}_x(t) + 2\zeta_x\omega_x\dot{q}_x(t) + \omega_x{}^2 q_x(t) = \frac{g(t)}{m_x} F_x\left(t, \tau(t)\right)$$
$$\ddot{q}_u(t) + 2\zeta_u\omega_u\dot{q}_u(t) + \omega_u{}^2 q_u(t) = \frac{g(t)}{m_u} F_x\left(t, \tau(t)\right)$$

the equation of motion during the non-cutting period $t_j \le t < t_{j+1}^-$ is found to be

$$\ddot{q}_x(t) + 2\zeta_x\omega_x\dot{q}_x(t) + \omega_x{}^2 q_x(t) = 0$$
$$\ddot{q}_u(t) + 2\zeta_u\omega_u\dot{q}_u(t) + \omega_u{}^2 q_u(t) = 0$$

These linear, homogenous differential equations can be solved to be

$$q_x(t) = c_1 e^{-\zeta_x\omega_x t}\cos(\omega_x\sqrt{1-\zeta_x{}^2}\,t) + c_2 e^{-\zeta_x\omega_x t}\sin(\omega_x\sqrt{1-\zeta_x{}^2}\,t)$$
$$q_u(t) = c_3 e^{-\zeta_u\omega_u t}\cos(\omega_u\sqrt{1-\zeta_u{}^2}\,t) + c_4 e^{-\zeta_u\omega_u t}\sin(\omega_u\sqrt{1-\zeta_u{}^2}\,t)$$

where c_1, c_2, c_3, and c_4 are constants of integration. The first derivatives of these solutions yield

$$\begin{aligned}\dot{q}_x(t) = &-c_1\zeta_x\omega_x e^{-\zeta_x\omega_x t}\cos(\omega_x\sqrt{1-\zeta_x{}^2}\,t) - c_1\omega_x\sqrt{1-\zeta_x{}^2}\,e^{-\zeta_x\omega_x t}\sin(\omega_x\sqrt{1-\zeta_x{}^2}\,t)\\ &- c_2\zeta_x\omega_x e^{-\zeta_x\omega_x t}\sin(\omega_x\sqrt{1-\zeta_x{}^2}\,t) + c_2\omega_x\sqrt{1-\zeta_x{}^2}\,e^{-\zeta_x\omega_x t}\cos(\omega_x\sqrt{1-\zeta_x{}^2}\,t)\\ \dot{q}_u(t) = &-c_3\zeta_u\omega_u e^{-\zeta_u\omega_u t}\cos(\omega_u\sqrt{1-\zeta_u{}^2}\,t) - c_3\omega_u\sqrt{1-\zeta_u{}^2}\,e^{-\zeta_u\omega_u t}\sin(\omega_u\sqrt{1-\zeta_u{}^2}\,t)\\ &- c_4\zeta_u\omega_u e^{-\zeta_u\omega_u t}\sin(\omega_u\sqrt{1-\zeta_u{}^2}\,t) + c_4\omega_u\sqrt{1-\zeta_u{}^2}\,e^{-\zeta_u\omega_u t}\cos(\omega_u\sqrt{1-\zeta_u{}^2}\,t)\end{aligned}$$

The starting time of the non-cutting period t_j can be chosen for any initial conditions, say,

$$
\begin{aligned}
q_x(t_j) &= q_x(0) = c_1 \\
q_u(t_j) &= q_u(0) = c_3 \\
\dot{q}_x(t_j) &= \dot{q}_x(0) = -\zeta_x \omega_x c_1 + \omega_x \sqrt{1-\zeta_x{}^2}\, c_2 \\
\dot{q}_u(t_j) &= \dot{q}_u(0) = -\zeta_u \omega_u c_3 + \omega_u \sqrt{1-\zeta_u{}^2}\, c_4
\end{aligned}
$$

c_2 and c_4 then respectively equal

$$
\begin{aligned}
c_2 &= \frac{\dot{q}_x(0) + \zeta_x \omega_x q_x(0)}{\omega_x \sqrt{1-\zeta_x{}^2}} = \frac{\dot{q}_x(t_j) + \zeta_x \omega_x q_x(t_j)}{\omega_x \sqrt{1-\zeta_x{}^2}} \\
c_4 &= \frac{\dot{q}_u(0) + \zeta_u \omega_u q_u(0)}{\omega_u \sqrt{1-\zeta_u{}^2}} = \frac{\dot{q}_u(t_j) + \zeta_u \omega_u q_u(t_j)}{\omega_u \sqrt{1-\zeta_u{}^2}}
\end{aligned}
$$

To describe the state at the end of the non-cutting period for $q_x(t_{j+1}^-)$ and $\dot{q}_x(t_{j+1}^-)$, the time *t* is allowed to travel for one period τ_1. Due to loss of contact effects $\tau_2 \to 0$, and hence, $\tau_1 \to \tau$.

By substituting the constants of integration and by using the initial conditions established for $q_x(t_j)$, $q_u(t_j)$, $\dot{q}_x(t_j)$, and $\dot{q}_u(t_j)$, the equations mapping the end of the non-cutting period to its beginning are derived to be

$$q_x(t_{j+1}^-) = [e^{-\zeta_x\omega_x\tau}\cos(\omega_x\sqrt{1-\zeta_x^{\,2}}\tau) + \frac{\zeta_x\omega_x e^{-\zeta_x\omega_x\tau}}{\omega_x\sqrt{1-\zeta_x^{\,2}}}\sin(\omega_x\sqrt{1-\zeta_x^{\,2}}\tau)]q_x(t_j)$$
$$+[\frac{e^{-\zeta_x\omega_x\tau}}{\omega_x\sqrt{1-\zeta_x^{\,2}}}\sin(\omega_x\sqrt{1-\zeta_x^{\,2}}\tau)]\dot{q}_x(t_j)$$

$$q_u(t_{j+1}^-) = [e^{-\zeta_u\omega_u\tau}\cos(\omega_u\sqrt{1-\zeta_u^{\,2}}\tau) + \frac{\zeta_u\omega_u e^{-\zeta_u\omega_u\tau}}{\omega_u\sqrt{1-\zeta_u^{\,2}}}\sin(\omega_u\sqrt{1-\zeta_u^{\,2}}\tau)]q_u(t_j)$$
$$+[\frac{e^{-\zeta_u\omega_u\tau}}{\omega_u\sqrt{1-\zeta_u^{\,2}}}\sin(\omega_u\sqrt{1-\zeta_u^{\,2}}\tau)]\dot{q}_u(t_j)$$

$$\dot{q}_x(t_{j+1}^-) = [-\omega_x\sqrt{1-\zeta_x^{\,2}}e^{-\zeta_x\omega_x\tau}\sin(\omega_x\sqrt{1-\zeta_x^{\,2}}\tau) - \frac{\zeta_x^{\,2}\omega_x^{\,2}e^{-\zeta_x\omega_x\tau}}{\omega_x\sqrt{1-\zeta_x^{\,2}}}\sin(\omega_x\sqrt{1-\zeta_x^{\,2}}\tau)]q_x(t_j)$$
$$+[e^{-\zeta_x\omega_x\tau}\cos(\omega_x\sqrt{1-\zeta_x^{\,2}}\tau) - \frac{\zeta_x\omega_x e^{-\zeta_x\omega_x\tau}}{\omega_x\sqrt{1-\zeta_x^{\,2}}}\sin(\omega_x\sqrt{1-\zeta_x^{\,2}}\tau)]\dot{q}_x(t_j)$$

$$\dot{q}_u(t_{j+1}^-) = [-\omega_u\sqrt{1-\zeta_u^{\,2}}e^{-\zeta_u\omega_u\tau}\sin(\omega_u\sqrt{1-\zeta_u^{\,2}}\tau) - \frac{\zeta_u^{\,2}\omega_u^{\,2}e^{-\zeta_u\omega_u\tau}}{\omega_u\sqrt{1-\zeta_u^{\,2}}}\sin(\omega_u\sqrt{1-\zeta_u^{\,2}}\tau)]q_u(t_j)$$
$$+[e^{-\zeta_u\omega_u\tau}\cos(\omega_u\sqrt{1-\zeta_u^{\,2}}\tau) - \frac{\zeta_u\omega_u e^{-\zeta_u\omega_u\tau}}{\omega_u\sqrt{1-\zeta_u^{\,2}}}\sin(\omega_u\sqrt{1-\zeta_u^{\,2}}\tau)]\dot{q}_u(t_j)$$

Simplifying these equations produces the two degree-of-freedom non-cutting phase map given by equation (2.25); that is,

$$\begin{bmatrix} q_x(t_{j+1}^-) \\ q_u(t_{j+1}^-) \\ \dot{q}_x(t_{j+1}^-) \\ \dot{q}_u(t_{j+1}^-) \end{bmatrix} = \mathrm{C}\begin{bmatrix} q_x(t_j) \\ q_u(t_j) \\ \dot{q}_x(t_j) \\ \dot{q}_u(t_j) \end{bmatrix}$$

where the state-transition matrix C is

$$\begin{bmatrix} e^{-\zeta_x\omega_x\tau}[\hat{c}_x+\frac{\zeta_x\omega_x}{\omega_{xd}}\hat{s}_x] & 0 & \frac{e^{-\zeta_x\omega_x\tau}}{\omega_{xd}}\hat{s}_x & 0 \\ 0 & e^{-\zeta_u\omega_u\tau}[\hat{c}_u+\frac{\zeta_u\omega_u}{\omega_{ud}}\hat{s}_u] & 0 & \frac{e^{-\zeta_u\omega_u\tau}}{\omega_{ud}}\hat{s}_u \\ -\frac{\omega_x^{\,2}}{\omega_{xd}}e^{-\zeta_x\omega_x\tau}\hat{s}_x & 0 & e^{-\zeta_x\omega_x\tau}[\hat{c}_x-\frac{\zeta_x\omega_x}{\omega_{xd}}\hat{s}_x] & 0 \\ 0 & -\frac{\omega_u^{\,2}}{\omega_{ud}}e^{-\zeta_u\omega_u\tau}\hat{s}_u & 0 & e^{-\zeta_u\omega_u\tau}[\hat{c}_u-\frac{\zeta_u\omega_u}{\omega_{ud}}\hat{s}_u] \end{bmatrix}$$

and $\omega_{xd}=\omega_x\sqrt{1-\zeta_x^{\,2}}$ is the damped natural frequency of the tool, $\omega_{ud}=\omega_u\sqrt{1-\zeta_u^{\,2}}$ is the damped natural frequency of the workpiece, and $\hat{c}_x=\cos(\omega_{xd}\tau)$, $\hat{s}_x=\sin(\omega_{xd}\tau)$, $\hat{c}_u=\cos(\omega_{ud}\tau)$, and $\hat{s}_u=\sin(\omega_{ud}\tau)$.

Inserting the third and fourth expressions from equation (2.25); that is,

$$\dot{q}_x(t_{j+1}^-)=\mathrm{C}_{31}q_x(t_j)+\mathrm{C}_{33}\dot{q}_x(t_j)$$
$$\dot{q}_u(t_{j+1}^-)=\mathrm{C}_{42}q_u(t_j)+\mathrm{C}_{44}\dot{q}_u(t_j)$$

into equation (2.30), the result is

$$\dot{q}_x(t_{j+1})=\dot{q}_x(t_{j+1}^-)+\tau_2\frac{K_t w}{m_x}\left[q_x(t_j)-q_x(t_{j+1}^-)+q_u(t_j)-q_u(t_{j+1}^-)+\mathrm{h}_0\right]$$
$$\dot{q}_u(t_{j+1})=\dot{q}_u(t_{j+1}^-)+\tau_2\frac{K_t w}{m_u}\left[q_x(t_j)-q_x(t_{j+1}^-)+q_u(t_j)-q_u(t_{j+1}^-)+\mathrm{h}_0\right]$$

The following equations for the linear cutting force can be obtained:

$$\begin{aligned}\dot{q}_x(t_{j+1})&=\mathrm{C}_{31}q_x(t_j)+\mathrm{C}_{33}\dot{q}_x(t_j)\\&\quad+\tau_2\frac{K_t w}{m_x}[q_x(t_j)-\mathrm{C}_{11}q_x(t_j)-\mathrm{C}_{13}\dot{q}_x(t_j)+q_u(t_j)-\mathrm{C}_{22}q_u(t_j)-\mathrm{C}_{24}\dot{q}_u(t_j)+\mathrm{h}_0]\\ \dot{q}_u(t_{j+1})&=\mathrm{C}_{42}q_u(t_j)+C_{44}\dot{q}_u(t_j)\\&\quad+\tau_2\frac{K_t w}{m_u}[q_x(t_j)-\mathrm{C}_{11}q_x(t_j)-\mathrm{C}_{13}\dot{q}_x(t_j)+q_u(t_j)-\mathrm{C}_{22}q_u(t_j)-\mathrm{C}_{24}\dot{q}_u(t_j)+\mathrm{h}_0]\end{aligned}$$

Assuming that the position of the oscillating tool and workpiece remain constant during interaction so that $q_x(t_{j+1}) \approx q_x(t_{j+1}^-)$ and $q_u(t_{j+1}) \approx q_u(t_{j+1}^-)$, one has

$$q_x(t_{j+1}) = \mathrm{C}_{11} q_x(t_j) + \mathrm{C}_{13} \dot{q}_x(t_j)$$
$$q_u(t_{j+1}) = \mathrm{C}_{22} q_u(t_j) + \mathrm{C}_{24} \dot{q}_u(t_j)$$

from the first and second expressions in equation (2.25).

Combining the previous two pairs of equations together, one arrives at equation (2.32) for the linear cutting force model.

$$\begin{bmatrix} q_x(t_{j+1}) \\ q_u(t_{j+1}) \\ \dot{q}_x(t_{j+1}) \\ \dot{q}_u(t_{j+1}) \end{bmatrix} = \mathrm{C} \begin{bmatrix} q_x(t_j) \\ q_u(t_j) \\ \dot{q}_x(t_j) \\ \dot{q}_u(t_j) \end{bmatrix} + \begin{bmatrix} 0 \\ 0 \\ \tau_2 \dfrac{K_t w}{m_x} [(1-\mathrm{C}_{11}) q_x(t_j) - \mathrm{C}_{13} \dot{q}_x(t_j) + (1-\mathrm{C}_{22}) q_u(t_j) - \mathrm{C}_{24} \dot{q}_u(t_j) + \mathrm{h}_0] \\ \tau_2 \dfrac{K_t w}{m_u} [(1-\mathrm{C}_{11}) q_x(t_j) - \mathrm{C}_{13} \dot{q}_x(t_j) + (1-\mathrm{C}_{22}) q_u(t_j) - \mathrm{C}_{24} \dot{q}_u(t_j) + \mathrm{h}_0] \end{bmatrix}$$

By using equations (2.25) and (2.31), the same process can be used for the 3/4 rule cutting force model to obtain equation (2.33).

$$\begin{bmatrix} q_x(t_{j+1}) \\ q_u(t_{j+1}) \\ \dot{q}_x(t_{j+1}) \\ \dot{q}_u(t_{j+1}) \end{bmatrix} = \mathrm{C} \begin{bmatrix} q_x(t_j) \\ q_u(t_j) \\ \dot{q}_x(t_j) \\ \dot{q}_u(t_j) \end{bmatrix} + \begin{bmatrix} 0 \\ 0 \\ \tau_2 \dfrac{K w}{m_x} [(1-\mathrm{C}_{11}) q_x(t_j) - \mathrm{C}_{13} \dot{q}_x(t_j) + (1-\mathrm{C}_{22}) q_u(t_j) - \mathrm{C}_{24} \dot{q}_u(t_j) + \mathrm{h}_0]^{3/4} \\ \tau_2 \dfrac{K w}{m_u} [(1-\mathrm{C}_{11}) q_x(t_j) - \mathrm{C}_{13} \dot{q}_x(t_j) + (1-\mathrm{C}_{22}) q_u(t_j) - \mathrm{C}_{24} \dot{q}_u(t_j) + \mathrm{h}_0]^{3/4} \end{bmatrix}$$

To derive the fixed points for the two degree-of-freedom system with the linear cutting force model, one sets

$$
\begin{aligned}
x_e &= q_x(t_{j+1}) = q_x(t_j) \\
u_e &= q_u(t_{j+1}) = q_u(t_j) \\
v_e &= \dot{q}_x(t_{j+1}) = \dot{q}_x(t_j) \\
w_e &= \dot{q}_u(t_{j+1}) = \dot{q}_u(t_j)
\end{aligned}
$$

By substituting x_e, u_e, v_e, and w_e into equation (2.33),

$$
\begin{bmatrix} x_e \\ u_e \\ v_e \\ w_e \end{bmatrix} = \begin{bmatrix} \mathrm{C}_{11} & 0 & \mathrm{C}_{13} & 0 \\ 0 & \mathrm{C}_{22} & 0 & \mathrm{C}_{24} \\ \mathrm{C}_{31} & 0 & \mathrm{C}_{33} & 0 \\ 0 & \mathrm{C}_{42} & 0 & \mathrm{C}_{44} \end{bmatrix} \begin{bmatrix} x_e \\ u_e \\ v_e \\ w_e \end{bmatrix}
$$

$$
+ \begin{bmatrix} 0 \\ 0 \\ \tau_2 \dfrac{K_t w}{m_x}[(1-\mathrm{C}_{11})x_e - \mathrm{C}_{13}v_e + (1-\mathrm{C}_{22})u_e - \mathrm{C}_{24}w_e + \mathrm{h}_0] \\ \tau_2 \dfrac{K_t w}{m_u}[(1-\mathrm{C}_{11})x_e - \mathrm{C}_{13}v_e + (1-\mathrm{C}_{22})u_e - \mathrm{C}_{24}w_e + \mathrm{h}_0] \end{bmatrix}
$$

and solving explicitly for x_e, u_e, v_e, and w_e, the fixed points for the linear cutting force are found to be

$$
\begin{aligned}
x_e &= \frac{K_t w \tau_2 \mathrm{h}_0 \mathrm{C}_{13}}{m_x[1 + \det(\hat{\mathrm{C}}) - \mathrm{tr}(\hat{\mathrm{C}})]} \\
u_e &= \frac{K_t w \tau_2 \mathrm{h}_0 \mathrm{C}_{24}}{m_u[1 + \det(\overset{*}{\mathrm{C}}) - \mathrm{tr}(\overset{*}{\mathrm{C}})]} \\
v_e &= \frac{K_t w \tau_2 \mathrm{h}_0 (1-\mathrm{C}_{11})}{m_x[1 + \det(\hat{\mathrm{C}}) - \mathrm{tr}(\hat{\mathrm{C}})]} \\
w_e &= \frac{K_t w \tau_2 \mathrm{h}_0 (1-\mathrm{C}_{22})}{m_u[1 + \det(\overset{*}{\mathrm{C}}) - \mathrm{tr}(\overset{*}{\mathrm{C}})]}
\end{aligned}
$$

where $\hat{C}$ is obtained from the state-transition matrix A of the tool in equation (2.11)

$$\hat{C} = A = \begin{bmatrix} A_{11} & A_{12} \\ A_{21} & A_{22} \end{bmatrix} = \begin{bmatrix} C_{11} & C_{13} \\ C_{31} & C_{33} \end{bmatrix}$$

and $\overset{*}{C}$ is the state-transition matrix of the workpiece

$$\overset{*}{C} = \begin{bmatrix} C_{22} & C_{24} \\ C_{42} & C_{44} \end{bmatrix}$$

To solve for the fixed points for the 3/4 rule cutting force model, the Taylor series is expanded for

$$h_{xu}{}^{3/4}(t_j) = [h_0 + \Delta h_{xu}(t_j)]^{3/4}$$

where

$$\Delta h_{xu}(t_j) = (1 - C_{11})q_x(t_j) - C_{13}\dot{q}_x(t_j) + (1 - C_{22})q_u(t_j) - C_{24}\dot{q}_u(t_j)$$

Taking only linear terms from the Taylor series expansion

$$\begin{aligned} h_{xu}{}^{3/4}(t_j) &\approx h_0{}^{3/4} + \frac{3}{4}\frac{\Delta h_{xu}(t_j)}{h_0{}^{1/4}} \\ &\approx h_0{}^{3/4} + \frac{3}{4}\frac{(1 - C_{11})q_x(t_j) - C_{13}\dot{q}_x(t_j) + (1 - C_{22})q_u(t_j) - C_{24}\dot{q}_u(t_j)}{h_0{}^{1/4}} \end{aligned}$$

the linearized form of equation (2.33) now becomes

$$\begin{bmatrix} q_x(t_{j+1}) \\ q_u(t_{j+1}) \\ \dot{q}_x(t_{j+1}) \\ \dot{q}_u(t_{j+1}) \end{bmatrix} = \mathrm{C} \begin{bmatrix} q_x(t_j) \\ q_u(t_j) \\ \dot{q}_x(t_j) \\ \dot{q}_u(t_j) \end{bmatrix}$$

$$+ \begin{bmatrix} 0 \\ 0 \\ \tau_2 \dfrac{Kw}{m_x}[\mathrm{h_0}^{3/4} + \dfrac{3}{4}\dfrac{(1-\mathrm{C}_{11})q_x(t_j) - \mathrm{C}_{13}\dot{q}_x(t_j) + (1-\mathrm{C}_{22})q_u(t_j) - \mathrm{C}_{24}\dot{q}_u(t_j)}{\mathrm{h_0}^{1/4}}] \\ \tau_2 \dfrac{Kw}{m_u}[\mathrm{h_0}^{3/4} + \dfrac{3}{4}\dfrac{(1-\mathrm{C}_{11})q_x(t_j) - \mathrm{C}_{13}\dot{q}_x(t_j) + (1-\mathrm{C}_{22})q_u(t_j) - \mathrm{C}_{24}\dot{q}_u(t_j)}{\mathrm{h_0}^{1/4}}] \end{bmatrix}$$

By substituting x_e, u_e, v_e, and w_e into this linearized form

$$\begin{bmatrix} x_e \\ u_e \\ v_e \\ w_e \end{bmatrix} = \mathrm{C} \begin{bmatrix} x_e \\ u_e \\ v_e \\ w_e \end{bmatrix} + \begin{bmatrix} 0 \\ 0 \\ \tau_2 \dfrac{Kw}{m_x}[\mathrm{h_0}^{3/4} + \dfrac{3}{4}\dfrac{(1-\mathrm{C}_{11})x_e - \mathrm{C}_{13}v_e + (1-\mathrm{C}_{22})u_e - \mathrm{C}_{24}w_e}{\mathrm{h_0}^{1/4}}] \\ \tau_2 \dfrac{Kw}{m_u}[\mathrm{h_0}^{3/4} + \dfrac{3}{4}\dfrac{(1-\mathrm{C}_{11})x_e - \mathrm{C}_{13}v_e + (1-\mathrm{C}_{22})u_e - \mathrm{C}_{24}w_e}{\mathrm{h_0}^{1/4}}] \end{bmatrix}$$

and solving explicitly for x_e and v_e, the fixed points for the 3/4 rule cutting force are found to be

$$x_e = \frac{Kw\tau_2 \mathrm{h_0}^{3/4}\mathrm{C}_{13}}{m_x[1 + \det(\hat{\mathrm{C}}) - \mathrm{tr}(\hat{\mathrm{C}})]}$$

$$u_e = \frac{Kw\tau_2 \mathrm{h_0}^{3/4}\mathrm{C}_{24}}{m_u[1 + \det(\overset{*}{\mathrm{C}}) - \mathrm{tr}(\overset{*}{\mathrm{C}})]}$$

$$v_e = \frac{Kw\tau_2 \mathrm{h_0}^{3/4}(1-\mathrm{C}_{11})}{m_x[1 + \det(\hat{\mathrm{C}}) - \mathrm{tr}(\hat{\mathrm{C}})]}$$

$$w_e = \frac{Kw\tau_2 \mathrm{h_0}^{3/4}(1-\mathrm{C}_{22})}{m_u[1 + \det(\overset{*}{\mathrm{C}}) - \mathrm{tr}(\overset{*}{\mathrm{C}})]}$$

To solve for the Jacobian matrix of the linear cutting force model, equation (2.32) is rearranged to form

$$\begin{bmatrix} q_x(t_{j+1}) \\ q_u(t_{j+1}) \\ \dot{q}_x(t_{j+1}) \\ \dot{q}_u(t_{j+1}) \end{bmatrix} = \mathrm{E}_{\mathrm{LCF}}^{\mathrm{2DOF}} \begin{bmatrix} q_x(t_j) \\ q_u(t_j) \\ \dot{q}_x(t_j) \\ \dot{q}_u(t_j) \end{bmatrix} + \begin{bmatrix} 0 \\ 0 \\ \tau_2 \dfrac{K_t w \mathrm{h}_0}{m_x} \\ \tau_2 \dfrac{K_t w \mathrm{h}_0}{m_u} \end{bmatrix}$$

where matrix $\mathrm{E}_{\mathrm{LCF}}^{\mathrm{2DOF}}$ is determined to be

$$\begin{bmatrix} \mathrm{C}_{11} q_x(t_j) & 0 & \mathrm{C}_{13}\dot{q}_x(t_j) & 0 \\ 0 & \mathrm{C}_{22} q_u(t_j) & 0 & \mathrm{C}_{24}\dot{q}_u(t_j) \\ [\mathrm{C}_{31} + \dfrac{K_t w \tau_2}{m_x}(1-\mathrm{C}_{11})] q_x(t_j) & \dfrac{K_t w \tau_2}{m_x}(1-\mathrm{C}_{22}) q_u(t_j) & [\mathrm{C}_{33} - \dfrac{K_t w \tau_2}{m_x}\mathrm{C}_{13}]\dot{q}_x(t_j) & -\dfrac{K_t w \tau_2}{m_x}\mathrm{C}_{24}\dot{q}_u(t_j) \\ \dfrac{K_t w \tau_2}{m_u}(1-\mathrm{C}_{11}) q_x(t_j) & [\mathrm{C}_{24} + \dfrac{K_t w \tau_2}{m_u}(1-\mathrm{C}_{22})] q_u(t_j) & -\dfrac{K_t w \tau_2}{m_u}\mathrm{C}_{13}\dot{q}_x(t_j) & [\mathrm{C}_{44} - \dfrac{K_t w \tau_2}{m_u}\mathrm{C}_{24}]\dot{q}_u(t_j) \end{bmatrix}$$

Forming the Jacobian from $\mathrm{E}_{\mathrm{LCF}}^{\mathrm{2DOF}}$ leads to

$$\mathrm{D} = \begin{bmatrix} \mathrm{C}_{11} & 0 & \mathrm{C}_{13} & 0 \\ 0 & \mathrm{C}_{22} & 0 & \mathrm{C}_{24} \\ \mathrm{C}_{31} + \hat{\mathrm{w}}_x(1-\mathrm{C}_{11}) & \hat{\mathrm{w}}_x(1-\mathrm{C}_{22}) & \mathrm{C}_{33} - \hat{\mathrm{w}}_x\mathrm{C}_{13} & -\hat{\mathrm{w}}_x\mathrm{C}_{24} \\ \hat{\mathrm{w}}_u(1-\mathrm{C}_{11}) & \mathrm{C}_{42} + \hat{\mathrm{w}}_u(1-\mathrm{C}_{22}) & -\hat{\mathrm{w}}_u\mathrm{C}_{13} & C_{44} - \hat{\mathrm{w}}_u\mathrm{C}_{24} \end{bmatrix}$$

where the dimensionless chip widths for the linear cutting force are

$$\hat{w}_x = \frac{K_t w \tau_2}{m_x}$$

$$\hat{w}_u = \frac{K_t w \tau_2}{m_u}$$

To solve for the Jacobian matrix for the system with the 3/4 rule cutting force, the linearized form of equation (2.33) is rearranged to obtain

$$\begin{bmatrix} q_x(t_{j+1}) \\ q_u(t_{j+1}) \\ \dot{q}_x(t_{j+1}) \\ \dot{q}_u(t_{j+1}) \end{bmatrix} = \mathrm{E}_{3/4\mathrm{CF}}^{2\mathrm{DOF}} \begin{bmatrix} q_x(t_j) \\ q_u(t_j) \\ \dot{q}_x(t_j) \\ \dot{q}_u(t_j) \end{bmatrix} + \begin{bmatrix} 0 \\ 0 \\ \tau_2 \dfrac{K w \mathrm{h}_0^{3/4}}{m_x} \\ \tau_2 \dfrac{K w \mathrm{h}_0^{3/4}}{m_u} \end{bmatrix}$$

where matrix $\mathrm{E}_{3/4\mathrm{CF}}^{2\mathrm{DOF}}$ is determined to be

$$\begin{bmatrix} \mathrm{C}_{11} q_x(t_j) & 0 & \mathrm{C}_{13}\dot{q}_x(t_j) & 0 \\ 0 & \mathrm{C}_{22} q_u(t_j) & 0 & \mathrm{C}_{24}\dot{q}_u(t_j) \\ [\mathrm{C}_{31} + \frac{3}{4}\frac{K w \tau_2}{m_x \mathrm{h}_0^{1/4}}(1-\mathrm{C}_{11})] q_x(t_j) & \frac{3}{4}\frac{K w \tau_2}{m_x \mathrm{h}_0^{1/4}}(1-\mathrm{C}_{22}) q_u(t_j) & [\mathrm{C}_{33} - \frac{3}{4}\frac{K w \tau_2}{m_x \mathrm{h}_0^{1/4}}\mathrm{C}_{13})]\dot{q}_x(t_j) & -\frac{3}{4}\frac{K w \tau_2}{m_x \mathrm{h}_0^{1/4}}\mathrm{C}_{24}\dot{q}_u(t_j) \\ \frac{3}{4}\frac{K w \tau_2}{m_u \mathrm{h}_0^{1/4}}(1-\mathrm{C}_{11}) q_x(t_j) & [\mathrm{C}_{42} + \frac{3}{4}\frac{K w \tau_2}{m_u \mathrm{h}_0^{1/4}}(1-\mathrm{C}_{22})] q_u(t_j) & -\frac{3}{4}\frac{K w \tau_2}{m_u \mathrm{h}_0^{1/4}}\mathrm{C}_{13}\dot{q}_x(t_j) & [\mathrm{C}_{44} - \frac{3}{4}\frac{K w \tau_2}{m_u \mathrm{h}_0^{1/4}}\mathrm{C}_{24}\dot{q}_u(t_j) \end{bmatrix}$$

Constructing the Jacobian from $\mathrm{E}_{3/4\mathrm{CF}}^{2\mathrm{DOF}}$ leads to

$$\mathrm{D} = \begin{bmatrix} \mathrm{C}_{11} & 0 & \mathrm{C}_{13} & 0 \\ 0 & \mathrm{C}_{22} & 0 & \mathrm{C}_{24} \\ \mathrm{C}_{31} + \hat{\mathrm{w}}_x(1-\mathrm{C}_{11}) & \hat{\mathrm{w}}_x(1-\mathrm{C}_{22}) & \mathrm{C}_{33} - \hat{\mathrm{w}}_x \mathrm{C}_{13} & -\hat{\mathrm{w}}_x \mathrm{C}_{24} \\ \hat{\mathrm{w}}_u(1-\mathrm{C}_{11}) & \mathrm{C}_{42} + \hat{\mathrm{w}}_u(1-\mathrm{C}_{22}) & -\hat{\mathrm{w}}_u \mathrm{C}_{13} & C_{44} - \hat{\mathrm{w}}_u \mathrm{C}_{24} \end{bmatrix}$$

where the dimensionless chip widths for the 3/4 rule cutting force are given by

$$\hat{w}_x = \frac{3}{4}\frac{K w \tau_2}{m_x \mathrm{h}_0^{1/4}}$$

$$\hat{w}_u = \frac{3}{4}\frac{K w \tau_2}{m_u \mathrm{h}_0^{1/4}}$$

Linearizing around the fixed points, the generalized local dynamics is described by

$$\begin{bmatrix} q_x(t_{j+1}) \\ q_u(t_{j+1}) \\ \dot{q}_x(t_{j+1}) \\ \dot{q}_u(t_{j+1}) \end{bmatrix} = \begin{bmatrix} x_e \\ u_e \\ v_e \\ w_e \end{bmatrix} + \mathrm{D} \begin{bmatrix} q_x(t_j) \\ q_u(t_j) \\ q_x(t_j) \\ \dot{q}_u(t_j) \end{bmatrix}$$

where x_e, u_e, v_e, w_e, $\hat{w}_x$, and $\hat{w}_u$ are based on respective cutting force models.

Appendix B

MATLAB Programs for Stability Computations

In this appendix, MATLAB programs used to carry out stability computations (flip and Neimark-Sacker bifurcations) are provided. These programs are used to generate the analytical predictions shown in Figures 5.9 to 5.14.

B.1 Two DOF System: Flip Bifurcation Computations

```
% Parameter Inputs
rpmmin=13000;                                   % Min Spindle Speed (rpm)
rpmmax=22000;                                   % Max Spindle Speed (rpm)
s=5;                                            % # of steps

% Corrects Inputs for Matrix Calculations
rpm=rpmmin:s:rpmmax;
one=linspace(1,1,((rpmmax-rpmmin)/s)+1);

% Parameter Inputs (continued)

% tool:
m_x=linspace(0.02,0.02,((rpmmax-rpmmin)/s)+1);     % mass (kg)
zeta_x=linspace(0.01,0.01,((rpmmax-rpmmin)/s)+1);  % damping ratio
k_x=linspace(8e5,8e5,((rpmmax-rpmmin)/s)+1);       % stiffness (N/m)

% workpiece:
m_u=linspace(0.1,0.1,((rpmmax-rpmmin)/s)+1);       % mass (kg)
zeta_u=linspace(0.01,0.01,((rpmmax-rpmmin)/s)+1);  % damping ratio
k_u=linspace(1e6,1e6,((rpmmax-rpmmin)/s)+1);       % stiffness (N/m)
Kt=linspace(600e6,600e6,((rpmmax-rpmmin)/s)+1);    % mat const (N/m^2)
rho=linspace(0.1,0.1,((rpmmax-rpmmin)/s)+1);       % cut pd to total pd
N=2;                                               % # teeth on tool

% Unit Definitions/Conversions
omega=rpm./60;
t=1./(N.*omega);
w_x=sqrt(k_x./m_x);
w_xd=w_x.*sqrt(1-zeta_x.^2);
w_u=sqrt(k_u./m_u);
w_ud=w_u.*sqrt(1-zeta_u.^2);
mh=m_x./m_u;
```

```
% State Transition Matrix Terms for the Non-Cutting Period
A11=exp(zeta_x.*w_x.*t).*(cos(w_xd.*t)+zeta_x.*w_x./w_xd.*...
    sin(w_xd.*t));
A13=exp(-zeta_x.*w_x.*t)./w_xd.*sin(w_xd.*t);
A22=exp(-zeta_u.*w_u.*t).*(cos(w_ud.*t)+zeta_u.*w_u./w_ud.*...
    sin(w_ud.*t));
A24=exp(-zeta_u.*w_u.*t)./w_ud.*sin(w_ud.*t);
A31=-exp(-zeta_x.*w_x.*t).*w_x.^2./w_xd.*sin(w_xd.*t);
A33=exp(-zeta_x.*w_x.*t).*(cos(w_xd.*t)-zeta_x.*w_x./w_xd.*...
    sin(w_xd.*t));
A42=-exp(-zeta_u.*w_u.*t).*w_u.^2./w_ud.*sin(w_ud.*t);
A44=exp(-zeta_u.*w_u.*t).*(cos(w_ud.*t)-zeta_u.*w_u./w_ud.*...
    sin(w_ud.*t));

% ADOC calculations
wh_crf=1/2.*(1+A44.*A11.*A33+A11.*A22.*A44+A22.*A11.*A33-...
    A44.*A13.*A31-A22.*A13.*A31-A11.*A24.*A42+A11+A22+A33+A44+...
    A22.*A33.*A44+A11.*A22.*A33.*A44-A11.*A42.*A24.*A33-...
    A31.*A22.*A13.*A44+A31.*A42.*A13.*A24-A42.*A24.*A33+...
    A33.*A44+A22.*A44-A24.*A42+A11.*A33-...
    A13.*A31+A11.*A22+A11.*A44+A33.*A22)./...
    (A13+A13.*A22+A13.*A44+A22.*A13.*A44-A42.*A13.*A24+mh.*A24+...
    mh.*A24.*A11+mh.*A24.*A33+mh.*A24.*A11.*A33-mh.*A24.*A13.*A31);
w_crf=wh_crf.*m_x./(Kt.*rho.*t);

% Stability Prediction Plot for the 2 DOF Linear Cutting Force Model
plot(rpm,w_crf,'b-');
axis([1.3e4 2.2e4 0 .008]);
xlabel('Spindle Speed (rpm)');
ylabel('ADOC (m)');
title('2 DOF Linear Cutting Force - Flip Bifurcations');
```

B.2 Two DOF System: Neimark Sacker Bifurcation Computations

```
% Parameter Inputs
m_x=0.02;                       % tool mass (kg)
zeta_x=0.01;                    % tool damping ratio
k_x=8e5;                        % tool stiffness (N/m)
m_u=0.01;                       % workpiece mass (kg)
zeta_u=0.01;                    % workpiece damping ratio
k_u=1e6;                        % workpiece stiffness (N/m)
Kt=6e8;                         % workpiece material constant (N/m^2)
rho=0.1;                        % cutting pd to total spindle pd
N=2;                            % # of teeth on the tool
rpm=16000;                      % Spindle Speed (rpm)

% Eigenvalue Guess: a + bi
a=0.8408;
b=0.11469;

% Unit Definitions/Conversions
omega=rpm/60;
t=1/(N*omega);
w_x=sqrt(k_x/m_x);
```

```
w_xd=w_x*sqrt(1-zeta_x^2);
w_u=sqrt(k_u./m_u);
w_ud=w_u*sqrt(1-zeta_u^2);
mh=m_x/m_u;

% State Transition Matrix Terms for the Non-Cutting Period
A11=exp(-zeta_x*w_x*t)*(cos(w_xd*t)+zeta_x*w_x/w_xd*sin(w_xd*t));
A13=exp(-zeta_x*w_x*t)/w_xd*sin(w_xd*t);
A22=exp(-zeta_u*w_u*t)*(cos(w_ud*t)+zeta_u*w_u/w_ud*sin(w_ud*t));
A24=exp(-zeta_u*w_u*t)/w_ud*sin(w_ud*t);
A31=-exp(-zeta_x*w_x*t)*w_x^2/w_xd*sin(w_xd*t);
A33=exp(-zeta_x*w_x*t)*(cos(w_xd*t)-zeta_x*w_x/w_xd*sin(w_xd*t));
A42=-exp(-zeta_u*w_u*t)*w_u^2/w_ud*sin(w_ud*t);
A44=exp(-zeta_u*w_u*t)*(cos(w_ud*t)-zeta_u*w_u/w_ud*sin(w_ud*t));

% ADOC calculations
wh_crns=(A11*A22*A33*A44+A13*A24*A31*A42-A11*A24*A33*A42-...
    A13*A22*A31*A44-a^2-b^2)/(A13*A22*A44-A13*A24*A42+...
    mh*A11*A24*A33-mh*A13*A24*A31);
w_crns=wh_crns*m_x/(Kt*rho*t);
w=w_crns;
wh=w*rho*Kt*t/m_x;

% State Transition Matrix for the Cutting Period
B=[A11 0 A13 0; 0 A22 0 A24;...
    A31+wh*(1-A11) wh*(1-A22) A33-wh*A13 -wh*A24;...
    mh*wh*(1-A11) A42+mh*wh*(1-A22) -mh*wh*A13 A44-mh*wh*A24];

% Solve for the Eigenvalues of Matrix B
e=eig(B);
c=e(1,:);
d=e(2,:);

% Checks for the Magnitude of the Eigenvalue Guess
magab=sqrt(a^2+b^2);

% Checks for Product of Magnitudes of other Eigenvalue Pair to = 1
check=c*d;
```

Appendix C

MATLAB Programs for DDE Numerical Computations

In this appendix, MATLAB programs used to carry out integration of the delay differential equations are provided. These programs are used to generate the delay differential equation numerical predictions shown in Figures 5.1 and 5.9.

C.1 Single DOF System: DDE Numerical Computations

Main Program

```
global g
close all; clf; clc;

% Parameter Inputs
m=0.0431;                       % tool mass (kg)
zeta=0.016691;                  % tool damping ratio
k=1.4e+6;                       % tool stiffness (N/m)
kt=500e+6;                      % workpiece material constant (N/m^2)
rho=0.14;                       % cutting pd to total spindle pd
feed=0.000102;                  % feed (m/tooth)
N=2;                            % number of teeth on the tool
w=.00203;                       % ADOC (m)
omega_rpm=13500;                % spindle speed (rpm)
q0=[0.0006;0.001];              % initial conditions (m)
T=200;                          % # of total spindle periods divided by 2

% Unit Definitions/Conversions
c=zeta*2.0*sqrt(m*k);
omega=2*pi*omega_rpm/60;
f=omega/(2*pi)*N*feed;

% Time Delays
tau=2*pi/(N*omega);
tau1=rho*tau;
tau2=(1-rho)*tau;

% Initial Settings
ti=0;
tf=0;
q_0=zeros(2,2*T);
q_0(:,1)=q0;
q=q0(1);
```

```
q_dot=q0(2);
t=0;

for i=1:2*T;

    if (mod(i,2)==1)            % Cutting Period

        g=1;
        tf=ti+tau2;

    else                        % Non-cutting Period

        g=0;
        tf=ti+tau1;

    end

    tlength=[ti;tf];

    % Option 1 - Call the 1 DOF Linear Cutting Force equation
    sol=dde23(@LinearCF1DOFf,...
        [tau],q_0(:,i),tlength,[],m,k,kt,w,c,f,rho,tau);

    % Option 2 - Call the 1 DOF 3/4 Cutting Force equation
    %sol=dde23(@ThreeQuarterCF1DOFf,...
    %    [tau],q_0(:,i),tlength,[],m,k,kt,w,c,f,rho,tau);

    q_0(:,i+1)=sol.y(:,length(sol.y));
    ti=tf;
    q=cat(1,q,sol.y(1,2:length(sol.y(1,:)))');
    q_dot=cat(1,q_dot,sol.yp(1,2:length(sol.yp(1,:)))');
    t=cat(1,t,sol.x(1,2:length(sol.x))');

end

% Response Plot
figure(1);
subplot(2,1,1);
plot(t,real(q));
xlabel('t (s)');
ylabel('q_x(t) (m)');
hold on;

% Phase Portrait Plot
subplot(2,1,2);
plot(real(q),real(q_dot));
xlabel('q_x(t) (m)');
ylabel('q_x''(t) (m/s)');
```

Linear Cutting Force Function

```
function v=LinearCF1DOFf(t,y,Z,m,k,kt,w,c,f,rho,tau)
global g
ylag1 = Z(:,1);
```

```
v = zeros(2,1);

% Linear Cutting Force Model 1 DOF State Space Equations
v=[y(2); -k/m*y(1)-c/m*y(2)+g*kt*w/m*(ylag1(1)-y(1)+f*tau)];
```

3/4 Rule Cutting Force Function

```
function v=ThreeQuarterCF1DOFf(t,y,Z,m,k,kt,w,c,f,rho,tau)
global g
ylag1 = Z(:,1);
v = zeros(2,1);

% 3/4 Cutting Force Model 1 DOF State Space Equations
v=[y(2); -k/m*y(1)-c/m*y(2)+g*kt*(f*tau)^(1/4)*w/m*(ylag1(1)-...
    y(1)+f*tau)^(3/4)];
```

C.2 Two DOF System: DDE Numerical Computations

Main Program

```
global g
close all; clf; clc;

% Parameter Inputs
mx=0.02;                        % tool mass (kg)
zetax=0.01;                     % tool damping ratio
kx=8e+5;                        % tool stiffness (N/m)
mu=0.1;                         % workpiece mass (kg)
zetau=0.01;                     % workpiece damping ratio
ku=1.0e+6;                      % workpiece stiffness (N/m)
kt=600e+6;                      % workpiece material constant (N/m^2)
rho=0.2;                        % cutting pd to total spindle pd
feed=5.1e-4;                    % feed (m/tooth)
N=2;                            % number of teeth on the tool
w=.00023;                       % ADOC (m)
omega_rpm=17000;                % spindle speed (rpm)
q0=[0.0006;0.0006;0.001;0.001]; % initial conditions (m)
T=300;                          % # of total spindle pds divided by 2

% Unit Definitions/Conversions
cx=zetax*2.0*sqrt(mx*kx);
cu=zetau*2.0*sqrt(mu*ku);
omega=2*pi*omega_rpm/60;
f=omega/(2*pi)*N*feed;
```

```
% Time Delays
tau=2*pi/(N*omega);
tau1=tau*rho;
tau2=tau*(1-rho);

% Initial Settings
ti=0;
tf=0;
q_0=zeros(4,2*T);
q_0(:,1)=q0;
qx=q0(1);
qu=q0(2);
qx_dot=q0(3);
qu_dot=q0(4);
t=0;

for i=1:2*T;

    if (mod(i,2)==1)            % Cutting Period

        g=1;
        tf=ti+tau2;

    else                        % Non-cutting Period

        g=0;
        tf=ti+tau1;

    end

    tlength=[ti;tf];

    % Option 1 - Call the 2 DOF Linear Cutting Force equation
    %sol = dde23(@LinearCF2DOFf,[tau],...
    %    q_0(:,i),tlength,[],mx,kx,mu,ku,kt,w,cx,cu,f,rho,tau);

    % Option 2 = Call the 2 DOF Linear Cutting Force equation
    sol = dde23(@ThreeQuarterCF2DOFf,...
        [tau],q_0(:,i),tlength,[],mx,kx,mu,ku,kt,w,cx,cu,f,rho,tau);

    q_0(:,i+1)=sol.y(:,length(sol.y));
    ti=tf;
    qx=cat(1,qx,sol.y(1,2:length(sol.y(1,:)))');
    qu=cat(1,qu,sol.y(1,2:length(sol.y(2,:)))');
    qx_dot=cat(1,qx_dot,sol.yp(1,2:length(sol.yp(1,:)))');
    qu_dot=cat(1,qu_dot,sol.yp(1,2:length(sol.yp(2,:)))');
    t=cat(1,t,sol.x(1,2:length(sol.x))');

end

% Response Plot for q_x
figure(1);
subplot(2,2,1);
plot(t,real(qx));
xlabel('time t');
ylabel('q_x(t)');
hold on;
```

```
% Response Plot for q_u
subplot(2,2,2);
plot(t,real(qu));
xlabel('time t');
ylabel('q_u(t)');

% Phase Portrait Plot for q_x
subplot(2,2,3);
plot(real(qx),real(qx_dot));
xlabel('q_x(t)');
ylabel('q_x''(t)');

% Phase Portrait Plot for q_u
subplot(2,2,4);
plot(real(qu),real(qu_dot));
xlabel('q_u(t)');
ylabel('q_u''(t)');
```

Linear Cutting Force Function

```
function v=LinearCF2DOFf(t,y,Z,mx,kx,mu,ku,kt,w,cx,cu,f,rho,tau)
global g
ylag1 = Z(:,1);
v = zeros(4,1);

% Linear Cutting Force Model 2 DOF State Space Equations
v=[y(3);...
    y(4);...
    -kx/mx*y(1)-cx/mx*y(3)+g*kt*w/mx*(ylag1(1)+ylag1(2)-y(1)-...
    y(2)+f*tau);...
    -ku/mu*y(2)-cu/mu*y(4)+g*kt*w/mu*(ylag1(1)+ylag1(2)-y(1)-...
    y(2)+f*tau)];
```

3/4 Rule Cutting Force Function

```
function v=ThreeQuarterCF2DOFf(t,y,Z,mx,kx,mu,ku,kt,w,cx,cu,f,rho,tau)
global g
ylag1 = Z(:,1);
v = zeros(4,1);

% 3/4 Cutting Force Model 2 DOF State Space Equations
v=[y(3);...
    y(4);...
    -kx/mx*y(1)-cx/mx*y(3)+g*kt*(f*tau)^(1/4)*w/mx*(ylag1(1)+...
    ylag1(2)-y(1)-y(2)+f*tau)^(3/4);...
    -ku/mu*y(2)-cu/mu*y(4)+g*kt*(f*tau)^(1/4)*w/mu*(ylag1(1)+...
    ylag1(2)-y(1)-y(2)+f*tau)^(3/4)];
```

Appendix D

UMCP Numerical Stability Prediction Programs

In this appendix, the original UMCP numerical stability prediction program and the modified UMCP numerical stability prediction program, used to carry out stability computations (flip and Neimark-Sacker bifurcations) are provided. These programs are used to generate UMCP stability program predictions for linear and 3/4 rule cutting forces shown in Figures 5.2 to 5.8 and Figures 5.10 to 5.14.

D.1 Matlab Programs for Linear Cutting Force Model

Main Program <linear_millingmain.m>

```
% MAIN PROGRAM TO GET THE STABILITY LOBE BY SEMI-DISCRETIZATION METHOD
% IN THIS CASE, WE WILL CONSIDER THE EFFECT OF FEED RATE ON TIME DELAY

function main
% num_tooth   - Number of teeth on the cutter
% r           - Radius of cutter (m)
% phi_n       - Normal rake angle (degree)
% omega       - Spindle Speed (rpm)
% feed        - Feed rate along x direction (m/s)
% feedcut     - Feed per tooth along x direction (m/tooth)
% rdoc        - Radial depth of cut (m)
% adoc        - Axial depth of cut (m)
% kt          - Tangential cutting coef from orthogonal cutting (N/m^2)
% kn          - Cutting coefficient proportional constant
% cp          - Viscous damping in the cutting process (N*s/m^2)
% friction    - Coulomb friction coefficient
% eta         - Helix angle of cylindrical end mill (degrees)
% mx          - Modal mass in x direction (kg)
% kx          - Modal stiffness in x direction (N/m)
% cx          - Viscous damping in x direction (N*s/m)
% theta_enter - Cutter entering angle (degree)
% theta_exit  - Cutter exit angle (degree)
% z1          - Dynamic integration lower limit (m)
% z2          - Dynamic integration upper limit (m)
% step        - Integration time step (s)

global mx xix kx my xiy ky mu ku xiu mv kv xiv feed;
```

```
global kt kn friction cp r eta phi_n num_tooth feedcut;
global omega1 omega2 delta_omega theta_enter theta_exit;
global adocL adocH delta_adoc int_time;

PI=3.14159;

% THE NUMBER OF STEPS FOR EVERY PERIOD
N=40;

% CALLS THE INPUT FUNCTION TO INPUT THE SYSTEM PARAMETERS
input_stepan;

% CHANGES THE DIMENSIONLESS DAMPING INTO cx, cy, cu, AND cv
cx=xix*2.0*sqrt(mx*kx);
cy=xiy*2.0*sqrt(my*ky);
cu=xiu*2.0*sqrt(mu*ku);
cv=xiv*2.0*sqrt(mv*kv);

% FORMS THE MASS, DAMPING AND STIFFNESS MATRICES
mm=[mx,my,mu,mv];
MC=diag(mm,0);
MC=inv(MC);
cc=[cx,cy,cu,cv];
CC=diag(cc,0);
kk=[kx,ky,ku,kv];
KC=diag(kk,0);

% CREATES TWO MATRICES FOR STATE SPACE EQUATIONS
AA=zeros(8,8);
BB=zeros(8,8);
kbar=zeros(4,4);
cbar=zeros(4,4);
zerobar=zeros(4,1);

s=zeros(2,2);
q=zeros(2,2);


% UNIT CONVERSIONS - CHANGES THE ANGLES FROM DEGREES TO RADIANS
eta=eta*PI/180.0;
omega1=2*PI*omega1/60.0;
omega2=2*PI*omega2/60.0;
delta_omega=2*PI*delta_omega/60.0;
theta_enter=theta_enter*PI/180.0;
theta_exit=theta_exit*PI/180.0;

% CALLS K1 AND K2
k1 = kn/cos(eta);
k2 = 1.0 + friction*(cos(phi_n)-kn*sin(phi_n))*tan(eta);

% DEFINES THE RANK OF THE MAPPING MATRICS
rankn=(N+1)*8;

% STABILITY PREDICTION USING PARAMETERS OF SPINDLE SPEED AND ADOC
BI=zeros(rankn,rankn);
jj=1;
ii=0;
```

```
for omega=omega1:delta_omega:omega2
   step=2*PI/omega/(N+0.5)/num_tooth;
   tn=2*PI/omega/num_tooth;
   excite_harmonics=(-omega:omega:6*omega)/2/PI;
   feed=omega/(2*PI)*num_tooth*feedcut;

   % CUTTING ENTRANCE OR EXIT ANGLE VARIATIONS DUE TO THE FEED
   delta_theta = asin(2*PI*feed/(2*omega*r*num_tooth));

   % TWO TIME DELAYS
   % FOR A SINGLE TIME DELAY, SET xdelay=ydelay AND xresidue=yresidue
   xdelay = floor(2*PI/(omega*num_tooth*step));
   ydelay = floor(4*PI*r/(num_tooth*step*(2*r*omega+feed)));
   xresidue = 2*PI/(omega*num_tooth*step)-xdelay+0.5;
   yresidue = 4*PI*r/(num_tooth*step*(2*r*omega+feed))-ydelay+0.5;
   adoc1=adocL;
   adoc2=adocH;
   adoc=adocH/2.0;

   while (adoc-adoc1)>1e-6 & (adoc2-adoc)>1e-6
      PHI=eye(rankn,rankn);

      for t=0:step:tn-step
         BI=[zeros(8,rankn);eye(rankn-8),zeros(rankn-8,8)];

% CALLS THE LINEAR CUTTING FORCE SUBROUTINE TO GET THE S AND Q MATRICES

[s,q]=cutzone1(t,theta_enter,theta_exit,delta_theta,adoc,r,omega,...
    eta,num_tooth,step,k1,k2,kt,cp);
         kbar=[s,s;s,s];
         cbar=[q,q;q,q];
         kbar1=kbar(:,1);
         cbar1=cbar(:,1);
         kbar2=kbar(:,2);
         cbar2=cbar(:,2);

         % X DIRECTION DELAY COEFFICIENT MATRICES
         kbar11=[kbar1,zerobar,kbar1,zerobar];
         cbar11=[cbar1,zerobar,cbar1,zerobar];

         % Y DIRECTION DELAY COEFFICIENT MATRICES
         kbar22=[zerobar,kbar2,zerobar,kbar2];
         cbar22=[zerobar,cbar2,zerobar,cbar2];

         % THE STATE SPACE EQUATION MATRIX
         AA=[zeros(4,4),eye(4,4);-MC*(KC-kbar),-MC*(CC-cbar)];
         INVA=inv(AA);

         % THE EFFECTIVE COEFFICIENTS OF DELAY
         BB1=[zeros(4,8);-MC*kbar11,-MC*cbar11];
         BB2=[zeros(4,8);-MC*kbar22,-MC*cbar22];
         mi0=expm(AA*step);
         mi1=(1-xresidue)*(mi0-eye(8,8))*INVA*BB1;
         mi2=xresidue*(mi0-eye(8,8))*INVA*BB1;
         mi3=(1-yresidue)*(mi0-eye(8,8))*INVA*BB2;
         mi4=yresidue*(mi0-eye(8,8))*INVA*BB2;
         BI(1:8,1:8)=BI(1:8,1:8)+mi0;
```

```
          BI(1:8,8*xdelay-7:8*xdelay)=BI(1:8,8*xdelay-7:8*xdelay)+mi1;
          BI(1:8,8*xdelay+1:8*xdelay+8)=BI(1:8,8*xdelay+...
              1:8*xdelay+8)+mi2;
          BI(1:8,8*ydelay-7:8*ydelay)=BI(1:8,8*ydelay-7:8*ydelay)+mi3;
          BI(1:8,8*ydelay+1:8*ydelay+8)=BI(1:8,8*ydelay+...
              1:8*ydelay+8)+mi4;
          PHI=BI*PHI;

       end
          E=eig(PHI);
          max_eig=max(abs(E));

       if max_eig>1
          adoc2=adoc;
          adoc=(adoc1+adoc)/2;

       else
           adoc1=adoc;
           adoc=(adoc2+adoc)/2;

       end

    end
    [y,i]=sort(abs(E));

    if abs(E(i(rankn))+1)<1e-2
        ii=1+ii;
        E(i(rankn))
        period2(ii)=adoc
        omega2(ii)=omega*60/2/pi

    end

    Floquetmult=E(i(rankn))
    chatter_freq1=-imag(log(Floquetmult))/tn/2/PI+excite_harmonics;
    chatter_freq2=imag(log(Floquetmult))/tn/2/PI+excite_harmonics;
    l_c_f=length(chatter_freq1);
    chatter_freq(1+2*(jj-1)*l_c_f:2*(jj-1)*l_c_f+l_c_f)=chatter_freq1;
    chatter_freq(2*(jj-1)*l_c_f+l_c_f+1:2*jj*l_c_f)=chatter_freq2;
    s_spindle(1+2*(jj-1)*l_c_f:2*jj*l_c_f)=omega*60/2/PI*...
        ones(1,2*l_c_f);
    adoc
    omega*60/2/PI
    omeg(jj)=omega*60/2/PI;
    ado(jj)=adoc;
    jj=jj+1;

end

save f0_s_d4r25.dat omeg ado -ascii -double;
save f0_s_d4r25_cf.dat s_spindle chatter_freq -ascii -double;
save f0_s_d4r25p2.dat omega2 period2 -ascii -double;

% PLOTS THE STABILITY LOBE PREDICTIONS
load f0_s_d4r25.dat;
figure(1)
plot(f0_s_d4r25(2,:),1000*f0_s_d4r25(1,:));
```

```
xlabel('Spindle Speed (krpm)');
ylabel('ADOC (mm)');

% PLOTS THE BIFURCATIONS CORRESPONDING TO THE STABILITY LOBE
PREDICTIONS
load f0_s_d4r25_cf.dat;
figure(2)
plot(f0_s_d4r25_cf(2,:),f0_s_d4r25_cf(1,:)/1000,'.');
xlabel('Spindle Speed (krpm)');
ylabel('Chatter Frequency (Hz)');
```

Subroutine Program <cutzone1.m>

```
% DEFINES THE CUTTING ZONE
% FORMS THE STIFFNESS AND DAMPING MATRICES DUE TO THE CUTTING FORCE

function [s,q]=cutzone1(tn,theta_enter,theta_exit,delta_theta,adoc,...
    r,omega,eta,num_tooth,step,k1,k2,kt,cp)

   PI=3.14159;
   tn_1=tn-step;
   s=zeros(2,2);
   q=zeros(2,2);
   normal1=zeros(num_tooth,1);
   normal2=zeros(num_tooth,1);

   for i = 1:num_tooth
      normal1(i) = -2*PI*(i-1)/num_tooth + theta_enter;
      normal2(i) = normal1(i) - 2*PI;

   end
   theta_en=theta_enter;
   theta_ex=theta_exit;

      % COMPENSATION OF delta_theta FOR UP AND DOWN MILLING
    if theta_en == 0.0
        theta_en = theta_en - delta_theta;
    end
    if theta_ex == PI
        theta_ex = theta_ex + delta_theta;
    end
    if theta_en >= theta_ex
        theta_en = -PI;
        theta_ex = -PI;
    end
    for i = 1:num_tooth

      % FOR CYLINDRICAL END MILLS WITH NON-ZERO HELIX ANGLES

      if(eta ~= 0.0)

          theta_en1 = theta_en;
          theta_ex1 = theta_ex;
```

```
% NORMALIZATION OF THE CUTTING ZONE ANGLES
if (theta_en1-normal1(i))*(theta_en1-normal2(i)) > 0.0
    while (theta_en1-normal2(i)) > 2*PI
        theta_en1 = theta_en1 - 2*PI;
    end
end
if (theta_en1-normal1(i))*(theta_en1-normal2(i)) > 0.0
    while (theta_en1-normal1(i)) < (-2*PI)
        theta_en1 = theta_en1 + 2*PI;
    end
end
if (theta_en1-normal1(i))*(theta_en1-normal2(i)) == 0.0
    theta_en1 = normal1(i);
end
if (theta_ex1-normal1(i))*(theta_ex1-normal2(i)) > 0.0
    while (theta_ex1-normal2(i)) > 2*PI
        theta_ex1 = theta_ex1 - 2*PI;
    end
end
if (theta_ex1-normal1(i))*(theta_ex1-normal2(i)) > 0.0
    while (theta_ex1-normal1(i)) < (-2*PI)
        theta_ex1 = theta_ex1 + 2*PI;
    end
end
if (theta_ex1-normal1(i))*(theta_ex1-normal2(i)) == 0.0
    theta_ex1 = normal1(i);
end

% ROTATES THE CUTTING ZONE IN THE OPPOSITE DIRECTION
theta_en1 = theta_en1 - omega*tn;
theta_ex1 = theta_ex1 - omega*tn;
if theta_en1 <= normal2(i)
    theta_en1 = theta_en1 + 2*PI;
end
if (theta_ex1 <= normal2(i))
    theta_ex1 = theta_ex1 + 2*PI;
end

% z_en AND z_ex VALUES ARE ALWAYS POSITIVE
z_en = (-(i-1)*2*PI/num_tooth+theta_enter-theta_en1)*r/...
    tan(eta);
z_ex = (-(i-1)*2*PI/num_tooth+theta_enter-theta_ex1)*r/...
    tan(eta);

% NON-CUTTING POSITIONS
if ((z_ex>=adoc)&(z_en>z_ex))|((z_en<=0.0)&(z_ex>adoc))|...
    (z_en==z_ex)
    z1 = 0.0;
    z2 = 0.0;

% CUTTING POSITIONS
else
    if (z_en<adoc)&(z_en>0.0)&((z_ex<=0.0)|(z_ex>adoc))
        z1 = 0.0;
        z2 = z_en;
    elseif (z_en>=adoc)&((z_ex<=0.0)|(z_ex>adoc))
        z1 = 0.0;
```

```
            z2 = adoc;
        elseif (z_en<adoc)&(z_ex<adoc)&(z_ex<z_en)&(z_ex>0.0)
            z1 = z_ex;
            z2 = z_en;
        elseif (z_en>=adoc)&(z_ex<adoc)&(z_ex>0.0)
            z1 = z_ex;
            z2 = adoc;
        else
    % YOU SHOULD NOT ENTER HERE IF ALL SCENARIOS INCLUDED
            %puts("There is a bug for helical tooth cutter!\n");
            z1 = 0.0;
            z2 = 0.0;
        end
    end

    % NON-CUTTING OR CUTTING COEFFICIENTS
    s_s = (z2-z1)/2.0+r*sin(tan(eta)*(z1-z2)/r)*...
        cos(2*omega*tn-(i-1)*4*PI/num_tooth-tan(eta)*(z1+z2)/...
        r+2*theta_enter)/(2*tan(eta));
    cc = (z2-z1)/2.0-r*sin(tan(eta)*(z1-z2)/r)*...
        cos(2*omega*tn-(i-1)*4*PI/num_tooth-tan(eta)*(z1+z2)/...
        r+2*theta_enter)/(2*tan(eta));
    sc = r*sin(tan(eta)*(z2-z1)/r)*sin(2*omega*tn-(i-1)*4*PI/...
        num_tooth-tan(eta)*(z1+z2)/r+2*theta_enter)/(2*tan(eta));

% FOR FLAT END MILLS WITH ZERO HELIX ANGLE

elseif(eta==0)
    theta_t = omega*tn - (i-1)*2*PI/num_tooth + theta_enter;
    theta_angle= theta_t;

    % NORMALIZATION OF THE CUTTING ZONE ANGLES
    if ((theta_t-theta_enter)*(theta_t-theta_enter-2*PI) > 0.0)
        while ((theta_t-theta_enter) > 2*PI)
            theta_t = theta_t - 2*PI;
        end
    end
    if ((theta_t-theta_enter)*(theta_t-theta_enter-2*PI) > 0.0)
        while ((theta_t-theta_enter-2*PI) < (-2*PI))
            theta_t = theta_t + 2*PI;
        end
    end
    if ((theta_t-theta_enter)*(theta_t-theta_enter-2*PI) == 0.0)
        theta_t = theta_enter;
    end

    % NON-CUTTING POSITIONS AND COEFFICIENTS
    if (((theta_t-theta_en)*(theta_t-theta_ex)>0.0)|...
        ((theta_en==-PI)&(theta_ex==-PI)))

        s_s=0.0;
        cc=0.0;
        sc=0.0;

    % CUTTING POSITIONS AND COEFFICIENTS
    elseif (((theta_t-theta_en)*(theta_t-theta_ex)<=0.0)&...
            (theta_en~=-PI)&(theta_ex~=-PI))
```

```
            s_s = adoc*sin(theta_t)*sin(theta_t);
            cc = adoc*cos(theta_t)*cos(theta_t);
            sc = 0.5*adoc*sin(2*theta_t);
        end
    end

    bs1= -k1*kt*s_s-k2*kt*sc-omega*cp*(k2*cc+k1*sc);
    bq1= -k1*cp*s_s-k2*cp*sc;
    bs2= -k2*kt*cc-k1*kt*sc+omega*cp*(k1*s_s+k2*sc);
    bq2= -k2*cp*cc-k1*cp*sc;
    bs3= k2*kt*s_s-k1*kt*sc+omega*cp*(k2*sc-k1*cc);
    bq3= k2*cp*s_s-k1*cp*sc;
    bs4= k2*kt*sc-k1*kt*cc+omega*cp*(k1*sc-k2*s_s);
    bq4= k2*cp*sc-k1*cp*cc;
    s(1:1,1:1) = s(1:1,1:1) + bs1;
    s(1:1,2:2) = s(1:1,2:2) + bs2;
    s(2:2,1:1) = s(2:2,1:1) + bs3;
    s(2:2,2:2) = s(2:2,2:2) + bs4;
    q(1:1,1:1) = q(1:1,1:1) + bq1;
    q(1:1,2:2) = q(1:1,2:2) + bq2;
    q(2:2,1:1) = q(2:2,1:1) + bq3;
    q(2:2,2:2) = q(2:2,2:2) + bq4;

end
```

Input Program <input_stepan.m> for Figure 5.6

```
% FUNCTION INPUT NAME
function input_stepan

global mx xix kx my xiy ky mu ku xiu mv kv xiv feed;
global kt kn friction cp r eta phi_n num_tooth feedcut;
global omega1 omega2 delta_omega theta_enter theta_exit;
global adocL adocH delta_adoc int_time;

% PARAMETER INPUTS

% MASS (kg); DAMPING; STIFFNESS (N/m) - X DIRECTION
mx=2.586;
xix=0.0038;
kx=2.2e+6;

% MASS (kg); DAMPING; STIFFNESS (N/m) - Y DIRECTION
my=1.0e+5;
xiy=1.0;
ky=1.0e+15;
% MASS (kg); DAMPING; STIFFNESS (N/m) - U DIRECTION
mu=1.0e+5;
xiu=1.0;
ku=1.0e+15;
```

```
% MASS (kg); DAMPING; STIFFNESS (N/m) - V DIRECTION
mv=1.0e+5;
xiv=1.0;
kv=1.0e+15;
% WORKPIECE MATERIAL
material='aluminum';
% WORKPIECE MATERIAL CONSTANTS
kt=1.89e+9; % (N/m^2)
kn=0.364;
% CUTTING FRICTION AND DAMPING
friction=0.20;
cp=0.0;
% CUTTING RADIUS OF TOOL (m)
r=9.53e-3;
% HELIX ANGLE OF TOOL (degrees)
eta=0.0;
% NORMAL RAKE ANGLE OF TOOL (degrees)
phi_n=12.0;
% NUMBER OF TEETH ON TOOL
num_tooth=1;
% FEEDRATE (m/tooth)
feedcut=0.0001016;
% MIN AND MAX SPINDLE SPEEDS (rpm)
omega1=2900.0;
omega2=3700.0;
% STEP CHANGE BETWEEN SPINDLE SPEED CALCULATIONS
delta_omega=10.0;
% CUTTING ENTRY AND EXIT ANGLES (degrees)
theta_enter=0;
theta_exit=19.57;
% MIN AND MAX ADOC (m)
adocL=50.0e-6;
adocH=8.0e-3;
% CHANGE IN ADOC
delta_adoc=0.0;
```

D.2 Matlab Programs for 3/4 Cutting Force Model

Main Program <threequarter_millingmain.m>

```
% MAIN PROGRAM TO GET THE STABILITY LOBE BY SEMI-DISCRETIZATION METHOD
% IN THIS CASE, WE WILL CONSIDER THE EFFECT OF FEED RATE ON TIME DELAY

function main
% num_tooth   - Number of teeth on the cutter
% r           - Radius of cutter (m)
% phi_n       - Normal rake angle (degree)
% omega       - Spindle Speed (rpm)
% feed        - Feed rate along x direction (m/s)
% feedcut     - Feed per tooth along x direction (m/tooth)
% rdoc        - Radial depth of cut (m)
```

```
% adoc        - Axial depth of cut (m)
% kt          - Tangential cutting coef from orthogonal cutting (N/m^2)
% kn          - Cutting coefficient proportional constant
% cp          - Viscous damping in the cutting process (N*s/m^2)
% friction    - Coulomb friction coefficient
% eta         - Helix angle of cylindrical end mill (degree)
% mx          - Modal mass in x direction (Kg)
% kx          - Modal stiffness in x direction (N/m)
% cx          - Viscous damping in x direction (N*s/m)
% theta_enter - Cutter entering angle (degree)
% theta_exit  - Cutter exit angle (degree)
% z1          - Dynamic integration lower limit (m)
% z2          - Dynamic integration upper limit (m)
% step        - Integration time step (s)

global mx xix kx my xiy ky mu ku xiu mv kv xiv feed;
global kt kn friction cp r eta phi_n num_tooth feedcut;
global omega1 omega2 delta_omega theta_enter theta_exit;
global adocL adocH delta_adoc int_time;
global xdelay ydelay feed;

PI=3.14159;

% THE NUMBER OF STEPS FOR EVERY PERIOD
N=40;

% CALLS THE INPUT FUNCTION TO INPUT THE SYSTEM PARAMETERS
input_stepan;

% CHANGES THE DIMENSIONLESS DAMPING INTO cx, cy, cu, AND cv
cx=xix*2.0*sqrt(mx*kx);
cy=xiy*2.0*sqrt(my*ky);
cu=xiu*2.0*sqrt(mu*ku);
cv=xiv*2.0*sqrt(mv*kv);

% FORMS THE MASS, DAMPING AND STIFFNESS MATRICES
mm=[mx,my,mu,mv];
MC=diag(mm,0);
MC=inv(MC);
cc=[cx,cy,cu,cv];
CC=diag(cc,0);
kk=[kx,ky,ku,kv];
KC=diag(kk,0);

% CREATES TWO MATRICES FOR STATE SPACE EQUATIONS
AA=zeros(8,8);
BB=zeros(8,8);
kbar=zeros(4,4);
cbar=zeros(4,4);
zerobar=zeros(4,1);

s=zeros(2,2);
q=zeros(2,2);

% UNIT CONVERSIONS - CHANGES THE ANGLES FROM DEGREES TO RADIANS
eta=eta*PI/180.0;
omega1=2*PI*omega1/60.0;
```

```
omega2=2*PI*omega2/60.0;
delta_omega=2*PI*delta_omega/60.0;
theta_enter=theta_enter*PI/180.0;
theta_exit=theta_exit*PI/180.0;

% CALLS K1 AND K2
k1 = kn/cos(eta);
k2 = 1.0 + friction*(cos(phi_n)-kn*sin(phi_n))*tan(eta);

% DEFINES THE RANK OF THE MAPPING MATRICS
rankn=(N+1)*8;

% STABILITY PREDICTION USING PARAMETERS OF SPINDLE SPEED AND ADOC
BI=zeros(rankn,rankn);
jj=1;
ii=0;
for omega=omega1:delta_omega:omega2
   step=2*PI/omega/(N+0.5)/num_tooth;
   tn=2*PI/omega/num_tooth;
   excite_harmonics=(-omega:omega:6*omega)/2/PI;
   feed=omega/(2*PI)*num_tooth*feedcut;

   % CUTTING ENTRANCE OR EXIT ANGLE VARIATIONS DUE TO THE FEED
   delta_theta = asin(2*PI*feed/(2*omega*r*num_tooth));

   % TWO TIME DELAYS
   % FOR A SINGLE TIME DELAY, SET xdelay=ydelay AND xresidue=yresidue
   xdelay = floor(2*PI/(omega*num_tooth*step));
   ydelay = xdelay;
   xresidue = 2*PI/(omega*num_tooth*step)-xdelay+0.5;
   yresidue = xresidue;
   adoc1=adocL;
   adoc2=adocH;
   adoc=adocH/2.0;

   while (adoc-adoc1)>1e-6 & (adoc2-adoc)>1e-6
      PHI=eye(rankn,rankn);

      for t=0:step:tn-step
         BI=[zeros(8,rankn);eye(rankn-8),zeros(rankn-8,8)];

% CALLS 3/4 RULE CUTTING FORCE SUBROUTINE TO GET THE S AND Q MATRICES

[s,q]=cutzone2(t,theta_enter,theta_exit,delta_theta,adoc,r,omega,...
    eta,num_tooth,step,k1,k2,kt,cp,xdelay,ydelay,feed);
         kbar=[s,s;s,s];
         cbar=[q,q;q,q];
         kbar1=kbar(:,1);
         cbar1=cbar(:,1);
         kbar2=kbar(:,2);
         cbar2=cbar(:,2);

         % X DIRECTION DELAY COEFFICIENT MATRICES
         kbar11=[kbar1,zerobar,kbar1,zerobar];
         cbar11=[cbar1,zerobar,cbar1,zerobar];

         % Y DIRECTION DELAY COEFFICIENT MATRICES
```

```
      kbar22=[zerobar,kbar2,zerobar,kbar2];
      cbar22=[zerobar,cbar2,zerobar,cbar2];

      % THE STATE SPACE EQUATION MATRIX
      AA=[zeros(4,4),eye(4,4);-MC*(KC-kbar),-MC*(CC-cbar)];
      INVA=inv(AA);

      % THE EFFECTIVE COEFFICIENTS OF DELAY
      BB1=[zeros(4,8);-MC*kbar11,-MC*cbar11];
      BB2=[zeros(4,8);-MC*kbar22,-MC*cbar22];
      mi0=expm(AA*step);
      mi1=(1-xresidue)*(mi0-eye(8,8))*INVA*BB1;
      mi2=xresidue*(mi0-eye(8,8))*INVA*BB1;
      mi3=(1-yresidue)*(mi0-eye(8,8))*INVA*BB2;
      mi4=yresidue*(mi0-eye(8,8))*INVA*BB2;
      BI(1:8,1:8)=BI(1:8,1:8)+mi0;
      BI(1:8,8*xdelay-7:8*xdelay)=BI(1:8,8*xdelay-7:8*xdelay)+mi1;
      BI(1:8,8*xdelay+1:8*xdelay+8)=BI(1:8,8*xdelay+...
          1:8*xdelay+8)+mi2;
      BI(1:8,8*ydelay-7:8*ydelay)=BI(1:8,8*ydelay-7:8*ydelay)+mi3;
      BI(1:8,8*ydelay+1:8*ydelay+8)=BI(1:8,8*ydelay+...
          1:8*ydelay+8)+mi4;
      PHI=BI*PHI;

   end
      E=eig(PHI);
      max_eig=max(abs(E));

   if max_eig>1
      adoc2=adoc;
      adoc=(adoc1+adoc)/2;
   else
      adoc1=adoc;
      adoc=(adoc2+adoc)/2;
   end

end
[y,i]=sort(abs(E));

if abs(E(i(rankn))+1)<1e-2
    ii=1+ii;
    E(i(rankn))
    period2(ii)=adoc
    omega2(ii)=omega*60/2/pi

end

Floquetmult=E(i(rankn))
chatter_freq1=-imag(log(Floquetmult))/tn/2/PI+excite_harmonics;
chatter_freq2=imag(log(Floquetmult))/tn/2/PI+excite_harmonics;
l_c_f=length(chatter_freq1);
chatter_freq(1+2*(jj-1)*l_c_f:2*(jj-1)*l_c_f+l_c_f)=chatter_freq1;
chatter_freq(2*(jj-1)*l_c_f+l_c_f+1:2*jj*l_c_f)=chatter_freq2;
s_spindle(1+2*(jj-1)*l_c_f:2*jj*l_c_f)=...
    omega*60/2/PI*ones(1,2*l_c_f);
adoc
omega*60/2/PI
```

```
   omeg(jj)=omega*60/2/PI;
   ado(jj)=adoc;
   jj=jj+1;

end

save f0_s_d4r25.dat omeg ado -ascii -double;
save f0_s_d4r25_cf.dat s_spindle chatter_freq -ascii -double;
save f0_s_d4r25p2.dat omega2 period2 -ascii -double;

% PLOTS THE STABILITY LOBE PREDICTIONS
load f0_s_d4r25.dat;
figure(1)
plot(f0_s_d4r25(2,:),1000*f0_s_d4r25(1,:));
xlabel('Spindle Speed (krpm)');
ylabel('ADOC (mm)');

% PLOTS THE BIFURCATIONS CORRESPONDING TO THE STABILITY LOBE
PREDICTIONS
load f0_s_d4r25_cf.dat;
figure(2)
plot(f0_s_d4r25_cf(2,:),f0_s_d4r25_cf(1,:)/1000,'.');
xlabel('Spindle Speed (krpm)');
ylabel('Chatter Frequency (Hz)');
```

Subroutine Program <cutzone2.m>

```
% DEFINES THE CUTTING ZONE
% FORMS THE STIFFNESS AND DAMPING MATRICES DUE TO THE CUTTING FORCE

function [s,q]=cutzone2(tn,theta_enter,theta_exit,delta_theta,adoc,...
    r,omega,eta,num_tooth,step,k1,k2,kt,cp,xdelay,ydelay,feed)

   PI=3.14159;
   tn_1=tn-step;
   s=zeros(2,2);
   q=zeros(2,2);
   normal1=zeros(num_tooth,1);
   normal2=zeros(num_tooth,1);

   for i = 1:num_tooth
      normal1(i) = -2*PI*(i-1)/num_tooth + theta_enter;
      normal2(i) = normal1(i) - 2*PI;
   end
   theta_en=theta_enter;
   theta_ex=theta_exit;

      % COMPENSATION OF delta_theta FOR UP AND DOWN MILLING
    if theta_en == 0.0
        theta_en = theta_en - delta_theta;
    end
    if theta_ex == PI
        theta_ex = theta_ex + delta_theta;
    end
```

```
if theta_en >= theta_ex
    theta_en = -PI;
    theta_ex = -PI;
end
for i = 1:num_tooth

  % FOR CYLINDRICAL END MILLS WITH NON-ZERO HELIX ANGLES

  if(eta ~= 0.0)
      theta_en1 = theta_en;
      theta_ex1 = theta_ex;

      % NORMALIZATION OF THE CUTTING ZONE ANGLES
      if (theta_en1-normal1(i))*(theta_en1-normal2(i)) > 0.0
          while (theta_en1-normal2(i)) > 2*PI
              theta_en1 = theta_en1 - 2*PI;
          end
      end
      if (theta_en1-normal1(i))*(theta_en1-normal2(i)) > 0.0
          while (theta_en1-normal1(i)) < (-2*PI)
              theta_en1 = theta_en1 + 2*PI;
          end
      end
      if (theta_en1-normal1(i))*(theta_en1-normal2(i)) == 0.0
          theta_en1 = normal1(i);
      end
      if (theta_ex1-normal1(i))*(theta_ex1-normal2(i)) > 0.0
          while (theta_ex1-normal2(i)) > 2*PI
              theta_ex1 = theta_ex1 - 2*PI;
          end
      end
      if (theta_ex1-normal1(i))*(theta_ex1-normal2(i)) > 0.0
          while (theta_ex1-normal1(i)) < (-2*PI)
              theta_ex1 = theta_ex1 + 2*PI;
          end
      end
      if (theta_ex1-normal1(i))*(theta_ex1-normal2(i)) == 0.0
          theta_ex1 = normal1(i);
      end

      % ROTATES THE CUTTING ZONE IN THE OPPOSITE DIRECTION
      theta_en1 = theta_en1 - omega*tn;
      theta_ex1 = theta_ex1 - omega*tn;
      if theta_en1 <= normal2(i)
          theta_en1 = theta_en1 + 2*PI;
      end
      if (theta_ex1 <= normal2(i))
          theta_ex1 = theta_ex1 + 2*PI;
      end

      % z_en AND z_ex VALUES ARE ALWAYS POSITIVE
      z_en = (-(i-1)*2*PI/num_tooth+theta_enter-theta_en1)*r/...
          tan(eta);
      z_ex = (-(i-1)*2*PI/num_tooth+theta_enter-theta_ex1)*r/...
          tan(eta);
```

```
    % NON-CUTTING POSITIONS
    if ((z_ex>=adoc)&(z_en>z_ex))|((z_en<=0.0)&(z_ex>adoc))|...
        (z_en==z_ex)
        z1 = 0.0;
        z2 = 0.0;

    % CUTTING POSITIONS
    else
        if (z_en<adoc)&(z_en>0.0)&((z_ex<=0.0)|(z_ex>adoc))
            z1 = 0.0;
            z2 = z_en;
        elseif (z_en>=adoc)&((z_ex<=0.0)|(z_ex>adoc))
            z1 = 0.0;
            z2 = adoc;
        elseif (z_en<adoc)&(z_ex<adoc)&(z_ex<z_en)&(z_ex>0.0)
            z1 = z_ex;
            z2 = z_en;
        elseif (z_en>=adoc)&(z_ex<adoc)&(z_ex>0.0)
            z1 = z_ex;
            z2 = adoc;
        else

  % YOU SHOULD NOT ENTER HERE IF ALL SCENARIOS INCLUDED
            %puts("There is a bug for helical tooth cutter!\n");
            z1 = 0.0;
            z2 = 0.0;
        end
    end

    % NON-CUTTING OR CUTTING COEFFICIENTS
    s_s = (z2-z1)/2.0+r*sin(tan(eta)*(z1-z2)/r)*...
        cos(2*omega*tn-(i-1)*4*PI/num_tooth-tan(eta)*(z1+z2)/...
        r+2*theta_enter)/(2*tan(eta));
    cc = (z2-z1)/2.0-r*sin(tan(eta)*(z1-z2)/r)*...
        cos(2*omega*tn-(i-1)*4*PI/num_tooth-tan(eta)*(z1+z2)/...
        r+2*theta_enter)/(2*tan(eta));
    sc = r*sin(tan(eta)*(z2-z1)/r)*sin(2*omega*tn-(i-1)*4*PI/...
        num_tooth-tan(eta)*(z1+z2)/r+2*theta_enter)/(2*tan(eta));

% FOR FLAT END MILLS WITH ZERO HELIX ANGLE

elseif(eta==0)
    theta_t = omega*tn - (i-1)*2*PI/num_tooth + theta_enter;
    theta_angle= theta_t;

    % NORMALIZATION OF THE CUTTING ZONE ANGLES
    if ((theta_t-theta_enter)*(theta_t-theta_enter-2*PI) > 0.0)
        while ((theta_t-theta_enter) > 2*PI)
            theta_t = theta_t - 2*PI;
        end
    end
    if ((theta_t-theta_enter)*(theta_t-theta_enter-2*PI) > 0.0)
        while ((theta_t-theta_enter-2*PI) < (-2*PI))
            theta_t = theta_t + 2*PI;
        end
    end
    if ((theta_t-theta_enter)*(theta_t-theta_enter-2*PI) == 0.0)
```

```
            theta_t = theta_enter;
        end

        % NON-CUTTING POSITIONS AND COEFFICIENTS
        if (((theta_t-theta_en)*(theta_t-theta_ex)>0.0)|...
                ((theta_en==-PI)&(theta_ex==-PI)))

            s_s=0.0;
            cc=0.0;
            sc=0.0;

        % CUTTING POSITIONS AND COEFFICIENTS
        elseif (((theta_t-theta_en)*(theta_t-theta_ex)<=0.0)&...
                (theta_en~=-PI)&(theta_ex~=-PI))

                s_s = adoc*sin(theta_t)*sin(theta_t);
                cc = adoc*cos(theta_t)*cos(theta_t);
                sc = 0.5*adoc*sin(2*theta_t);
        end
    end

% MODIFIED FOR THE LINEARIZED 3/4 RULE CUTTING FORCE MODEL

if(eta ~= 0.0)
    bs1= (-k1*kt*s_s-k2*kt*sc)*3/4*(xdelay*feed*sin(tan(eta)*...
        (z1-z2)/r)+1/(2*r)*(xdelay*feed*...
        cos(2*omega*tn-(i-1)*4*PI/num_tooth-tan(eta)*...
        (z1+z2)/r+2*theta_enter))^2)^(-1/4)-omega*cp*(k2*cc+k1*sc);
    bs2= (-k1*kt*sc-k2*kt*cc)*3/4*(ydelay*feed*...
        sin(tan(eta)*(z1-z2)/r)+1/(2*r)*(ydelay*feed*...
        cos(2*omega*tn-(i-1)*4*PI/num_tooth-tan(eta)*...
        (z1+z2)/r+2*theta_enter))^2)^(-1/4)+omega*cp*(k1*s_s+k2*sc);
    bs3= (-k1*kt*sc+k2*kt*s_s)*3/4*(xdelay*feed*...
        sin(tan(eta)*(z1-z2)/r)+1/(2*r)*(xdelay*feed*...
        cos(2*omega*tn-(i-1)*4*PI/num_tooth-tan(eta)*...
        (z1+z2)/r+2*theta_enter))^2)^(-1/4)+omega*cp*(k2*sc-k1*cc);
    bs4= (-k1*kt*cc+k2*kt*sc)*3/4*(ydelay*feed*...
         sin(tan(eta)*(z1-z2)/r)+1/(2*r)*(ydelay*feed*...
         cos(2*omega*tn-(i-1)*4*PI/num_tooth-tan(eta)*...
        (z1+z2)/r+2*theta_enter))^2)^(-1/4)+omega*cp*(k1*sc-k2*s_s);

elseif(eta == 0.0)
    bs1= (-k1*kt*s_s-k2*kt*sc)*3/4*(xdelay*feed*...
        sin(theta_t)+1/(2*r)*(xdelay*feed*...
        cos(theta_t))^2)^(-1/4)-omega*cp*(k2*cc+k1*sc);
    bs2= (-k1*kt*sc-k2*kt*cc)*3/4*(ydelay*feed*...
        sin(theta_t)+1/(2*r)*...
        (ydelay*feed*cos(theta_t))^2)^(-1/4)+omega*cp*(k1*s_s+k2*sc);
    bs3= (-k1*kt*sc+k2*kt*s_s)*3/4*(xdelay*feed*...
        sin(theta_t)+1/(2*r)*(xdelay*feed*...
        cos(theta_t))^2)^(-1/4)+omega*cp*(k2*sc-k1*cc);
    bs4= (-k1*kt*cc+k2*kt*sc)*3/4*(ydelay*feed*...
        sin(theta_t)+1/(2*r)*(ydelay*feed*...
        cos(theta_t))^2)^(-1/4)+omega*cp*(k1*sc-k2*s_s);

end
```

```
      bq1= -k1*cp*s_s-k2*cp*sc;
      bq2= -k2*cp*cc-k1*cp*sc;
      bq3= k2*cp*s_s-k1*cp*sc;
      bq4= k2*cp*sc-k1*cp*cc;
      s(1:1,1:1) = s(1:1,1:1) + bs1;
      s(1:1,2:2) = s(1:1,2:2) + bs2;
      s(2:2,1:1) = s(2:2,1:1) + bs3;
      s(2:2,2:2) = s(2:2,2:2) + bs4;
      q(1:1,1:1) = q(1:1,1:1) + bq1;
      q(1:1,2:2) = q(1:1,2:2) + bq2;
      q(2:2,1:1) = q(2:2,1:1) + bq3;
      q(2:2,2:2) = q(2:2,2:2) + bq4;

    end
```

Input Program <input_stepan.m> for Figure 5.6

```
% FUNCTION INPUT NAME
function input_stepan

global mx xix kx my xiy ky mu ku xiu mv kv xiv feed;
global kt kn friction cp r eta phi_n num_tooth feedcut;
global omega1 omega2 delta_omega theta_enter theta_exit;
global adocL adocH delta_adoc int_time;

% PARAMETER INPUTS

% MASS (kg); DAMPING; STIFFNESS (N/m) - X DIRECTION
mx=2.586;
xix=0.0038;
kx=2.2e+6;
% MASS (kg); DAMPING; STIFFNESS (N/m) - Y DIRECTION
my=1.0e+5;
xiy=1.0;
ky=1.0e+15;
% MASS (kg); DAMPING; STIFFNESS (N/m) - U DIRECTION
mu=1.0e+5;
xiu=1.0;
ku=1.0e+15;
% MASS (kg); DAMPING; STIFFNESS (N/m) - V DIRECTION
mv=1.0e+5;
xiv=1.0;
kv=1.0e+15;
% WORKPIECE MATERIAL
material='aluminum';
% WORKPIECE MATERIAL CONSTANTS
kt=1.89e+9; % (N/m^2)
kn=0.364;
% CUTTING FRICTION AND DAMPING
friction=0.20;
cp=0.0;
% CUTTING RADIUS OF TOOL (m)
r=9.53e-3;
```

```
% HELIX ANGLE OF TOOL (degrees)
eta=0.0;
% NORMAL RAKE ANGLE OF TOOL (degrees)
phi_n=12.0;
% NUMBER OF TEETH ON TOOL
num_tooth=1;
% FEEDRATE (m/tooth)
feedcut=0.0001016;
% MIN AND MAX SPINDLE SPEEDS (rpm)
omega1=2900.0;
omega2=3700.0;
% STEP CHANGE BETWEEN SPINDLE SPEED CALCULATIONS
delta_omega=10.0;
% CUTTING ENTRY AND EXIT ANGLES (degrees)
theta_enter=0;
theta_exit=19.57;
% MIN AND MAX ADOC (m)
adocL=50.0e-6;
adocH=8.0e-3;
% CHANGE IN ADOC
delta_adoc=0.0;
```

References

Arnold, R. N., 1946, "Mechanism of Tool Vibration in Cutting of Steel," Proc. of the Inst. of Mech. Eng., **154**(4), pp. 261-276.

Balachandran, B., 2001, "Nonlinear Dynamics of Milling Processes," Phil. Trans. R. Soc. Lond. A., **359**, pp. 793-819.

Davies, M. A., and Balachandran, B., 2000, "Impact Dynamics in the Milling of Thin-Walled Structures," Nonlinear Dynamics **22**(4), pp. 375-392.

Davies, M.A., Pratt, J. R., Dutterer, B., and Burns, T. J., 2002, "Stability Prediction for Low Radial Immersion Milling," Journal of Manufacturing Science and Engineering, **124**(2), pp. 217-225.

Halley, J. E., Helvey, A. M., Smith, K. S., and Winfough, W. R., 1999, "The Impact of High-Speed Machining on the Design and Fabrication of Aircraft Components," *Proc. of 1999 ASME Design and Tech. Conf.*, Paper No. DETC99/VIB-8057, Las Vegas, NV.

Insperger, T., Mann, B. P., Stepan, G., and Bayly, P. V., 2003, "Stability of Up-Milling and Down-Milling, Part 1: Alternative Analytical Methods," International Journal of Machine Tools and Manufacture, **43**(1), pp. 25-34.

Insperger, T., Mann, B. P., Stepan, G., and Bayly, P. V., 2003, "Stability of Up-Milling and Down-Milling, Part 2: Experimental Verification," International Journal of Machine Tools and Manufacture, **43**(1), pp. 35-40.

Long, X. H., 2006, "Loss of Contact and Time Delay Dynamics of Milling Processes," Ph.D. thesis, University of Maryland at College Park, College Park, MD.

Long, X. H., Balachandran, B., and Mann, B. P., 2007, "Dynamics of Milling Processes with Variable Time Delays," Nonlinear Dynamics, **47**(1-3), pp. 49-63.

Nayfeh, A. H., and Balachandran, B., 1995, *Applied Nonlinear Dynamics*, Wiley, New York, NY.

Stepan, G., Szalai, R., and Insperger, T., 2003, "Stability of High-Speed Milling," *Nonlinear Dynamics of Production Systems*, G. Radons, ed, Wiley VCH, New York, NY, pp. 111-128.

Stepan, G., Szalai, R., Mann, B. P., Bayly, P.V., Insperger, T., Gradisek, J., and Govekar, E., 2005, "Nonlinear Dynamics of High-Speed Milling - Analyses, Numerics, and Experiments," Journal of Vibration and Acoustics, **127**(2), pp. 197-203.

Szalai, R., 2006, “Nonlinear Dynamics of High-Speed Milling,” Ph.D. thesis, Budapest University of Technology and Economics, Budapest, Hungary.

Szalai, R., Stepan, G., and Hogan, S. J., 2004, “Global Dynamics of Low Immersion High-Speed Milling,” American Institute of Physics, **14**(4), pp. 1069-1077.

Tlusty, J., 2000, *Manufacturing Process and Equipment*, Prentice Hall, Englewood Cliffs, NJ.

Tlusty, J., and Polacek, M., 1963, “The Stability of the Machine Tool Against Self-Excited Vibration in Machining,” *Proc. of the International Research in Production Engineering*, Pittsburgh, PA, pp. 465-474.

Tobias, S. A., 1965, *Machine-Tool Vibration*, Wiley, New York, NY.

Zhao, M. X., 2000, “Dynamics and Stability of Milling Processes,” Ph.D. thesis, University of Maryland at College Park, College Park, MD.